

Harmonization of Global Land-Use Change and Management for the Period 850-2100 (LUH2) for CMIP6

George C. Hurtt^{1*} ϕ , Louise Chini¹, Ritvik Sahajpal¹, Steve Frohking², Benjamin L. Bodirsky³,
 Katherine Calvin⁴, Jonathan C. Doelman⁵, Justin Fisk^{1,6}, Shinichiro Fujimori⁷, Kees Klein
 Goldewijk^{5,8}, Tomoko Hasegawa⁷, Peter Havlik⁹, Andreas Heinemann¹⁰, Florian Humpenöder³,
 Johan Jungclauss¹¹, Jed O. Kaplan¹², Jennifer Kennedy¹, Tamás Krisztin⁹, David Lawrence¹³,
 Peter Lawrence¹³, Lei Ma¹, Ole Mertz¹⁴, Julia Pongratz^{11,15}, Alexander Popp³, Benjamin
 Poulter¹⁶, Keywan Riahi⁹, Elena Shevliakova¹⁷, Elke Stehfest⁵, Peter Thornton¹⁸, Francesco N.
 Tubiello¹⁹, Detlef P. van Vuuren^{5,8}, Xin Zhang²⁰

*Correspondence to: gchurtt@umd.edu

ϕ authors alphabetical after Frohking.

¹Department of Geographical Sciences, University of Maryland, U.S.A.

²Institute for the Study of Earth, Oceans, and Space, University of New Hampshire, U.S.A.

³Potsdam Institute for Climate Impact Research, Germany

⁴Joint Global Change Research Institute, Pacific Northwest National Laboratory, U.S.A.

⁵PBL Netherlands Environmental Assessment Agency, Netherlands

⁶Applied Geosolutions, U.S.A.

⁷National Institute for Environmental Studies, Japan

⁸Copernicus Institute of Sustainable Development, University of Utrecht, Netherlands

⁹International Institute for Applied Systems Analysis, Austria

¹⁰Institute of Geography and Centre for Development and Environment, University of Bern, Switzerland

¹¹Max Planck Institute for Meteorology, Hamburg, Germany

¹²Department of Earth Sciences, The University of Hong Kong, Hong Kong

¹³National Center for Atmospheric Research, U.S.A.

¹⁴Department of Geosciences and Natural Resource Management, University of Copenhagen, Denmark

¹⁵Ludwig-Maximiliansuniversität Munich, Department of Geography, Germany

¹⁶NASA Goddard Space Flight Center, Biospheric Sciences Lab, Greenbelt, MD 20771, U.S.A.

¹⁷Geophysical Fluid Dynamics Lab, Princeton, NJ, U.S.A.

¹⁸Oak Ridge National Laboratory, U.S.A.

¹⁹Statistics Division, Food and Agriculture Organization of the United Nations

²⁰Appalachian Laboratory, University of Maryland Center for Environmental Science, U.S.A.

Abstract. Human land-use activities have resulted in large changes to the biogeochemical and biophysical properties of the Earth surface, with consequences for climate and other ecosystem services. In the future, land-use activities are likely to expand and/or intensify further to meet growing demands for food, fiber, and energy. As part of the World
45 Climate Research Program Coupled Model Intercomparison Project (CMIP6), the international community has developed the next generation of advanced Earth System Models (ESMs) to estimate the combined effects of human activities (e.g. land use and fossil fuel emissions) on the carbon-climate system. A new set of historical data based on the History of the Global Environment database (HYDE), and multiple alternative scenarios of the future (2015-2100) from Integrated Assessment Model (IAM) teams, are required as input for these models. With most ESM simulations
50 for CMIP6 now completed, it is important to document and the land use patterns used by those simulations. Here we present results from the Land-use Harmonization 2 (LUH2) project, which smoothly connects updated historical reconstructions of land-use with eight new future projections in the format required for ESMs. The harmonization strategy estimates the fractional land-use patterns, underlying land-use transitions, key agricultural management information, and resulting secondary lands annually, while minimizing the differences between the end of the
55 historical reconstruction and IAM initial conditions and preserving changes depicted by the IAMs in the future. The new approach builds off a similar effort from CMIP5, and is now provided at higher resolution (0.25 x 0.25 degree), over a longer time domain (850-2100, with extensions to 2300), with more detail (including multiple crop and pasture types and associated management practices), using more input datasets (including Landsat remote sensing data), updated algorithms (wood harvest and shifting cultivation), and is assessed via a new diagnostic package. The new
60 LUH2 products contain >50 times the information content of the datasets used in CMIP5, and are designed to enable new and improved estimates of the combined effects of land-use on the global carbon-climate system.

1. Introduction

65 Over the past several centuries to millennia, human land-use activities have grown and intensified to provide food, feed, energy, and fiber to support an expanding human population. These same land-use activities have also resulted in large changes to the underlying biogeophysical properties of the Earth surface, with impacts on climate, biogeochemical cycling, and habitat for biodiversity. In the future, land-use activities are likely to expand and/or intensify further to meet future demands for food, feed, energy, and fiber. What have been the effects of land-use
70 activities on the climate system? What will be the impacts on climate of future land-use scenarios? Addressing these questions requires an integrated set of historical land-use data, integrated assessment models of the future, and climate models. To be most useful, requisite land-use data must be global, spatially and temporally and conceptually consistent from the past through to the future, and in a format that is usable by Earth System Models (ESMs).

75 Previously, in preparation for the Fifth Assessment Report (AR5) of the Intergovernmental Panel on Climate Change (IPCC) and as part of CMIP5, the Land-use Harmonization (LUH1) project provided harmonized land-use data for the years 1500-2100, at $0.5^\circ \times 0.5^\circ$ resolution (Hurtt et al., 2011). These data served as required land-use forcing for CMIP5 climate model experiments and have been used in numerous related studies to assess the effects of land-use change on carbon and climate (Brovkin et al., 2013; Jones et al., 2011; Shevliakova et al., 2009;
80 Shevliakova et al., 2013). They have also been extended for use in uncoupled DGVM modeling studies (e.g. TRENDY) and as input to the Global Carbon Project (Le Quéré et al., 2013; Le Quéré et al., 2014; Le Quéré et al., 2015) and other studies (Jones et al., 2013; Di Vittorio et al., 2014; Collins et al., 2015; Arneeth et al., 2017; Thornton et al., 2017; Di Vittorio et al., 2018)

Now, as part of the World Climate Research Program Coupled Model Intercomparison Project (CMIP6, Eyring et al., 2016), the international research community has developed the next generation of advanced ESMs able to estimate the combined effects of human activities (e.g. land use and fossil fuel emissions) on the carbon-climate system. In addition, a set of historical data based on the History of the Global Environment database (HYDE) (Klein Goldewijk et al. 2017), and multiple alternative scenarios of the future (2015-2100), developed by Integrated Assessment Model (IAM) teams (Riahi et al. 2017), including global land-use projections (Popp et al.
85 2017), have been developed as drivers for these models. The goal of the Land-Use Harmonization (LUH2) project is to prepare a new harmonized set of land-use scenarios that smoothly connects the historical reconstructions of land-use with eight future projections in the format required for ESMs. This ambitious land-use harmonization strategy estimates the fractional land-use patterns, underlying land-use transitions, and key agricultural management information, annually for the time period 850-2100 at $0.25^\circ \times 0.25^\circ$ resolution, while minimizing the differences at the transition between the historical reconstruction ending conditions and IAM initial conditions,
90 and working to preserve changes depicted by the IAMs in the future to create a consistent set of IAM simulations specifically for this project. The resulting data products are a required input for multiple CMIP6 model experiments, including the historical all-forcing experiment, and related model intercomparison project

100 experiments including PaleoMIP (Junclaus et al., 2017), ScenarioMIP (O'Neill et al., 2016), LUMIP (Lawrence
 et al., 2016). Extensions are also provided for 2100-2300 as input to climate stabilization experiments. To bracket
 the ranges of uncertainty in the historical reconstruction, two alternative scenarios (“low” and “high”) are provided
 in addition to the “baseline” historical scenario.

2. Methods

105 Like its predecessors, The Global Land Use Model (Hurtt et al., 2006; Hurtt et al., 2011), GLM2 (the model
 underlying the LUH2 dataset) computes subgrid-scale land-use states and corresponding transition rates using an
 accounting-based method that tracks the fractional state of the land surface in each grid cell as a function of the land
 surface at the previous time step, and a transition matrix. This can be represented using the following matrix
 equation:

$$110 \quad l(x, t+1) = A(x, t)l(x, t)$$

$$x = (1, \dots, N), t = (t_0, \dots, t_f) \quad (1)$$

where $l(x, t)$ is a vector giving the fractions of grid cell area in each land-use category in a grid cell x and time t , and
 $A(x, t)$ is a matrix giving the land-use transition rates between N land-use categories in grid cell x and time t . Each
 115 element, $a_{ij}(x, t)$ of the matrix $A(x, t)$ gives the rate at which land-use type j was converted to land-use type i between t
 and $t+1$.

$$A(x, t) = \begin{bmatrix} a_{11}(x, t) & \cdots & a_{1n}(x, t) \\ \vdots & a_{ij}(x, t) & \vdots \\ a_{n1}(x, t) & \cdots & a_{nn}(x, t) \end{bmatrix} \quad (i, j = 1 \dots N) \quad (2)$$

120 GLM2 was adapted and extended from GLM1 to track a larger list of 12 subgrid scale land-use types (4 “natural
 land” types, 5 crop types, 2 pasture types, and urban), and key management information (i.e. fraction irrigated,
 fraction flooded, fraction biofuel, and rate of industrial N fertilizer application) related to agriculture. The vector
 $m(x, t)$ gives the cropland management information for grid cell x at time t , and the state of the full system is
 therefore described by both the vectors $l(x, t)$ and $m(x, t)$.

125 GLM2 was used to solve Eq. 1 and associated values of $A(x, t)$ and $m(x, t)$ annually for every $0.25^\circ \times 0.25^\circ$ terrestrial
 grid cell globally for 850-2100 (with extensions to 2300). In the process, the framework was used to determine on
 the order of 10^{10} unknowns. Since this was a large and underdetermined system, the approach was to solve the
 system for every grid cell at each time step by constraining with inputs including: (i) land-use maps, (ii) crop type

130 and rotation rates, (iii) shifting cultivation rates, (iv) agriculture management, (v) wood harvest, (vi) forest
transitions, and (vii) potential biomass and biomass recovery rates. Because these inputs do not uniquely constrain
the system, additional assumptions were made including: (viii) the priority of primary (not harvested, cut or
converted since 850 CE) or secondary land for wood harvesting and agricultural conversion, (ix) the inclusiveness in
135 wood harvest statistics of wood cut in conversion of forest to agricultural use, and (x) the spatial pattern of wood
harvest. These model inputs, constraints, and assumptions that are used to compute the state of the system and the
associated values of $A(x,t)$ are described in the following sections. The model input-output is illustrated in Fig. 1,
and described below.

2.1 Historical Maps of Land Use

140 Historical maps of land use were based on the History of the Global Environment database (HYDE). HYDE
provides long-term historical, spatially-explicit time series on a 5 arc minute resolution of population estimates as
well as land use reconstructions covering the Holocene period, defined here as 10 000 BCE until the present (Table
1). It is an effort to quantify the agricultural expansion of humankind over time. In principle, HYDE uses a simple
approach of combining historical population estimates with assumptions on the trajectory of historical land use per
capita. Allocation of land use patterns is steered at present day by satellite information and UN FAO agricultural
145 data, and this is gradually replaced towards the past by a combination of spatially explicit maps such as climate, soil,
slope, and neighborhood of rivers and lakes. The latest version (3.2; Klein Goldewijk et al., 2017) presents land use
categories such as built-up area, managed pastures and more extensive rangelands, cropland excluding rice, and rice
as a separate crop because of its relevancy for greenhouse gas emissions. A distinction was made between irrigated
and rain-fed cropland (both for other crops and rice). Besides the baseline reconstruction, two alternative historical
150 land-use reconstructions were provided based on uncertainties. For a full description of the methodology see Klein
Goldewijk et al. (2017).

The version of the HYDE 3.2 dataset used for the baseline LUH2 historical product was the “2016_beta_release”
version, and the version used for the high and low scenarios was the “2017_beta_release_000” version. Data was
provided at 5’ spatial resolution, every 100 years from 800 to 1700, every 10 years from 1700 to 2000, and then
155 annually from 2000 to 2015. These data were aggregated to $0.25^\circ \times 0.25^\circ$ resolution and converted from absolute area
of each grid cell to grid cell fractional area. Data were then linearly interpolated in time to produce annual maps of
the fraction of each 0.25° grid-cell occupied by each of the following land-use types: cropland, grazing land, pasture,
and urban. The ice and water fractions of each grid cell were also taken from the HYDE dataset and were assumed
constant over time. By subtracting the land-use and ice and water fractions from each grid cell, the fractions of each
160 grid cell occupied by natural vegetation (either primary or secondary forest or grassland) were also determined. The
HYDE 3.2 dataset also includes a global map that assigns a country code to each terrestrial grid cell, at 5’ resolution.
This map served as a basis to generate a similar map at 0.25° resolution, consistent with the 0.25° maps of land-use
data. In this map every grid cell with ice/water fraction less than 1.0 was assigned a country code, resulting in a
global map containing 199 countries.

165 2.2 Historical Maps of Crop types and Crop Rotations

The cropland fraction of each grid-cell, along with transitions to/from cropland, are further sub-divided into five different crop functional types (CFTs): C3 annuals, C4 annuals, C3 perennials, C4 perennials, and C3 nitrogen fixers. For the years 850 to 2015 the CFT fractions of total cropland are primarily based on data from Monfreda et al. (2008), which provides global maps of harvested areas of 175 different crops, at 5-minute spatial resolution, for the year 2000. For use in the LUH2 methodology, these maps were aggregated into five CFT classes at 0.25° spatial resolution and then normalized so that all CFT fractions sum to 1 in each grid-cell. For grid cells that do not have crop-type data from Monfreda et al., national crop-type data from FAO (FAO 2016) is used instead (i.e. by aggregating the 169 FAO crop types into the 5 CFT classes represented in LUH, averaging over all years of FAO data from 1961 to 2013, then assigning the normalized national CFT fractions to any grid-cells within each country that did not have Monfreda data). The resulting map of CFT fractions is used for all years 850-2015 to sub-divide the gridded cropland fraction and cropland-related transitions into CFT fractions and CFT-related transitions, by multiplying the cropland fraction of each grid-cell (and the cropland-related transitions to/from each grid-cell) by the CFT fractions map. Note that this process includes the inherent assumption that the fraction of a grid cell that was harvested for a crop type (i.e. the Monfreda et al. data) was roughly correlated with the fraction of the total cropland area that was occupied by that crop type.

For the years 2015-2100, we first identify one or two CFTs in the IAM data that have the greatest global area increase over the 85-year period. We then attempt to follow the gridded changes in fraction of cropland occupied by those CFTs, by first assigning as much of the cropland expansion transitions as possible to the expansion of those one or two CFTs, and then, when needed, by adding transitions between CFTs to re-assign area from CFTs with lower rates of increase (or even reductions) of area in the IAM data to the CFTs with large global increases in area. The result of this process is typically that the global area changes of CFTs in LUH2 tend to follow global area changes of CFTs in the IAM data, not just for the CFTs with the largest area changes, but for others as well. When there were no CFTs with significant changes over the 2015-2100 period, the contemporary CFT ratios were used to disaggregate total cropland area into CFT fractions for all years 2015-2100.

Crop rotations or the practice of growing a sequence of crops on an agricultural field, within or across growing seasons, is a key component of agricultural management, and has impacts on overall crop yields, nutrient cycling, fertilizer and water usage, water quality and biodiversity (Bullock, 1992). An example of such a crop rotation is the corn-soybean-corn rotation practiced extensively in the U.S. Midwest. We generated a national scale crop rotation dataset for the U.S to quantify rates of transition from one crop functional type to another and applied those rates to the crop functional types in LUH2. We use the USDA Cropland Data Layer (CDL, Sahajpal et al., 2014) to quantify unique crop rotations for U.S from 2012 – 2014 (Sahajpal et al., 2014). Assuming a crop rotation span of 3 years, and nearly 100 unique crops in the CDL, we could potentially have 10^6 unique crop rotations. Empirically, there are close to 100,000 unique crop rotations in the U.S for that time-period. However, by aggregating different crop types to the crop functional types in LUH2 and merging similar rotations, we estimated transition rates between different

200 crop functional types in LUH2 and applied them after all other transitions between land-use types have been
 computed.

2.3 Historical Data on Agriculture Management Activities

205 Historical information on crop management activities included data on irrigation, flooded agriculture, and industrial
 nitrogen fertilizer application rates. Data on irrigated area, and area of flooded rice, were obtained from HYDE. The
 irrigated fraction of each crop type was computed during the historical period by dividing the HYDE 3.2 irrigated
 fraction of each grid-cell by the HYDE 3.2 cropland fraction of each grid-cell. This fraction is then used as the
 irrigated fraction of each crop sub-type. The fraction of C3 annuals that are flooded for rice is computed historically
 by dividing the HYDE 3.2 flooded fraction of each grid-cell by the C3 annual fraction of each grid-cell (rice is the
 only C3 annual considered to be flooded in our dataset. Non-flooded rice is not explicitly represented here, but
 210 would be included in the non-flooded C3 annual fraction). For industrial nitrogen fertilizers, we used a recent global
 compilation of N fertilizer use for 1961-2011 (Zhang et al., 2015) as our base data set. Countries without fertilizer
 data reported in Zhang et al. (2015) were assigned regional mean values, based on the regional grouping of countries
 defined in Zhang et al. (2015). Fertilizer use between 1915 and 1960 was hindcast using global synthetic N fertilizer
 use totals from Smil (2001), and was forecast from 2012 to 2015 using an estimate of global industrial N fertilizer
 215 use based on data from the International Fertilizer Association (IFA, 2015). Decadal mean N-fertilizer rates by crop
 and country were computed from the Zhang et al. (2015) data and were assigned to mid-decade year (e.g., the 1961-
 1970 mean was assigned to 1965). To generate country fertilizer application rates for 2015, which we did not
 compute as a decadal mean, we assumed that the fertilization rate since 2005 has changed with a same scaling factor
 across all countries and crop types (as in Zhang et al., 2015). Using the harvested area in 2015 from HYDE 3.2 (see
 220 Section 2.1), the fertilization rate for country j and crop k in 2015 is determined by

$$R_{j,k,2015} = R_{j,k,2005} \cdot (F_{2015,IFA}/A_{2015}) \div (F_{2005}/A_{2005}),$$

225 where $R_{j,k,t}$ is the N-fertilization rate by crop type (j) by country (k) by year (t) [$\text{kg N ha}^{-1} \text{y}^{-1}$], and A_t is the global
 total crop area in year t from HYDE 3.2, $F_{2015,IFA}$ is the global N fertilizer application in 2015, estimated by applying
 the trend in 2006-2012 from the IFA data to extrapolate to 2015 from 2012, yielding $F_{2015,IFA} = 115 \text{ Tg N y}^{-1}$, and
 F_{2005} is the global total N fertilizer application estimated as the product of N fertilizer application rate in 2005
 computed from Zhang et al. (2015) and LUH2 cropland area ($F_{2005} = 94 \text{ Tg N}$, the mean of 2001-2010, as above).

230 Fertilizer application rates were hindcast from the 1960s to rates for 1950, 1930, and 1915. Synthetic N fertilizer
 rates in 1915 are set to 0.0 kg N km^{-2} for all countries and crop types, as this was when the Haber-Bosch industrial
 process was invented. Using global N consumption data from Smil (2001) for 1950 ($F_{1950,Smil} = 3.7 \text{ Tg N y}^{-1}$) and
 1930 ($F_{1930,Smil} = 1.0 \text{ Tg N y}^{-1}$), and crop area from LUH2 ($A_{j,k,t}$, see Section 2.1), the synthetic N rates by crop and
 country ($R_{j,k,t}$) were estimated for 1950, 1930, and 1915 as follows

$$R_{j,k,1950} = R_{j,k,1965} \cdot (F_{1950,Smil}) \div \Sigma[R_{j,k,1965} \cdot A_{j,k,1950}],$$

$$R_{j,k,1930} = R_{j,k,1965} \cdot (F_{1930,Smit}) \div \Sigma[R_{j,k,1965} \cdot A_{j,k,1930}],$$

$$R_{j,k,1915} = 0.$$

235 where the sum is over all countries (j index) and crops (k index). Finally, we generated annual synthetic N fertilizer rate values by country and crop functional type and year ($R_{j,k,t}$) by linearly interpolating between values for 1915, 1930, 1950, 1965, 1975, 1985, 1995, 2005, 2015.

2.4 Rates of Shifting Cultivation

240 We considered shifting cultivation to be a specific land use sequence of clearing, agricultural use typically for one to several years, and subsequent abandonment of land to forest (or other natural vegetation) regeneration for three years to several decades ('fallow'). While likely widespread in the early millennia of agriculture (Olofsson & Hickler, 2007), more recently it has been restricted to the tropics (Ruthenberg, 1980). We use the recent analysis of the past, present, and future extent of shifting cultivation (Heinimann et al., 2017) to constrain its occurrence in LUH2. Heinimann et al. (2017) based their analysis on the early global map of the distribution of 'primitive subsistence agriculture' (Butler 1980), a visual inspection of the distribution of shifting cultivation based on the 2000-2014 Global Forest Change (GFC) data set (Hansen et al., 2013) coupled with high-resolution satellite imagery, and an extensive expert survey on regional trends in shifting cultivation, querying lead authors of scientific publications on shifting cultivation over the past decade (Heinimann et al., 2017).

250 Heinimann et al. (2017) estimated the current area under shifting cultivation (cultivated + fallow) to be about 280 Mha, distributed extensively and heterogeneously across Central and tropical South America, tropical Africa, and tropical Southeast Asia (see Fig. 5 in Heinimann et al., 2017). For each $1 \times 1^\circ$ grid cell with detected signs of shifting cultivation, they also estimated its level of occurrence, including both active cropland and fallows, aggregated into five classes of the total land area in each grid cell: none (<1%), very low (1-9%), low (10-19%), moderate (20-39%) or high ($\geq 40\%$). They project significant declines in shifting cultivation extent through the 21st century, with losses by the end of the century of more than 80% in Africa and Latin America, and 100% in Asia, and extent at $1 \times 1^\circ$ in remaining areas to be low or very low (see Fig. 7 in Heinimann et al., 2017).

260 We created annual LUH2 shifting cultivation maps by linearly interpolating between the assumed shifting cultivation rates in 1850 and the expert opinion-based rates of 2010 (Heinimann et al., 2017). The 1850 shifting cultivation rates were assumed to fall in the 'high' category of 70%. The future shifting cultivation rates were similarly computed by linearly interpolating between the 2010 and the assumed 2100 rates from the expert opinion survey of Heinimann et al., 2017. For LUH2, shifting cultivation involved cropland only (grazing land was included as part of shifting cultivation in LUH1 but not in LUH2). For all grid cells, we used the mid-range of shifting cultivation occurrence (e.g., 5% for 'very low', 15% for 'low', 30% for 'moderate', and 70% for 'high'), and assumed that these fractions also applied to the fraction of cropland involved in shifting cultivation. We also 265 assumed that the residence time for a patch of cropland involved in shifting cultivation was only 1 year. At each

time-step in our model, we then abandoned the Heinimann et al. (2017) prescribed percentage of total cropland area in the grid cell (e.g. cropland to secondary land), and cleared the same area from natural vegetation (e.g. forest to cropland), with a prioritization of clearing secondary land first unless the available secondary land was less than 10 times the cropland area involved in shifting cultivation (based on an assumption of a 10-year fallow period). The global area of shifting cultivation activity tends to track global changes in cropland area from HYDE 3.2 (Klein Goldewijk et al., 2017, or see Section 2.1), and global future cropland area changes from IAMs, although this relationship between cropland area and shifting cultivation area declines over time due to the extent of shifting cultivation declining significantly, especially through the 21st century.

2.5 Historical Statistics on Wood Harvest

Historical wood harvest in LUH2 is based on national statistics, and partitioned into fuelwood and non-fuelwood, for 199 countries, based on a 1990 country list from HYDE 3.2 (Klein Goldewijk et al., 2017). These national wood harvest statistics are used to solve Equation 1 and assigned to individual grid-cells using the methodology described in Sections 2.10 and 2.11. For the years 1961-2015 the LUH2 wood harvest data is based on FAO national wood harvest volume data (FAO 2016) for both coniferous and non-coniferous round wood, which is combined with wood density values of 0.225 Mg C m⁻³ for coniferous wood and 0.325 Mg C m⁻³ for non-coniferous wood (Houghton and Hackler, 2000) to convert volume statistics to mass of carbon harvested. Harvest rates were hindcast to 1920 by interpolating from mean FAO per capita harvest rates from 1961-1965, using national population totals from HYDE 3.2 (see section 2.1), and national per capita fuelwood ('firewood') and timber ('sawtimber') wood harvest totals from 1920 (Zon and Sparhawk 1923). Note that Zon and Sparhawk totals for timber consumption include volume of wood for construction, industry, and pulp, and so, with firewood, should be roughly comparable to FAO 'total roundwood'.

For the years prior to 1920, national annual per capita wood harvest rates were computed in three different ways for low, baseline, and high LUH2 scenarios, and use the same national population data from HYDE 3.2 to compute the total national wood harvest (in Mg C) per year for each scenario. For the "low" wood harvest scenario, the national annual per capita wood harvest rates from Zon and Sparhawk (1923) were held constant for all years from 850 to 1920. However, prior to the fossil fuel era, global mean per capita wood harvest was likely significantly higher than in 1920, so for the "high" scenario we used a national per capita wood harvest demand reconstruction for "fuelwood" and "durable wood" from Kaplan et al. (2017) for the period 850-1800. Per capita wood harvest rates then transitioned linearly from 1800 rates to the 1920 rates of Zon and Sparhawk (1923), to mimic the global shift in energy sources from biomass towards fossil fuels (Smil, 2003). These high and low wood harvest scenarios represented two different extremes in terms of cumulative wood harvested and total area of forests removed. In addition, the high scenario is significantly higher than the LUH1 wood harvest reconstruction. To provide a scenario somewhere between these two extremes, we also generated a "baseline" wood harvest scenario in which we modified the Kaplan national wood harvest rates from 850 to 1800 by national scale factors. These scale factors are defined as twice the contemporary FAO national per capita wood harvest rates divided by the national per capita

wood harvest rates in 1800 from the Kaplan data, and this definition was determined from analysis of the global time-series figure of historical biofuels consumption (Smil 2003) which shows current global per capita biofuels consumption of around 6 GJ per capita and around 21 GJ per capita in 1800. Reducing the Kaplan wood harvest rates via these scale factors does not imply that the original Kaplan rates are too high, rather that the Kaplan data is likely to be capturing types of wood harvest and related processes that our model does not currently simulate. For years between 1800 and 1920 we linearly interpolate between the modified year 1800 rates from Kaplan and the Zon and Sparhawk (1923) rates in 1920.

For the “low” and “baseline” scenarios, the reconstructed national wood harvest data were increased by a slash fraction of 30% (as in LUH1, Hurtt et al., 2011) to account for non-harvested losses from forests that occur during the wood harvesting process. For the “high” scenario, we do not add a slash fraction to the data for the years 850-1800 since it is assumed this is already included in the Kaplan data (Kaplan et al. 2017). In this scenario, the slash fraction is linearly increased from 0% to 30% during 1800 to 1920, and held constant thereafter.

All national wood harvest totals from FAO and Zon and Sparhawk are assumed to represent the amount of wood produced by each country. In contrast, the data from Kaplan represents the wood harvest demand from each country, although it is assumed that during the years 850-1800 there was limited wood trade in most parts of the world, and hence demand would equal production. In Europe, however, international wood trade occurred during 850-1800 (Kaplan et al., 2017). So, for European countries only, if the available national biomass is not sufficient to meet the national wood harvest demand in a particular year, we seek the unmet demand from other European countries (i.e. increase the wood harvest production in other countries) proportional to the available biomass in each country. From 1500–2005, the global cumulative total wood harvest in the baseline scenario was 190 Pg C including slash (Fig. 2), compared with 142 Pg C and 381 Pg C in the “low” and “high” scenarios, respectively.

2.6 Historical Maps of Forest Transitions

The spatial patterns of forest transitions, particularly those related to wood harvesting, were constrained by the Landsat-based gridded forest loss observations from Hansen et al. (2013). This product consists of global 30m grids of tree canopy cover for year 2000 and gross forest cover loss and gain for the 2000-2012 time interval mapped using the entire global Landsat data archive (although only the forest loss data was used within LUH2). Within this dataset, forest was defined using a single tree canopy cover threshold to match the global forest extent provided by the FAO FRA report (FAO 2000). Cumulative forest area was estimated by summing pixels with different tree canopy cover. Then the threshold was selected that most closely enabled a match to the total world forest cover for year 2000, which is 4085 million ha, according to FAO data. A threshold of 28% tree canopy cover produced 100.5% of the FAO forest area. This threshold was used to define forest area for the year 2000 at 30m spatial resolution. Gross forest cover loss was reported only within areas covered with forest in the year 2000. Gross forest cover gain was mapped independently outside areas forested in the year 2000 and represents gain of tree canopy cover to 30% or higher from non-forest state. The global maps of forest extent and change were then aggregated to the same spatial resolution and format as the LUH1 datasets ($0.5^\circ \times 0.5^\circ$ fractional). To aggregate the data to the

0.5° grid, the area of each class was computed within each grid cell, and then the class area percent of total cell area was calculated. The 0.5° product shows percent forest cover for year 2000 and percent gross forest cover loss and gain during the 2000-2012 time interval. The 0.5° product was later downscaled to 0.25° for consistency with the new LUH2 spatial resolution. A very simple downscaling method was employed that kept the fraction of forest area (or forest loss) equal within each 0.25° grid-cell inside the 0.5° grid-cell cells.

The resulting map of forest loss was used within LUH2 as part of the algorithm for determining the spatial pattern of forest loss from wood harvesting. However, it should be noted that the Landsat-based forest loss maps differ from the LUH2 forest loss maps in multiple ways, including definitions of “forest” (i.e. tree canopy cover vs. biomass density), whether or not a single grid-cell can contain both forest and non-forest (LUH2 grid-cells are either potentially forested or potentially non-forested), whether or not the forest loss includes natural disturbances such as fires or not (LUH2 forest loss results only from land-use-related changes). As a result, the match between these products is not perfect, and the Landsat-based forest loss data is used as a guide to improving the LUH2 forest loss patterns, rather than a hard constraint on those patterns.

2.7 Biomass Density and Recovery Rates

To discriminate forested land from non-forested land, and to convert quantities of harvested wood in biomass units into harvested area, information was needed on the historical distribution of forests and above ground carbon stocks. As no complete global, gridded, historical record of these quantities was available, a simple empirically-based global terrestrial model was used to provide a consistent set of both global forest cover and carbon stocks. Estimates of ecosystem properties were based on an updated version of the MIAMI-LU ecosystem model (Hurtt et al., 2002; Hurtt et al., 2006; Hurtt et al., 2011). Miami-LU was driven by the empirically-based Miami model of net primary production (Leith, 1972), which has integrated sub-models of plant mortality and disturbance. The model tracked sub-grid heterogeneity resulting from land-use changes in a manner similar to the more advanced Ecosystem Demography (ED) model (Hurtt et al., 1998; Moorcroft et al., 2001; Hurtt et al., 2002).

Miami-LU was run globally at 0.5° x 0.5° resolution for a spin-up period of 500 years using data from the Multi-Scale Synthesis and Terrestrial Model Intercomparison Project (MsTMIP) (Wei et al., 2013). These data are a combination of climatologies from the Climate Research Unit and National Centers for Environmental Protection, and has a global 0.5° x 0.5° climatology with a 6 hourly daily time step from 1901 – 2010. MIAMI-LU outputs were subsequently downscaled to 0.25° x 0.25° resolution to match the remaining LUH2 inputs (downscaling simply assigned all 0.25° x 0.25° grid-cells the same fraction value as the 0.5° x 0.5° grid-cell they were contained within). Aggregated globally, the NPP estimate from Miami-LU was 63 Pg C y⁻¹. This fell within a range of NPP estimates from various global biogeochemical models, ranging from 40 Pg C y⁻¹ to 81 Pg C y⁻¹ (Cramer et al. 1999). Miami-LU estimated a global stock of potential plant carbon of 718 Pg C (Figure 3). This falls within a range spanning 557 Pg C (Kucharik et al., 2000) to 923 Pg C (Sitch et al., 2003), with a more recent estimate of 772 Pg C (Pan et al., 2013). The total potential above-ground carbon stock was 563 Pg C. To differentiate forest from non-

370 forest areas, a definition based on potential above-ground standing stock of 2 kg C m⁻² was used (Hurtt et al., 2002; Hurtt et al., 2006; Hurtt et al., 2011). Each grid cell was thus identified as potential forest or potential non-forest based on potential biomass, providing a static map that is used for the entire time period from 850-2100. Using this definition, 48.8 x 10⁶ km² of the land surface was classified as potential forest. For comparison, potential forest area based on the BIOME model was estimated at 60 x 10⁶ km² (Klein Goldewijk, 2001). Finally, Miami-LU was also
375 used to estimate the recovery of carbon stocks on secondary lands by tracking the mean age of secondary land in each grid cell, although not explicitly account for the full age distribution or the potential effects of land degradation, management, or pollution that may have occurred.

2.8 Future Land Use, Wood Harvest, and Management from Integrated Assessment Models

380 For 2015-2100, we use land use and wood harvest information from eight different marker SSP-RCP scenarios derived from five different Integrated Assessment Models (Riahi et al. 2017). These marker scenarios were prioritized as input to CMIP6 climate model simulations by ScenarioMIP. They are fully described elsewhere (O'Neill et al., 2016, Riahi et al. 2017), and their main features are summarized below and in Table 2 in the order described in O'Neill et al. (2016).

385 2.8.1 SSP5-8.5 REMIND-MAGPIE

The scenario SSP5-8.5 is based on the REMIND-MAGPIE SSP5 baseline scenario, which has a radiative forcing close to RCP8.5 (Kriegler et al., 2017). SSP5 is characterized by rapid and resource intensive development and material-intensive consumption patterns, whereas technological progress, including agricultural productivity, is high. In consequence, the SSP5-RCP8.5 scenario exhibits very high levels of fossil fuel use, up to a doubling of
390 global food demand, and up to a tripling of greenhouse gas emissions over the course of the century, marking the upper end of the emission scenario literature. The REMIND-MAGPIE integrated assessment modeling framework consists of the Regionalized Model of Investment and Development (REMIND) and the Model of Agricultural Production and its Impacts on the Environment (MAGPIE). REMIND (Luderer et al., 2015) is a global multi-regional energy-economy general equilibrium model linking a macro-economic growth model with a bottom-up engineering-based energy model. MAGPIE (Popp et al., 2014) is a global multi-regional partial equilibrium model of
395 the land-use sector, which accounts for spatially explicit biophysical constraints derived by the vegetation, hydrology and crop growth model LPJmL (Müller and Robertson, 2014; Bondeau et al., 2007; Bodirsky et al., 2012). Land-use decisions in MAGPIE are modeled at a spatially-explicit level (Lotze-Campen et al., 2008). REMIND and MAGPIE are coupled by exchange of price and quantity information on bioenergy and GHG
400 emissions (Popp et al., 2011; Kriegler et al., 2017). As an outcome of the strongly increasing food and feed demand as well as highly intensified future livestock production systems relying on concentrates rather than roughage feed (Weindl et al., 2017), the SSP5-RCP8.5 scenario shows strong expansion of global cropland into pasture and forest land, with an increase of about 300 Mha (20%) between 2010 to 2100.

2.8.2 SSP3-7 AIM

405 The SSP3-7.0 is a simulation derived from the SSP3 baseline scenario (Fujimori et al., 2017) which has a radiative forcing close to 7.0 Wm^{-2} . The SSP3-7.0 was simulated using the Asia-Pacific Integrated assessment Model/Computable General Equilibrium model (AIM/CGE; (Fujimori et al., 2014; Fujimori et al., 2012)) combined with a land-use allocation model (Hasegawa et al., 2017). AIM/CGE is a global integrated assessment model, coupling representations of economy, energy systems, land, and climate. AIM/CGE is a recursive dynamic general
410 equilibrium model, adjusting prices until the supply and demand for energy, industrial, agriculture, forest commodities as well as all the other goods and services equilibrate. AIM/CGE includes 17 regions and 42 industrial classifications including 10 agricultural sectors. The land system is divided into nine agro-ecological zones. Land use and land cover were further downscaled to 0.5×0.5 grids using the land allocation approach developed by Hasegawa et al. (2017). SSP3 is a world of regional rivalry where countries increasingly focus on domestic and
415 regional issues. Economic development is slow, consumption is material-intensive, and population growth is low in industrialized and high in developing countries. Land use change is hardly regulated. Agricultural land intensification is low, especially due to very limited transfer of new agricultural technologies to developing countries. Unhealthy diets with high animal shares and high food waste prevail. A regionalized world leads to reduced trade flows for agricultural goods. The SSP3-RCP7.0 scenario includes strong expansion of global crop and
420 pasture land, with increases of 40% and 7% from 2010 to 2100, respectively, resulting in large-scale deforestation.

2.8.3 SSP2-4.5 MESSAGE

SSP2-4.5 is a low stabilization scenario that stabilizes radiative forcing at 4.5 Wm^{-2} (~650 ppm CO₂-equivalent) before 2100 without ever exceeding that value. RCP4.5 is simulated in a structure of interlinked disciplinary and sectorial models referred to as the IIASA Integrated Assessment Modelling (IAM) framework (Riahi et al. 2007,
425 Fricko et al. 2017). Within the framework, land-use dynamics are modelled with the GLOBIOM model, which is a recursive-dynamic partial-equilibrium model (Havlík et al., 2011). GLOBIOM includes a bottom-up representation of the agricultural, forestry and bio-energy sector, which allows for the inclusion of detailed grid-cell information on biophysical constraints and technological costs, as well as a rich set of environmental parameters, including comprehensive AFOLU (agriculture, forestry and other land use) GHG emission accounts and irrigation water use.
430 For spatially explicit projections of the change in afforestation, deforestation, forest management, and their related CO₂ emissions, GLOBIOM is coupled with the G4M model (Kindermann et al., 2006; Kindermann et al., 2008; Gusti, 2010). These models are linked to the MESSAGE energy system model (Messner and Strubegger, 1995; Riahi et al., 2012), while air pollution implications are derived with the help of the GAINS model. An important feature of the RCP4.5 is the initial decrease in forest by about 43 million ha from 2000 to 2050 (comparable to the
435 reference scenario), with a subsequent increase in forest by about 331 million ha from 2050 to 2100.

2.8.4 SSP1-2.6 IMAGE

The SSP1-2.6 scenario is developed using the IMAGE 3.0 integrated assessment model (Stehfest et al., 2014). IMAGE is a model framework describing the future agriculture system and energy system, as well the changes in future land cover, the carbon and hydrological cycle and climate change. While most socio-economic processes are described at the level of 26 regions, environmental processes are modeled on a grid -basis (30 or 5 arc-minutes). The LPJmL model is hard-coupled to IMAGE on a yearly basis (Mueller et al., 2016), and calculates for crops & grassland productivity, natural vegetation dynamics, hydrology, and the carbon cycle. The SSP1-RCP2.6 is derived from the SSP1 baseline scenario which projects a future under a green growth paradigm (van Vuuren et al, 2017). The SSP1 scenario is characterized by moderate population growth leveling off by mid-century, and by high economic growth and technological improvements including agricultural productivity. In addition, SSP1 describes an environmentally aware world concerned with limiting biodiversity loss and reduced appetite for animal product consumption. Mitigation policy is added to the SSP1 baseline scenario to achieve a maximum warming of 2 degrees consistent with the RCP2.6 scenario (van Vuuren et al., 2011). Important policies from the land-use perspective are increased bio-energy use in combination with carbon capture and storage, avoided deforestation policy to reduce deforestation, and restoration of degraded forests (Doelman et al., 2018).

In SSP1-2.6, the combination of socio-economic trends and climate policy results in substantial reductions in total agricultural land. At the same time, large areas are dedicated to bioenergy production, and also forest area increases (Doelman et al., 2018; Popp et al., 2017).

2.8.5 SSP4-6.0 GCAM

The SSP4-6.0 is a simulation derived from the SSP4 baseline (Calvin et al., 2017), with a modest climate policy imposed to limit 2100 radiative forcing to 6.0 Wm^{-2} . The SSP4-6.0 was simulated using the Global Change Assessment Model (GCAM; Wise et al., 2014). GCAM is a global integrated assessment model, coupling representations of energy, water, land, economy, and climate. GCAM is a market-equilibrium model, adjusting prices until the supply and demand for energy, agriculture, and forest commodities equilibrate. GCAM subdivides the world into 32 economic regions. The land system is further subdivided into as many as 18 agro-ecological zones, resulting in 283 agriculture and land use regions. Land use and land cover were further downscaled to $0.5^\circ \times 0.5^\circ$ grids using the approach developed by West et al. (2014) and implemented globally in Le Page et al. (2016). SSP4 is a world of inequality, both within and across regions. High-income regions continue to prosper, with increased demand for energy and food. Technological progress, including agricultural productivity, is high. Low-income regions, however, stagnate; increases in total consumption are due to increased population and not increased wealth. Agricultural productivity growth is low. Environmental policies, including reduced deforestation, reforestation, and afforestation programs, are present in high- and medium income countries only. The SSP4-60 scenario includes modest expansion of global crop and pasture land, with increases of 14% and 9% from 2010 to 2100, respectively.

470 The modest climate policy encourages afforestation in the high- and medium-income regions where environmental policies are strong, resulting in a global increase in forest cover of 3% between 2010 and 2100.

2.8.6 SSP4-3.4 GCAM

475 The SSP4-3.4 scenario starts from the same baseline as the SSP4-60, but includes a more stringent mitigation policy limiting radiative forcing to 3.4 Wm^{-2} in 2100. SSP4-3.4 was also simulated with GCAM (described above).
480 Limiting 2100 radiative forcing to 3.4 W/m^2 requires a much larger carbon price, exceeding \$1000/tCO₂ (2005 US\$) in 2100, than the SSP4-60. This increased carbon price has substantial effects on energy and land use. In particular, ~1200 million ha of land is allocated to the production of bioenergy, resulting in a large increase in total cropland area (80% increase between 2010 and 2100). Forest cover increases in the high and medium-income regions as the result of afforestation policies but decreases in the low-income regions as the result of agricultural land expansion. The net effect is that global forest cover increases through mid-century before returning to 2010 levels at the end of the century.

2.8.7 SSP5-3.4OS REMIND-MAGPIE

485 The SSP5-3.4OS scenario starts from the baseline SSP5-RCP8.5, but includes mitigation policy limiting radiative forcing to 3.4 Wm^{-2} in 2100. SSP5 RCP3.4OS was also simulated with REMIND-MAGPIE (described above) (Kriegler et al., 2017). This scenario is supposed to follow SSP5-8.5, an unmitigated baseline scenario, through 2040, but includes after 2040 strong mitigation action to rapidly reduce CO₂ emissions to zero around 2070 and to net negative levels thereafter. In consequence, the SSP5-RCP3.4OS pathway shows even stronger cropland expansion compared to the SSP5-RCP8.5 scenario, mainly due large-scale deployment of 2nd generation bioenergy crops after 2040. Globally, cropland in the SSP5-RCP3.4OS pathway increases by about 800 Mha (50%) between 490 2010 and 2100, mainly at the cost of pasture area.

2.8.8 SSP1-1.9 IMAGE

495 The SSP1-1.9 parallels SSP1-2.6 in all aspects, but reaches a lower radiative forcing target, namely 1.9 instead of 2.6 W m^{-2} . As SSP1-2.6, also SSP1-1.9 is derived from the IMAGE 3.0 integrated assessment model (Stehfest et al., 2014). IMAGE is a model framework describing the future agriculture system and energy system, as well the changes in future land cover, the carbon and hydrological cycle and climate change, as described above. The SSP1-1.9 is based on the SSP1 baseline scenario. As also described above, SSP1 projects a future under a green growth paradigm, with moderate population growth, and fast economic growth and technological improvements (van Vuuren et al, 2017). In terms of land use, SSP1 describes a world that is environmentally aware, and aims at limiting biodiversity loss and environmental impacts of food consumption. Mitigation policy is added to the SSP1 baseline scenario to limit warming 500 to 1.9 W m^{-2} (Rogelj et al., 2018; Doelman et al., 2018). As for SSP1-2.6, important policies from the land-use

perspective are increased bio-energy use in combination with carbon capture and storage, avoided deforestation policy to reduce deforestation, and restoration of degraded forests (Doelman et al., 2018).

2.9 Harmonization of LUH2 Inputs

505 Harmonization of inputs involved minimizing the difference between the end of the historical reconstruction and the beginning of future projections, and preserving as much information on the future from IAMs as possible. Five different IAMs provide future land-use, wood harvest, and management data using a variety of variables and units and at different spatial and temporal resolutions (Table 2). Prior to harmonization, inconsistencies in definitions, resolutions, and other factors resulted in significant discrepancies. The spread of global cropland values from the
510 IAMs in 2010 was 5% of the historical reconstruction values in that year, and the spread of global pasture values from the IAMs in 2010 was 23% of the historical values. Gridded values had even larger discrepancies, differing by as much as 100% from the historical values. After harmonization, these inconsistencies were eliminated by design of the harmonization methodology. Since some IAMs didn't simulate built-up area or urban spread, and for consistency of urban-land definitions across all scenarios, the IMAGE model provided land-use inputs for built-up area in all
515 scenarios (Doelman et al., 2018). Also, since the REMIND-MAGPIE model did not compute wood harvest amounts, these were provided for the SSP5-8.5 and SSP5-3.4OS scenarios from analogous scenarios computed by the GCAM model.

The first step in harmonizing inputs was to convert the IAM data into a standardized format for comparison with the historical product. Future land-use data were aggregated into the fractions of each grid-cell occupied by total
520 cropland, total grazing land (the sum of managed pasture and rangeland), urban land, and natural vegetation (the sum of primary and secondary forest and non-forest) annually at $0.25^\circ \times 0.25^\circ$ resolution. Future data on irrigation and flooded areas were standardized into national totals. Future wood harvest data were standardized into a total national wood harvest demand in Mg C y^{-1} , as well as the fuelwood component of that national wood harvest, either by aggregating gridded wood harvest data into national totals, or by disaggregating regional wood harvest data using
525 the ratio of national to regional wood harvest from the end-of-historical period (i.e. 2015). Wood harvest data that were provided in volume units (m^3) were converted to biomass (Mg C) using a conversion factor of $0.2688 \text{ Mg C m}^{-3}$. A 30% slash fraction was added to the wood harvest scenarios. Future fertilizer rates were standardized into national fertilizer application rates in $\text{kg N ha}^{-1} \text{ y}^{-1}$ per crop functional type. For future scenarios with only regional data, all countries within a region were assigned the same regional rates. When gridded future
530 fertilizer application rates were available these were also used in LUH2 and were standardized into annual rates per crop type ($\text{kg N ha}^{-1} \text{ y}^{-1}$) at $0.25^\circ \times 0.25^\circ$ resolution. For SSP4-3.4 and SSP4-6.0 (both from GCAM), the fertilizer rates for the GCAM crop types *misccrop* and *palmfruit* were used as estimates of fertilizer rates for C3 perennials, *sugarcrop* and *biomass* rates were used as estimates for C4 perennial rates, *oilcrop* and *misccrop* rates were used for C3 nitrogen fixing crops, *rice* and *wheat* were used for C3 annuals, and *corn* was used for C4 annuals.

535 Although the IAM land-use data were generally in good agreement with the end-of-historical period values at the
global scale, there were still significant differences both globally and spatially, particularly for pasture which has
less consistent definitions across models (Fig. 4). To address this issue, we applied IAM-based annual changes in
land use sequentially to the spatial pattern of land use at the end of the historical reconstruction. Annual future
changes in cropland, grazing land, and urban land were computed and aggregated to $2^\circ \times 2^\circ$. These changes were then
540 applied to the 2° -aggregated cropland, grazing land, and urban land, from the previous time-step, starting with the
end-of-historical period (i.e. 2015). When it was not possible to apply the annual change within a 2° grid-cell, due to
lack of available land to expand into, or lack of cropland, grazing, or urban land to abandon, the unmet changes were
applied in neighboring 2° grid-cells, starting with immediate neighbors and then radiating outward. The harmonized
grids of cropland, grazing land, and urban land were then disaggregated into $0.25^\circ \times 0.25^\circ$ grids according to the
545 following method: when disaggregating decreases, the percentage change in each land-use state was computed and
then applied to all underlying 0.25° land-use fractions; for increases in cropland, grazing, or urban land, the needed
change was applied across all underlying 0.25° grid-cells and was weighted by available land in each grid-cell.
Figure 5 shows how well the IAM 2015-2100 changes in cropland and pasture fractions are retained in the
harmonized data, which increases markedly with decreased spatial resolution. For wood harvest, analogous methods
550 were applied.

After the harmonization of total cropland, grazing land, and urban land, cropland and grazing areas were further
disaggregated into underlying sub-types. Assignment of future crop functional types were based on fixed
contemporary Monfreda/FAO proportions, and adjusted to match IAM specific information as needed. For grazing
land, a pasture/rangeland mask was generated for 2015 (and held constant for all years) to sub-divide future total
555 grazing land into the two grazing sub-types. For new grid cells projected to be converted to grazing land in the
future, national ratios were used.

Next, management data were harmonized by applying analogous algorithms to sequentially apply projected changes
in managed area and rates to the pattern at the end of the historical reconstruction. Annual change in national
irrigated areas were computed and then applied to the previous years gridded irrigation fractions for all crop types,
560 first increasing irrigated area on grid-cells with existing irrigation, and then adding any additional needed irrigated
area equally to all non-irrigated cropland grid-cells within each country. Annual national percentage change in
flooded area was computed and this percentage change was applied to all grid-cells that have a non-zero flooded
fraction in the previous time-step. Any resulting fractions that are greater than 1 are reset to 1. Finally, annual
national percentage changes in fertilizer rates per crop type are computed. These national percentage changes are
565 applied to the previous years gridded fertilizer rates for all grid-cells within each country. In an effort to ensure that
the final (year 2100) gridded fertilizer rates closely approximate the future IAM fertilizer rates, there are a few
exceptions to this method, which are based on simple assumptions that aim to keep the LUH2 rates from remaining
too low, or becoming too large, when compared to the IAM gridded rates. First, the gridded fertilizer rates are held
between 0 and $500 \text{ kg N ha}^{-1} \text{ yr}^{-1}$. Then, for grid-cells with fertilizer rates below $1 \text{ kg N ha}^{-1} \text{ yr}^{-1}$ on the previous time-
570 step, and with an increasing national percentage change in fertilizer rates, the actual gridded IAM fertilizer rates for

the next time step are used instead of the computed LUH2 rates. Also, if gridded fertilizer rates increase between time-steps and are above the gridded IAM fertilizer rates, the gridded fertilizer rates for the next time-step are held constant at the current LUH2 gridded rates. Finally, if the gridded LUH2 fertilizer rates are less than 80% of the IAM gridded fertilizer rates, and the national percentage change in fertilizer rates is positive, a small additional increase (1% of the total current difference between IAM gridded rates and LUH2 gridded rates) is added to the LUH2 fertilizer rates.

2.10 Additional Major Factors

2.10.1 Inclusiveness of Wood Harvest

Since it is not always known whether or not the wood cut on land cleared for agriculture is counted in national wood harvest statistics, assumptions are made in LUH2 about the amount of biomass from land clearing that is included towards meeting national wood harvest demands. The need to use wood from cleared land for fuel or wood products was probably higher in the past than it is now. To that end, we assumed all wood on land cleared for agriculture prior to 1850 was counted towards meeting the national wood harvest estimates and additional wood harvest was only conducted when the land cleared for agriculture did not provide enough wood to meet the estimates. We also assumed that after 1920 none of the wood from cleared land was counted toward meeting national wood harvest numbers and wood harvest demand was met only through explicit wood harvesting activities. Between 1850 and 1920 a fraction of the wood from cleared land was used to meet wood harvest demands, starting from 100% of wood from cleared lands in 1850 and decreasing linearly to 0% in 1920. If this fraction of wood from cleared lands was not enough to meet national wood harvest demands, additional explicit wood harvest was conducted to meet national totals.

2.10.2 Priority of Land Conversion

When converting natural land to agriculture, or using it for wood harvest, a decision must be made about whether to prioritize the use of primary or secondary land. The cumulative effect of these decisions has a large impact on the resulting secondary land area, age, and biomass in each grid-cell, and in aggregate at the regional and global scale. Although the decision of which natural vegetation type to prioritize is undoubtedly variable in space and time, for the sake of simplicity we have chosen a single priority rule for each land-use transition type, as follows. For urban expansion, secondary was prioritized. After all secondary land is used, further urban land-use demand (if any) was met on primary land. For expansion of cropland and grazing land, both primary and secondary land were used in relative proportion to their availability in each grid-cell. For example, if primary land and secondary land occupied 10% and 90% of natural vegetation in a grid-cell, respectively, then 10% of the converted natural vegetation would be taken from primary land, and 90% of the converted natural vegetation land would be taken from secondary land. For shifting cultivation, secondary land was prioritized unless the secondary land area was less than 10 times the cropland area in a grid-cell, in which case primary land was prioritized. For wood harvesting, the priority was to

605 take wood from both primary and secondary land in relative proportion to the amount of available biomass in each land type.

2.11 Methodology for Calculating Land Use Transitions

2.11.1 Determining agriculture land use transitions

Following Hurtt et al. (2011), a bookkeeping approach was used to calculate annual land-use transition rates between five aggregate land-use types—cropland, grazing land, urban, primary and secondary. To determine these, the annual change in urban area in each grid cell was first computed from either the HYDE data (for the historical period) or IAM data (for the future period) and applied proportionally to the cropland, grazing land, and secondary land-use categories within the grid cell. If there was not enough land available between cropland, grazing land and secondary land for a given urban land-use increase, the remaining area needed was taken from the primary land within the grid cell. Next, minimum transition rates were calculated between the remaining three land-use types (cropland, grazing land, and other; where other was defined as the sum of primary and secondary), based on the gridded annual input data on land-use patterns from HYDE or the IAMs (adjusted for the transitions into and out of those types associated with urban land-use change computed on the previous step). With only three land-use types, unique minimum transitions (i.e. solutions to Eq. 1) could be easily determined. Additional transitions associated with shifting cultivation and wood harvest were then determined. In cases of shifting cultivation, land-use transitions from cropland to other, and other to cropland, were both increased by the abandonment rate of agricultural land. Transitions from other were then partitioned into transitions from primary and secondary based on availability and the previously described shifting cultivation algorithm. All transitions from cropland or grazing land to other were defined as transitions to secondary. The amount of wood cut in converting land to agriculture was determined by overlaying these transitions with estimates of biomass density.

625

After computing transitions between the five aggregate land-use types, the transitions to/from both primary and secondary were further sub-divided into transitions to/from primary forest, primary non-forest, secondary forest, and secondary non-forest, based on the underlying map of potential forest (grid-cells with potential biomass density greater than 2 kg C m⁻² were designated as potentially forested). In addition, the transitions to/from grazing land were subdivided into transitions to/from managed pasture and rangeland, based on the annual gridded input data from HYDE. The HYDE maps of managed pasture and rangeland for the year 2015 were also used to sub-divide grazing land into the underlying grazing sub-types for all years in the future period (2015-2100). Transitions to/from total cropland in each grid-cell were further sub-divided into transitions to/from each of the five crop functional types (CFTs) using the data and methodology described in the section on “Historical Maps of Crop Types and Crop Rotations”.

2.11.2 Determining area cleared by wood harvest

Since the spatial patterns of wood harvest within each country are not generally known (especially for years outside the period of satellite observations), several assumptions were used to spatially allocate the reconstructed national annual wood harvest demands to individual grid-cells within each country, and to convert the biomass harvested to an area cleared per grid-cell. As a first step, within each country and at each time-step, a fraction of the biomass cleared from agricultural land expansion is subtracted from the national wood harvest demand, as described in the preceding section on the inclusiveness of wood harvest data. After wood from agricultural clearing has been subtracted, the remaining national wood demand is then explicitly harvested, first from grid-cells with available primary forest and/or mature secondary forest, then from grid-cells with young secondary forest, and finally from non-forested land (both primary and secondary). Mature secondary forests are defined using an average probability of harvest vs. biomass function parameterized from detailed age-specific harvesting algorithms previously developed and applied in the U.S. (Hurtt et al., 2002; Hurtt et al. 2006). Note that since the natural vegetation definitions are based on a *mean* biomass density, wood harvesting from non-forested land can imply either harvesting vegetation, such as shrubland, that is tree-based albeit with a mean biomass density below that of a forest, or harvesting isolated trees within other low-biomass-density vegetation such as grasslands.

Within the group of grid-cells containing primary forest and/or mature secondary forest in each country, the first cells to be harvested are all those with a “significant human presence” (SHP), followed by all neighboring cells, radiating outwards, taking only the fraction of biomass needed until the demand has been satisfied or the available biomass exhausted. The use of proximity to a SHP in this algorithm is based on the assumption that proximity to a SHP implies proximity to transportation infrastructure (accessibility) or local markets. Prior to the year 1900, grid-cells with a SHP are defined as those grid-cells having cropland, managed pasture, secondary land, or urban land area. Grid-cells that have Landsat-observed forest loss of at least 10% of the cell’s land area during the period 2000-2012 are gradually included in the definition of SHP between the years 1900 and 2000, until both the land-use-based

660 and Landsat-based definitions of SHP are given equal weighting between 2000 and 2015. The contribution of
Landsat-based forest loss to SHP then decreases again between 2015 and 2100.

When harvesting wood from a grid-cell chosen using these methods, if only a fraction of the biomass in a grid-cell is
needed, wood is harvested from both primary forest and secondary mature forest (or from primary non-forest and
secondary non-forest) in proportion to their available biomass. Wood harvested from primary land provides an area-
665 based transition “primary to secondary”, whereas wood harvested from secondary land provides an age- (and
biomass-) resetting/reduction transition “secondary to secondary”, with the resulting secondary mean age and
secondary mean biomass density tracked in the ‘secma’ and ‘secmb’ variables, respectively.. To calculate these
transitions in area units, the wood harvest biomass was converted using the carbon density of land affected (Hurtt et
al. 2006).

670 In addition to its use in the definition of SHP, the Landsat forest loss data is also used in two additional ways to
further constrain the spatial pattern of wood harvesting. First, primary forest and mature secondary forest land that
will experience a Landsat-observed forest loss during the period 2000-2012 is protected from wood harvest between
the years 1950 and 2000 so that it is available for harvesting during the period 2000-2012. Second, during the years
2000-2012, the Landsat forest loss data is used in LUH2 to constrain the spatial pattern of where wood harvest does,
675 or does not, occur, by checking whether the annualized gridded forest loss from the Landsat data has already been
met within LUH2 yet. Inclusion of Landsat-based forest loss data in the LUH2 algorithm generates a significant
improvement in the match between satellite observations of forest loss and the LUH2 representation of forest loss
between the years 2000-2012 (Fig. 6).

For European countries that are unable to meet their national wood harvest demand with the available biomass, the
680 unmet wood harvest from each country is reassigned to other European countries (including the former USSR),
proportional to available biomass, and the spatial pattern of this additional wood harvest is then allocated using the
same rules as outlined above. This is done to model the known trade in wood that was occurring between European
countries, even in the early years of our historical simulation (Kaplan et al., 2017).

2.12 Added Tree Cover

685 While it is primarily a land use dataset, LUH2 does also provide a simple estimate of forest cover change. For IAM
future scenarios with positive forest cover gain (SSP1-2.6, SSP2-4.5, SSP1-1.9), an algorithm was developed to
match the spatial pattern of forest gain from IAMs, preserve existing harmonized land-use transitions, and that could
be implemented relatively easily in ESMs. For each scenario, a supplementary file was created with a data variable
called ‘added_tree_cover’. The variable specifies the added tree cover that needs to be planted in each grid cell each
690 year to better represent the corresponding IAM Added Tree Cover estimates. For the other IAM scenarios that are
not affected by this issue, added_tree_cover values are set to zero. To produce these datasets, the spatial pattern of
differences in forest cover between LUH2 and each corresponding IAM were computed annually for 2015-2100. For
each year, each grid cell, if the difference could be met on LUH2 classified non-forest land, that difference was

695 noted as 'added_tree_cover' in the new file. If the gain could not be met on the non-forest area, the change was applied on nearby cells up to 4 grid cells away.

2.13 Extensions 2100-2300

700 In addition to the eight future scenarios for the period 2015-2100, the LUH2 dataset also includes extensions for the years 2100-2300 for three of the harmonized future land-use forcing datasets for use in long-term climate stabilization experiments. By design, in these extensions, all land-use states and management variables are held constant at year 2100 values for the years 2100-2300. As a result, almost all transitions between land-use states are set to zero, with the exception of crop rotations and shifting cultivation, which continue at their year 2100 rates, and wood harvest, which uses year 2099 national wood harvest demands for all years from 2100 to 2299. These
705 extensions to future scenarios are available for SSP1-2.6, SSP5-3.4OS, and SSP5-8.5.

3 Results

3.1 Aggregate Results

The annual, gridded land-use states are aggregated to annual global values by multiplying the grid-cell land-use fractions by the grid-cell area and summing over all grid-cells (Fig. 7). The 12 land-use states represented in the
710 LUH2 dataset can be further aggregated into the 5 broader land-use categories of total cropland (the sum of all 5 crop types), total grazing land (the sum of managed pasture and rangeland), primary land (the sum of primary forest and primary non-forest), secondary land (the sum of secondary forest and secondary non-forest), and urban land. Historically, the area of cropland increased at an accelerating rate from 1.7×10^6 km² in 850, to 4.3×10^6 km² in 1800, and 15.9×10^6 km² by 2015 (Fig. 7). Grazing lands increased more rapidly, from 3.3×10^6 km² in 850, to 9.2×10^6 km²
715 in 1800, and to 32.8×10^6 km² by 2015. Urban increased from 0 in 850 to 0.6×10^6 km² by 2015. See also HYDE 3.2 on the historic trends of cropland and pasture (Klein Goldewijk et al. 2017). During the historical period (850-2015 CE), primary land area decreased from 125×10^6 km² to 50.1×10^6 km² (of which 44% is forested), while secondary land increased from 0 to 30.4×10^6 km² (of which approximately 49% is forested); note that by definition LUH2 initializes secondary land area to zero in 850 CE. The new land-use history reconstruction derived here generally
720 compared favorably to prior reconstructions (Hurt et al, 2006; Hurt et al., 2011) and other references across a range of important diagnostics (Table 3), albeit at higher spatial resolution and with more process detail.

For the future, all eight scenarios projected increases in global cropland area, while six projected grazing land decreases (SSP4 RCP6.0 from GCAM, and SSP3 RCP7.0 from AIM projected grazing land increases). The global and regional trends of agriculture and land use in these eight projections are described in detail in Popp et al. (2017),
725 and underlying drivers of these land-use dynamics have been identified in Stehfest et al. (2019). For non-agricultural land, six out of eight scenarios projected large increases in wood harvesting, which contributed to large increases in

secondary area and corresponding reductions in primary area by 2100. In 2100 global cropland ranged from $17.8 \times 10^6 \text{ km}^2$ (SSP1 RCP2.6 from IMAGE) to $29.1 \times 10^6 \text{ km}^2$ (SSP4 RCP3.4 from GCAM). As shown in Table 4 and Figure 15 (panel a), for 6 out of 8 scenarios the dominant crop functional type in 2100 was C3 annuals, with C4 perennials (for biofuels) the dominant crop functional type in 2100 for the remaining two scenarios (SSP4 RCP3.4 from GCAM and SSP5 RCP3.4OS from REMIND-MAGPIE). Global grazing land in 2100 ranged from $25.4 \times 10^6 \text{ km}^2$ to $35.5 \times 10^6 \text{ km}^2$, with the majority of that coming from rangeland (Table 4). Secondary land in 2100 ranged from $36.5 \times 10^6 \text{ km}^2$ to $44.5 \times 10^6 \text{ km}^2$ (Table 4). In all cases, approximately half of all secondary land was forested, and the estimated mean age of secondary forest ranged from 58 yr to 74 yr. Added tree cover data layers, were computed to match the forest tree cover gains of the SSP1-2.6, SSP2-4.5, and SSP1-1.9 scenarios and were able to capture >80% of the global afforestation signal in the IAM scenarios. Extensions to year 2300 were computed for the SSP1-2.6, SSP5-3.4OS, and SSP5-8.5 scenarios, and by design did not change the gridded or global cropland, grazing land, or urban land areas. However, due to wood harvesting and shifting cultivation continuing at their end-of-century rates, the area of secondary vegetation continued to grow, and the area of primary vegetation continued to decline in these extensions. By 2300 the global secondary vegetation area in these extension scenarios ranged between $46.3 \times 10^6 \text{ km}^2$ and $51.2 \times 10^6 \text{ km}^2$, while the global primary vegetation area ranged between $28.6 \times 10^6 \text{ km}^2$ and $33.0 \times 10^6 \text{ km}^2$.

Gross transitions (the sum of the absolute value of all land-use transitions) are a measure of all land-use change activity. In general, the annual gross transitions tend to increase through time, beginning at $2 \times 10^5 \text{ km}^2$ in 850 and increasing to $1.86 \times 10^6 \text{ km}^2$ in 2000 (Table 3). The differences between the historical period low, baseline, and high scenarios in LUH2 (computed using 3 different HYDE land-use reconstructions and 3 different national wood harvest reconstructions) prior to 1920 are primarily due to the differences in rates of wood harvest between those three scenarios. After 1920 the three LUH2 historical scenarios share the same wood harvest reconstruction and their associated gross transitions are very similar. In the future scenarios, gross transitions mostly increased and by 2100 ranged from $2.0 \times 10^6 \text{ km}^2$ to $4.8 \times 10^6 \text{ km}^2$ (Table 5).

Net transitions measure only the net changes into land use (excluding wood harvest on secondary forests, shifting cultivation, and other agricultural land abandonment that is offset by land conversions to agriculture). Net transitions increase from $2 \times 10^4 \text{ km}^2$ in 850 to $2.3 \times 10^5 \text{ km}^2$ in 2000 (Table 3). The net transitions across all three historical LUH2 scenarios (low, baseline, and high) are all very similar at most time points. The LUH2 historical scenario shows a significant reduction in transitions to pasture around 1950-1960, with implications for carbon investigated separately (Ma et al., 2020). In the future, net transitions range from $-1.1 \times 10^5 \text{ km}^2$ to $1.6 \times 10^5 \text{ km}^2$ in 2100 (Table 5).

To visualize the magnitudes of transitions between variables, we present chord diagrams indicating the average net transitions occurring annually from 850-1849, 1850-2015, 850 – 2015, as well as 2015-2099 for all future scenarios amongst all the major land-use categories (Fig. 8). Each arc in a chord diagram represents the average annual area transitioning from one land-use to another. The color of the arc represents the land-use category from which transition occurs to a different category. For example, in Figure 8 the arc in light green color represents the transition

from cropland to other categories. Transitions involving croplands and secondary forest lands dominate land-use transitions in all three historical scenarios. The dominant land-use transition is secondary forest lands to croplands and it ranges from nearly $6 \times 10^4 \text{ km}^2 \text{ y}^{-1}$ in the low historical scenario to $8 \times 10^4 \text{ km}^2 \text{ y}^{-1}$ in the baseline scenario and $1 \times 10^5 \text{ km}^2 \text{ y}^{-1}$ in the high scenario when averaged from 850 – 2015. Cropland abandonment activities are also significant with nearly $1 \times 10^5 \text{ km}^2$, $1.4 \times 10^5 \text{ km}^2$ and $1.7 \times 10^5 \text{ km}^2$ of croplands transitioning annually to secondary lands (both forested and non-forested) in the low, baseline and high LUH2 historical scenarios respectively (averaged over the entire historical period). On an annual basis, the transitions to and from croplands and secondary lands are generally the same in all three LUH2 historical scenarios.

770 LUH2 historical results were compared to multiple diagnostics (Table 3). Almost all metrics are within, or very close to published reference ranges. These metrics show that 65% of the secondary land increase between 1700 and 2000 is forested, and 93% of U.S. forests in the year 2000 are on secondary land. Global natural vegetation in biodiversity hotspots in the year 2005 is estimated as 1.6% of the land surface (compared with the reference value of 2.3%). The mean age of secondary land can be calculated for each grid cell and aggregated to a global mean age.

775 For the first several hundred years of the simulation the global mean secondary age grew with time, due to primary land being used for land conversion and wood harvesting more often than secondary land (which was initialized to have zero area). Around 1700-1800, existing secondary land was used more often for new land conversions and wood harvesting and the global mean secondary age started to decrease with time. The median age of secondary forests in the year 2005 is 42 years, and is 43 years in the year 2015 (compared with the reference range of 30-40 years). The high scenario had the highest secondary mean age, because it had a larger secondary land area, which allows that secondary land to be used less frequently for wood harvesting and land conversions. Conversely, the low scenario had a lower secondary mean age than the baseline scenario. The overall land area impacted by human land use in the year 2000 is 59% of the land surface. The global area of secondary land increase between 1700 and 2000 is estimated as $13.2 \times 10^6 \text{ km}^2$ with $10.4 \times 10^6 \text{ km}^2$ of that area forested and $2.8 \times 10^6 \text{ km}^2$ non-forested.

785 Cumulative clearing for cropland and pasture between the years 1500 and 1990 resulted in 251 Pg C of wood removed (compared with a reference range of 121.9 to 356.3 Pg C). Total wood harvest over this period was 170 Pg C, of which 132 Pg C was from direct wood harvest and 38 Pg C was included from agricultural clearing. In the year 2000, an estimated $0.32 \times 10^6 \text{ km}^2$ of agricultural land was involved in shifting cultivation (compared with a reference value of $0.3 \times 10^6 \text{ km}^2$). Potential forest area $47 \times 10^6 \text{ km}^2$, compared to a reference value of $52 \times 10^6 \text{ km}^2$, and in the year 2015 global forest area was estimated at $37 \times 10^6 \text{ km}^2$, compared with a reference range of 32-41 $\times 10^6 \text{ km}^2$. In the year 2000 global wood harvest was 1.29 Pg C, of which 0.71 Pg C was for fuelwood. Global synthetic fertilizer usage in the year 2012 was 106.6 Tg N yr^{-1} (compared with a reference value of 100 Pg C), and the global area of irrigated cropland in 2003 was $2.51 \times 10^6 \text{ km}^2$ (compared with a reference value of $2.77 \times 10^6 \text{ km}^2$). In 2004, the area of cropland (primarily corn) used for biofuels was $0.03 \times 10^6 \text{ km}^2$ compared to the reference value of $0.033 \times 10^6 \text{ km}^2$. Total potential plant biomass on all lands was 718 Pg C (compared with a reference range between 557 and 923 Pg C), while total plant biomass in 2005 was 434 Pg C (compared with a reference value of 393 Pg C). Plant above-ground biomass on pantropical forested lands between years 2007-2008 was 184 Pg C

(compared with a reference range between 188 and 229 Pg C), and total plant biomass on forested lands in 2005 was 395 (compared with a reference value of 363 Pg C). In addition, the cumulative loss of above-ground biomass
800 resulting from land-use transitions (i.e., the sum of all losses) is an important metric of the gross effects of land use on the terrestrial carbon cycle and rose from 0 Pg C in 850 to 5.6×10^4 Pg C in 2015. Similarly, the cumulative net loss in above-ground biomass is the difference between the estimated above-ground biomass including land use, and the estimated biomass of potential vegetation, and includes both the losses of above-ground biomass due to land-use and the gains due to regrowth. During the historical period the global cumulative net loss of above ground biomass
805 carbon increases monotonically from nearly zero in 850AD to around 310 Pg C in 2015. The low, baseline, and high historical scenarios all give similar global estimates of this metric; the high scenario gives the highest estimates, which is presumably due to the high historical wood harvest in this scenario.

In the future scenarios secondary land increases between 6.0% and 13.27% across the years 2015 to 2100, with between 48.9% and 72.8% of that increase being on potentially forested land (Table 5). The median age of
810 secondary forest in the year 2100 ranges between 58 and 74 years. The global area covered by natural vegetation in the biodiversity hotspots ranges between 0.57% and 1.08% of the land surface. Wood clearing for cropland and pastures across the years 2015 to 2100 removes between 44 and 88 Pg C of above ground biomass, whereas direct wood harvest removes between 93 and 148 Pg C of above ground biomass. Global wood harvest in the year 2100 ranged between 0.9 and 1.87 Pg C, of which the fuelwood component was between 0.15 and 0.88 Pg C. Total forest
815 area change between 2015 and 2100 ranged from a decrease of 5.1×10^6 km² to an increase of 3.42×10^6 km², resulting in a global forest area in 2100 of between 32.1 and 38.1×10^6 km². Global fertilizer use in the year 2100 ranged between 110 Tg N yr⁻¹ and 240 Tg N yr⁻¹, while the global irrigated area in 2100 ranged between 2.6 and 4.1×10^6 km². Land flooded for rice in 2100 ranged from 0.23 to 0.96×10^6 km², and cropland used for growing biofuels in 2100 ranged from 0 to 18×10^6 km². Total biomass of natural vegetation on forested lands in 2100
820 ranged between 290 and 391 Pg C, of which between 170 and 239 Pg C is above ground biomass on pantropical forested lands. In 2100, the global cumulative net loss of above ground biomass carbon ranges widely across scenarios, from 320 Pg C to 385 Pg C.

3.2 Spatio-temporal Patterns of Land Use Transitions, Secondary Area, and Secondary Age

Regional results for the historical period, averaged for each century, are shown in Table 6. In each region or
825 continent, secondary land, gross transitions, and net transitions all tended to increase with time. Secondary land, along with both gross and net transitions, was highest in Eurasia and Africa. Mean regional secondary land area was 8.47×10^6 km² in Eurasia and 6.01×10^6 km² in Africa in the 1700s and increased to 12.4×10^6 km² and 6.82×10^6 km² in Eurasia and Africa respectively in the 1900s. Gross transitions peaked in Eurasia in the 1800s at 660×10^6 km² yr⁻¹, while net transitions peaked in Eurasia in the 1900s at 121×10^6 km² yr⁻¹. After 1700, secondary age tended to
830 decrease with time for most regions, although it has held relatively constant over the last three centuries for both Africa and Oceania. The range of secondary mean age in the 1900s was between 52 years to 289 years. In 1850 there are large areas of cropland in the Eastern USA, Europe, India, and China, and large areas of primary land

world-wide with the exception of Europe, Northern Africa and the Middle-East (Fig. 9). By 2015 cropland areas have expanded through-out Africa and the Americas as well, primary land is lost in large areas of the Eastern USA, Africa, Europe, India, and China, and mean secondary age is lower in most locations (Fig. 10).

Regional results are also averaged for the period 2000-2099 for each future scenario (Table 7). Across all scenarios, there were only small differences in regional secondary areas ($3.8-4.5 \times 10^6 \text{ km}^2$ for North America, $2.0-3.0 \times 10^6 \text{ km}^2$ for South America, $17-18 \times 10^6 \text{ km}^2$ for Eurasia, $9.2-11 \times 10^6 \text{ km}^2$ for Africa, and $0.7-0.87 \times 10^6 \text{ km}^2$ for Oceania) with SSP1-1.9 having the highest secondary area in each continent. Secondary land area was highest in Eurasia and Africa for all scenarios. Regional secondary age also did not vary significantly across scenarios; the SSP5-8.5 scenario had the highest secondary age for all regions except Oceania (67 years for North America, 49 years for South America, 209 years for Eurasia, 70 years for Africa, and 50 years for Oceania) and the SSP4-3.4 scenario had the lowest secondary age for most regions (60 years for North America, 45 years for South America, 197 years for Eurasia, 69 years for Africa, and 48 years for Oceania). Secondary age was highest in Eurasia for all scenarios. Gross transitions were highest in Eurasia in 7 out of 8 scenarios (with Africa the second highest), and highest in Africa in one scenario (with Eurasia the second highest). The highest overall rate of gross transitions was $1936 \times 10^6 \text{ km}^2 \text{ yr}^{-1}$ in Eurasia in the SSP5-3.4OS scenario, but comparable rates of gross transitions were also observed in Eurasia and/or Africa in the SSP4-3.4, SSP4-6.0, SSP3-7.0, and SSP5-8.5 scenarios. Net transitions were largest in Africa in all scenarios (between $34-143 \times 10^6 \text{ km}^2 \text{ yr}^{-1}$) and lowest in Oceania in 7 out of 8 scenarios (and negative in 6 of those), with South America having the lowest net transitions in the remaining scenario. The SSP4-3.4, SSP4-6.0, and SSP3-7.0 scenarios had the highest rates of net transitions overall at $143 \times 10^6 \text{ km}^2 \text{ yr}^{-1}$, $133 \times 10^6 \text{ km}^2 \text{ yr}^{-1}$, and $133 \times 10^6 \text{ km}^2 \text{ yr}^{-1}$ respectively.

Large-scale spatial patterns are similar across most scenarios in the year 2100 (Figs 11-14), with the trends of increased cropland area in South America, continued loss of primary land worldwide and particularly in Africa, and continued reduction of mean secondary age. Analogous mapped results for Tier 2 scenarios are provided in the Appendix.

3.3 Land-use Management

During the historical period, the use of synthetic nitrogen-based fertilizer on croplands was zero until the early 20th century. After 1950 fertilizer usage started increasing rapidly, and by 2015 global synthetic nitrogen fertilizer usage was 112 Tg N yr^{-1} (4150 Tg N cumulatively from 1915 to 2015; none prior to 1915), with the majority of this being applied in cropland-dominated locations including the North America, Europe, India, China, and South-East Asia. The eight harmonized future scenarios show a range of potential nitrogen futures; all except one scenario (the SSP5-8.5, which does increase but then falls again to close to current year values) project an increase in global nitrogen fertilizer usage. The range of harmonized global nitrogen fertilizer values in 2100 is between 110 Tg N yr^{-1} and 240 Tg N yr^{-1} , with a total cumulative use of synthetic nitrogen fertilizer from 2015 to 2100 between 9840 Tg N and 14800 Tg N (Figure 15, panel b).

The global area of irrigated cropland increased steadily throughout the historical period and was around 2.7 million km² in 2015. The spatial patterns of this irrigated area show that the majority of global irrigation occurs in India and China, with other significant areas in the USA, Europe, Middle East, and South-East Asia. Six out of eight future scenarios project the global irrigated area to remain steady, or even decrease slightly, whereas two future scenarios (SSP3-7.0 from AIM and SSP5-8.5) show large increases in global irrigated area. The range of values across all future scenarios in 2100 is between 2.6 and 4.1 million km² (Figure 15, panel c).

The global use of croplands area for purpose-grown biofuels was very low prior to the year 2000 when a small amount of first generation biofuels production began (such as corn or sugarcane). In the future scenarios the fraction of cropland area grown for first generation biofuels was held constant, although underlying changes in cropland area resulted in some small increases or decreases in the total area of first generation biofuels. Second generation biofuel area (such as miscanthus or switchgrass) expanded in each of the future scenarios, assumed to start from zero in 2015. Five of the eight scenarios (SSP1-1.9, SSP1-2.6, SSP4-3.4, SSP5-3.4OS, and SSP4-6.0) all showed significant increases in the area of second generation biofuels, while the remaining three scenarios have very little growth in this land management type. By the year 2100, global areas of biofuel crops ranged between 0 and 18 million km², and maps of the spatial distribution of total biofuels area (both first and second generation biofuels) show the dominant locations to be the USA, Europe, China, non-Amazonian Brazil, and Argentina. Large expansion of secondary biofuels primarily occurred in South-East Asia, Eastern Europe and the former USSR, and the Middle East (Figure 15, panel d).

885 4 DISCUSSION

Land use is essential for meeting human needs for food, fuel, fiber, and shelter, but also affects the biogeochemistry, biogeophysics, biodiversity, and climate of the Earth. Quantitatively understanding the effects of land-use activities on the Earth system requires that the best information on land use be incorporated into the best Earth system models. The strategy described here (LUH2) builds on the approach for harmonizing land-use patterns and transitions in CMIP5 (LUH1, Hurtt et al., 2011). This new version is completely updated with new inputs, and includes higher spatial resolution (0.25° vs 0.5°), increased detail (12 states vs. 5, and all associated transitions), added management layers, new future scenarios (8 vs. 4), and a longer time domain (850-2100 vs 1500-2100) - in all more than a 50-fold increase in data from its predecessor. As such, it is designed to facilitate more complete and more consistent treatments of how land-use changes influence the Earth system past-present-future.

895 In comparison to LUH1 (Hurtt et al., 2011), the LUH2 land-use history is spatially, temporally and thematically richer than the previous reconstruction. While not strictly comparable for these reasons, comparing the two products to each other and across a wide range of diagnostics reveals some important quantitative similarities and differences. Historically, the globally aggregated magnitudes of key land-use states (i.e., cropland, grazing area) and key land cover variables (forest area and biomass) are generally quite similar (<10% difference) over periods of overlap. 900 Larger differences between these datasets are found in transitions, resulting secondary lands, and spatial patterns of land-use activities, where contemporary global gross transitions are reduced by ~35%, contemporary net transitions

increased by ~35%, and estimated primary forest in biodiversity hotspots much closer to independent estimates relative to LUH1 (Jantz et al., 2015). Considering the past, LUH2 begins in 850AD, 650 years earlier than LUH1. Considering the future, the set of 8 future scenarios included in LUH2 doubles that of LUH1, expanding the range of
905 land-use forcing that can be considered and including additional cases. Like LUH1, LUH2 also includes extensions to 2100-2300 with no net change in forcing over the interval. LUH2 also includes new Added-tree-cover data, to better reflect the changes in tree cover projected by IAMs in afforestation scenarios.

Since management was a new input in LUH2, we do not have comparable values from LUH1. However, the estimates from LUH2 for key management variables are close to empirical estimates and reflect major alterations of
910 nutrient and water cycles, with implications for climate. For example, the ~100 Tg N y⁻¹ of industrial fertilizer use and irrigated area ~2.5 million km² by 2000 indicate major human impacts on the functioning of agro-ecosystems in addition to a general land-cover change metric. The inclusion of these activities here as part of the global harmonized dataset is intended to facilitate their inclusion in future global climate assessments, harmonized, and together with other concurring land-use changes.

915 These LUH2 datasets are part of the official CMIP6 input4MIPs data collection, and are required forcing datasets for the DECK and historical climate simulations (Meehl et al., 2014; Eyring et al., 2016). The data are also required for several of the CMIP6-MIP experiments including ScenarioMIP (O'Neill et al., 2016), LUMIP (Lawrence et al., 2016), PMIP (Junclaus et al., 2017) and others. ScenarioMIP defined the set of future scenarios for consideration and organized the official climate-model experiment to quantify the effects of future scenarios of anthropogenic
920 forcing on climate. LUMIP organized the set of model experiments focused on quantifying the effect of land-use forcing per se on climate. PMIP is organized to study the historical climate. The central use of these data in the DECK and across a range of important MIPs enhances consistency across CMIP6.

These datasets have also been adopted as required forcing for a range of other international studies including: ISIMIP (Frieler et al. 2017), Global Carbon Project (Le Quéré et al., 2016; Le Quéré et al., 2017; Le Quéré et al.,
925 2018; Friedlingstein et al., 2019), and IPBES (Kim et al. 2018). The LUH2 datasets are regularly employed by the TRENDY modeling group in the annual carbon budget estimates of the Global Carbon Project using a simple linear interpolation to update to year of current budget (Le Quéré et al., 2016; Le Quéré et al., 2017; Le Quéré et al., 2018; Friedlingstein et al., 2019). The Global Carbon Project also provides a comparison of land use and land use change emissions with quasi-independent data from two 'bookkeeping' models, of which one uses FAO statistics directly
930 and the other uses the LUH2 data. The bookkeeping and process-based model estimates of emissions tend to show high agreement, although in the last 3 years have begun to diverge (Friedlingstein et al., 2019). This standardization of land-use forcing across the breadth of CMIP6 studies, and other international assessments has the promise to facilitate maximum consistency in the treatment of land use across the range of interdisciplinary foci and spatial/temporal domains of studies.

935 Application of the LUH2 data in ESMs, LSMs, DGVMs and Biodiversity models depends on the model type for various aspects. For models with their own vegetation cover, different from LUH2, the conversion of forest/non-

forest vegetation to agricultural conversion needs to be handled. For conversion into grazing land, managed pasture should always trigger the removal of natural vegetation, while rangeland should only trigger removal of natural vegetation in forested areas (Ma et al. 2020). A general discussion of transition and conversion challenges in the various models has been described in (Prestele et al. 2017).

LUH2 preserves the land-use patterns of HYDE 3.2. For the gridded land use, HYDE 3.2 took into account the ESA-CCI land cover products (Klein Goldewijk et al. 2017). However, on a national scale, HYDE 3.2 is consistent with FAO and other statistical databases, and differences to satellite-based land cover products cannot be avoided, and can be large (Li et al. 2019).

The LUH2 dataset was developed to provide globally consistent and coherent gridded land use for more than a millennium, spanning the past and future, as a necessary input for earth system model simulations for CMIP6. The requirement of global consistency through time means that it did not always incorporate all of the best local, regional, or national historical data available. For this reason, it may not necessarily be the optimal dataset for a local or regional analysis of land use impacts on biogeochemistry or biodiversity.

Looking ahead, ongoing CMIP6 and several other international activities will be engaged in using LUH2 data as input to studies of global climate, carbon, biodiversity and other assessments. These data products are intended to meet current needs of models, and also provide new variables that most models do not yet include but that may be important. Examples of these features include transitions, introduced in LUH1 and now a growing feature of many models, and now management variables. Model development will need to continue to advance to utilize these features. Meanwhile, advances need to proceed for the next generation of land-use harmonization, which should build on these advances and include additional data constraints, more process detail, and a focus on reducing uncertainty of the most sensitive features. This should be part of larger effort to develop a robust process to provide the best forcing data sets for future global assessments.

Code Availability

The source code used to produce the LUH2 datasets, along with the sources and citations of necessary inputs, are archived at <http://doi.org/10.5281/zenodo.3954113>.

Data Availability

The data produced in this study are archived and publicly available at the U.S. Department of Energy input4MIPS site. The data are available in multiple files and fine-grain DOIs, and can be accessed and referenced using the following coarse grain citations, one historical (Hurtt et al., 2019a) and one future (Hurtt et al., 2019b). For dataset updates and supporting information, please visit the LUH2 website at <https://luh.umd.edu>.

Author Contributions

970 GH is the lead author and co-developed the method and conducted analyses with LC, RS, and SF. KKG, AH, JJ, JK,
OM, JP, XZ provided historical input. BB, KC, JD, SF, TH, PH, FH, TK, AP, KR, ES, DV provided future scenario
input. JF, JK, DL, PL, LM, BP, ES, PT provided modeling input. FT provided input on FAO data. All authors
contributed to writing the manuscript.

Competing Interests

The authors declare that they have no conflict of interest.

975

980

Acknowledgements

985 We gratefully acknowledge the support of the U.S. Department of Energy grant DESC0012972. This research was
supported as part of the Energy Exascale Earth System Model (E3SM) project, funded by the U.S. Department of
Energy, Office of Science, Office of Biological and Environmental Research. Additionally, this research was
supported by NASA grants NNX13AK84A (NASA-TE), 80NSSC17K0348 (NASA-IDS), and 80NSSC17K0710
(NASA-CMS).

BLB has received funding from the European Union's Horizon 2020 research and innovation programme under
grant agreement No 776479 (COACCH) and 821010 (CASCADES).

990 KC was supported by the US Department of Energy, Office of Science, Office of Biological and Environmental
Research.

KKG was supported by Dutch NWO VENI grant no. 016.158.021. Part of the material in the methods section is
from Hurtt et al. 2011.

995 TH and SF were supported by the Environment Research and Technology Development Fund (JPMEERF20202002)
of the Environmental Restoration and Conservation Agency of Japan and JSPS KAKENHI (JP20K20031,
19K24387) of the Japan Society for the Promotion of Science and the Sumitomo Foundation.

FH has received funding from the European Union's Horizon 2020 research and innovation programme under grant
agreement No 821124 (NAVIGATE) and 821471 (ENGAGE).

JOK was supported by the European Research Council (COEVOLVE 313797).

1000 DML is supported by the National Center for Atmospheric Research, which is a major facility sponsored by the NSF under Cooperative Agreement No. 1852977.

JP was supported by the German Research Foundation's Emmy Noether Program (PO 1751/1-1).

1005 FNT acknowledges funding from FAO's regular programme and the contribution of experts in specialized agencies in member countries. The Environment Team of FAO Statistics Division regularly supports the development and maintenance of the FAOSTAT Land Use database, with special thanks to Giorgia De Santis and Nathan Wanner. The views expressed in this publication are those of the author(s) and do not necessarily reflect the views or policies of FAO.

XZ was supported by National Science Foundation CNS-1739823.

1010

References

- 1015 Arneeth, A., S. Sitch, J. Pongratz, B. D. Stocker, P. Ciais, B. Poulter, A. D. Bayer, A. Bondeau, L. Calle, L. P. Chini, T. Gasser, M. Fader, P. Friedlingstein, E. Kato, W. Li, M. Lindeskog, J. E. M. S. Nabel, T. A. M. Pugh, E. Robertson, N. Viovy, C. Yue & S. Zaehle. Historical carbon dioxide emissions caused by land-use changes are possibly larger than assumed. *Nature Geoscience*, 2017.
- Bodirsky, B. L., Popp, A., Weindl, I., Dietrich J. P., Rolinski, S., Scheffele, L., Schmitz, C., and Lotze-Campen, H. 'N₂O Emissions from the Global Agricultural Nitrogen Cycle – Current State and Future Scenarios'. *Biogeosciences* 9 (10): 4169–97. <https://doi.org/10.5194/bg-9-4169-2012>, 2012.
- 1020 Bondeau, A., Smith, P. C., Zaehle, S., Schaphoff, S., Lucht, W., Cramer, W., Gerten, D., Lotze-Campen, H., Müller, C., Reichstein, M., and Smith, B. Modelling the role of agriculture for the 20th century global terrestrial carbon balance. *Global Change Biology*, 13, 679-706, 2007.
- 1025 Brovkin, V., Boysen, L., Arora, V. K., Boisier, J. P., Cadule, P., Chini, L., Claussen, M., Friedlingstein, P., Gayler, V., van den Hurk, B. J. J. M., Hurtt, G. C., Jones, C. D., Kato, E., de Noblet-Ducoudré, N., Pacifico, F., Pongratz, J., and Weiss, M. Effect of anthropogenic land-use and land cover changes on climate and land carbon storage in CMIP5 projections for the 21st century. *Journal of Climate*, 130325101629005. <http://doi.org/10.1175/JCLI-D-12-00623.1>, 2013.
- Bullock, D. G. Crop rotation. *Critical reviews in plant sciences*, 11(4), 309-326. 1992.
- 1030 Butler, J. H. *Economic Geography: Spatial and Environmental Aspects of Economic Activity*. New York: John Wiley, 1980.
- Calvin, K., Bond-Lamberty, B., Clarke, L., Edmonds, J., Eom, J., Hartin, C., Kim, S., Kyle, P., Link, R., Moss, R., McJeon, H., Patel, P., Smith, S., Waldhoff, S., and Wise, M. "The SSP4: A world of deepening inequality." *Global Environmental Change* 42: 284-296, 2017.
- 1035 Collins, W. D., Craig, A. P., Truesdale, J. E., Di Vittorio, A. V., Jones, A. D., Bond-Lamberty, B., Calvin, K. V., Edmonds, J. A., Kim, S. H., Thomson, A. M., Patel, P., Zhou, Y., Mao, J., Shi, X., Thornton, P. E., Chini, L. P., and Hurtt, G. C. The integrated Earth system model version 1: formulation and functionality, *Geosci. Model Dev.*, 8, 2203-2219, doi:10.5194/gmd-8-2203-2015, 2015.
- 1040 Cramer, W., Kicklighter, D.W., Bondeau, A., Iii, B.M., Churkina, G., Nemry, B., Ruimy, A., Schloss, A.L., Intercomparison, T. and Model, P.O.T.P.N. Comparing global models of terrestrial net primary productivity (NPP): overview and key results. *Global change biology*, 5(S1), pp.1-15, 1999.
- 1045 Di Vittorio, A. V., Chini, L. P., Bond-Lamberty, B., Mao, J., Shi, X., Truesdale, J., Craig, A., Calvin, K., Jones, A., Collins, W. D., Edmonds, J., Hurtt, G. C., Thornton, P., and Thomson, A. From land use to land cover: Restoring the afforestation signal in a coupled integrated assessment - earth system model and the implications for CMIP5 RCP simulations, *Biogeosciences*, 2014.
- Di Vittorio, A. V., Mao, J., Shi, X., Chini, L., Hurtt, G., & Collins, W. D. Quantifying the Effects of Historical Land Cover Conversion Uncertainty on Global Carbon and Climate Estimates. *Geophysical Research Letters*, 16(12), 3327–9. <http://doi.org/10.1002/2017GL075124>, 2018.
- 1050 Doelman, J. C., Stehfest, E., Tabeau, A., van Meijl, H., Lassaletta, L., Gernaat, D. E. H. J., Hermans, K., Harmsen, M., Diaoglou, V., Biemans, H., van der Sluis, S., and van Vuuren, D. P. Exploring SSP land-use dynamics using the IMAGE model: Regional and gridded scenarios of land-use change and land-based climate change mitigation. *Global Environmental Change*, 48, 119-135, 2018.

- 1055 Eyring, V., Bony, S., Meehl, G. A., Senior, C. A., Stevens, B., Stouffer, R. J., & Taylor, K. E. Overview of the Coupled Model Intercomparison Project Phase 6 (CMIP6) experimental design and organization. *Geoscientific Model Development*, 9(5), 1937–1958. <http://doi.org/10.5194/gmd-9-1937-2016>, 2016.
- FAO. FAOSTAT Database. Food and Agriculture Organization of the United Nations, Rome, Italy. Retrieved on July 28, 2016 from <http://www.fao.org/faostat/en/#data/FO>, 2016.
- FAO. Global Forest Resources Assessment 2000 – Main Report, FAO Forestry Paper 140, Food and Agriculture Organization of the United Nations, Rome, Italy, 2000.
- 1060 Fricko, O., Havlik, P., Rogelj, J., Klimont, Z., Gusti, M., Johnson, N., Kolp, P., Strubegger, M., Valin, H., Amann, M., Ermolieva, T., Forsell, N., Herrero, M., Heyes, C., Kindermann, G., Krey, V., McCollum, D. L., Obersteiner, M., Pachauri, S., Rao, S., Schmid, E., Schoepp, W., and Riahi, K. The marker quantification of the Shared Socioeconomic Pathway 2: A middle-of-the-road scenario for the 21st century. *Global Environmental Change*, 2017.
- 1065 Friedlingstein, P., Jones, M. W., O'Sullivan, M., Andrew, R. M., Hauck, J., Peters, G. P., Peters, W., Pongratz, J., Sitch, S., Le Quéré, C., Bakker, D. C. E., Canadell, J. G., Ciais, P., Jackson, R. B., Anthoni, P., Barbero, L., Bastos, A., Bastrikov, V., Becker, M., Bopp, L., Buitenhuis, E., Chandra, N., Chevallier, F., Chini, L. P., Currie, K. I., Feely, R. A., Gehlen, M., Gilfillan, D., Gkritzalis, T., Goll, D. S., Gruber, N., Gutekunst, S., Harris, I., Haverd, V., Houghton, R. A., Hurtt, G., Ilyina, T., Jain, A. K., Joetzier, E., Kaplan, J. O., Kato, E., Klein Goldewijk, K., Korbakken, J. I., Landschützer, P., Lauvset, S. K., Lefèvre, N., Lenton, A., Lienert, S., Lombardozi, D., Marland, G., McGuire, P. C., Melton, J. R., Metzl, N., Munro, D. R., Nabel, J. E. M. S., Nakaoka, S.-I., Neill, C., Omar, A. M., Ono, T., Peregón, A., Pierrot, D., Poulter, B., Rehder, G., Resplandy, L., Robertson, E., Rödenbeck, C., Séférian, R., Schwinger, J., Smith, N., Tans, P. P., Tian, H., Tilbrook, B., Tubiello, F. N., van der Werf, G. R., Wiltshire, A. J., and Zaehle, S. Global Carbon Budget 2019. *Earth Syst. Sci. Data*, 11, 1783–1838,
- 1070 <https://doi.org/10.5194/essd-11-1783-2019>, 2019.
- 1075 Fujimori, S., Masui, T., Matsuoka, Y. AIM/CGE [basic] manual. Discussion paper series. Center for Social and Environmental Systems Research, NIES, Tsukuba, Japan, 2012.
- Fujimori, S., Hasegawa, T., Masui, T., Takahashi, K. Land use representation in a global CGE model for long-term simulation: CET vs. logit functions. *Food Sec.* 6:685-699, 2014.
- 1080 Fujimori, S., Hasegawa, T., Masui, T., Takahashi, K., Herran, D. S., Dai, H., Hijioka, Y., and Kainuma, M. SSP3: AIM implementation of Shared Socioeconomic Pathways. *Global Environmental Change*. 2017.
- Gusti, M. An algorithm for simulation of forest management decisions in the global forest model *Artif. Intel.* N4 45–9, 2010.
- 1085 Hansen, M. C., Potapov, P. V., Moore, R., Hancher, M., Turubanova, S. A., Tyukavina, A., Thau, D., Stehman, S. V., Goetz, S. J., Loveland, T. R., Kommareddy, A., Egorov, A., Chini, L., Justice, C. O., Townshend, J. R. G. High-Resolution Global Maps of 21st-Century Forest Cover Change. *Science*. 342: 850–853. [doi.org/10.1126/science, 2013](http://doi.org/10.1126/science.2013).
- Hasegawa, T., Fujimori, S., Ito, A., Takahashi, K., and Masui, T. Global land-use allocation model linked to an integrated assessment model. *Science of The Total Environment* 580:787-796, 2017.
- 1090 Havlik, P., Schneider, U.A., Schmid, E., Böttcher, H., Fritz, S., Skalsky, R., Obersteiner, M. Global land use implications of first and second generation biofuel targets. *Energy Policy* 39 (10), 5690–5702, 2011.
- Heinimann, A., Mertz, O., Frolking, S., Egelund Christensen, A., Hurni, K., Sedano, F., Chini, L. P., Sahajpal, R., Hansen, M., Hurtt, G.. A global view of shifting cultivation: Recent, current, and future extent. *PLoS ONE*, 12(9), e0184479–21. <http://doi.org/10.1371/journal.pone.0184479>, 2017.

- 1095 Houghton, R. A. and Hackler, J. L. Changes in terrestrial carbon storage in the United States. 1. The roles of agriculture and forestry. *Global Ecol Biogeogr* 9:125–144, 2000.
- Hurtt, G. C., Moorcroft, P. R., Pacala, S. W., Levin, S. . Terrestrial models and global change: challenges for the future. *Global Change Biology* 4(5): 581-59, 1998.
- 1100 Hurtt, G. C., Pacala, S. W., Moorcroft, P. R., Caspersen, J., Shevliakova, E., Houghton, R. A. and Moore, B. I. I. I., Projecting the future of the US carbon sink. *Proceedings of the National Academy of Sciences*, 99(3), pp.1389-1394, 2002.
- Hurtt, G. C., Froliking, S., Fearon, M. G., Moore, B., Shevliakova, E., Malyshev, S., et al. The underpinnings of land-use history: three centuries of global gridded land-use transitions, wood-harvest, and resulting secondary lands. *Global Change Biology*, 12(1208-1229), 22, 2006.
- 1105 Hurtt, G. C., Chini, L. P., Froliking, S., Betts, R. A., Feddema, J., Fischer, G., et al. Harmonization of land-use scenarios for the period 1500–2100: 600 years of global gridded annual land-use transitions, wood harvest, and resulting secondary lands. *Climatic Change*. <http://doi.org/10.1007/s10584-011-0153-2>, 2011.
- Hurtt, G., Chini, L., Sahajpal, R., Froliking, S., Bodirsky, B. L., Calvin, K., Doelman, J., Fisk, J., Fujimori, S., Goldewijk, K., K., Hasegawa, T., Havlik, P., Heinemann, A., Humpenöder, F., Jungclaus, J., Kaplan, J., Krisztin, T., Lawrence, D., Lawrence, P., Mertz, O., Pongratz, J., Popp, A., Riahi, K., Shevliakova, E., Stehfest, E., Thornton, P., van Vuuren, D., and Zhang, X. Harmonization of Global Land Use Change and Management for the Period 850-2015. Version YYYYMMDD. Earth System Grid Federation. <https://doi.org/10.22033/ESGF/input4MIPs.10454>, 2019a.
- 1110
- 1115 Hurtt, G., Chini, L., Sahajpal, R., Froliking, S., Bodirsky, B. L., Calvin, K., Doelman, J., Fisk, J., Fujimori, S., Goldewijk, K., K., Hasegawa, T., Havlik, P., Heinemann, A., Humpenöder, F., Jungclaus, J., Kaplan, J., Krisztin, T., Lawrence, D., Lawrence, P., Mertz, O., Pongratz, J., Popp, A., Riahi, K., Shevliakova, E., Stehfest, E., Thornton, P., van Vuuren, D., and Zhang, X. Harmonization of Global Land Use Change and Management for the Period 2015-2300. Version YYYYMMDD. Earth System Grid Federation. <https://doi.org/10.22033/ESGF/input4MIPs.10468>, 2019b.
- 1120
- IFA. (International Fertilizer Association). IFA Database; <http://www.fertilizer.org/Statistics> (visited 21 Jan 2015), 2015.
- Jantz, S. M., Barker, B., Brooks, T. M., Chini, L. P., Huang, Q., Moore, R. M., et al. Future habitat loss and extinctions driven by land-use change in biodiversity hotspots under four scenarios of climate-change mitigation. *Conservation Biology*, n/a–n/a. <http://doi.org/10.1111/cobi.12549>, 2015.
- 1125
- Jones, A., Collins, W., Edmonds, J., Torn, M., Janetos, A., Calvin, K., Thomson, A., Chini, L. P., Mao, J., Shi, X., Thornton, P., Hurtt, G., and Wise, M. Greenhouse gas policy influences climate via direct effects of land-use change, *Journal of Climate*, 2013.
- Jones, C. D., Hughes, J. K., Bellouin, N., Hardiman, S. C., Jones, G. S., Knight, J., Liddicoat, S., O'Connor, F. M., Andres, R. J., Bell, C., Boo, K. -O., Bozzo, A., Butchart, N., Cadule, P., Corbin, K. D., Doutriaux-Boucher, M., Friedlingstein, P., Gornall, J., Gray, L., Halloran, P. R., Hurtt, G., Ingram, W. J., Lamarque, J. -F., Law, R. M., Meinshausen, M., Osprey, S., Palin, E. J., Chini, L. P., Raddatz, T., Sanderson, M. G., Sellar, A. A., Schurer, A., Valdes, P., Wood, N., Woodward, S., Yoshioka, M., Zerroukat, M. The HadGEM2-ES Implementation of CMIP5 Centennial Simulations, *Geoscientific Model Development*, 2011.
- 1130
- 1135 Jungclaus, J. H., Bard, E., Baroni, M., Braconnot, P., Cao, J., Chini, L. P., et al. The PMIP4 contribution to CMIP6 – Part 3: The last millennium, scientific objective, and experimental design for the PMIP4 <i>past1000</i> simulations. *Geoscientific Model Development*, 10(11), 4005–4033. <http://doi.org/10.5194/gmd-10-4005-2017>, 2017.

- 1140 Kaplan, J.O.; Krumhardt, K.M.; Gaillard, M.-J.; Sugita, S.; Trondman, A.-K.; Fyfe, R.; Marquer, L.; Mazier, F.; Nielsen, A.B. Constraining the Deforestation History of Europe: Evaluation of Historical Land Use Scenarios with Pollen-Based Land Cover Reconstructions. *Land*, 6, 91, 2017.
- 1145 Kim, H., Rosa, I., Alkemade, R., Leadley, P., Hurtt, G., Popp, A., Vuuren, D., Anthoni, P., Arneth, A., Baisero, D., Caton, E., Chaplin-Kramer, R., Chini, L., Palma, A., Fulvio, F., Marco, M., Espinoza, F., Ferrier, S., Fujimori, S., Gonzalez, R., Gueguen, M., Guerra, C., Harfoot, M., Harwood, T., Hasegawa, T., Haverd, V., Havlik, P., Hellweg, S., Hill, S., Hirata, A., Hoskins, A., Janse, J., Jetz, W., Johnson, J., Krause, A., Leclere, D., Martins, I., Matsui, T., Merow, C., Obersteiner, M., Ohashi, H., Poulter, B., Purvis, A., Quesada, B., Rondinini, C., Schipper, A., Sharp, R., Takahashi, K., Thuiller, W., Titeux, N., Visconti, P., Ware, C., Wolf, F., Pereira, H. A protocol for an intercomparison of biodiversity and ecosystem services models using harmonized land-use and climate scenarios *Geoscientific Model Development* 11(11), 4537 - 4562. <https://dx.doi.org/10.5194/gmd-11-4537-2018>, 2018.
- 1150 Kindermann, G. E., Obersteiner, M., Rametsteiner, E., and McCallum, I. Predicting the deforestation- trend under different carbon-prices *Carbon Balance Manag.* 1 1–17, 2006.
- Kindermann, G., Obersteiner, M., Sohngen, B., Sathaye, J., Andrasko, K., Rametsteiner, E., Beach, R., Global cost estimates of reducing carbon emissions through avoided deforestation. *Proc. Natl. Acad. Sci. U.S.A.* 105 (30), 10302–10307, 2008.
- 1155 Klein Goldewijk, K. Estimating global land use change over the past 300 years: The HYDE database. *Global Biogeochemical Cycles* 15(2):417–433, 2001.
- Klein Goldewijk, K., Beusen, A., Doelman, J., and Stehfest, E. Anthropogenic land-use estimates for the Holocene - HYDE 3.2, *Earth Syst. Sci. Data*, 9, 927 - 953, 2017.
- 1160 Kriegler, E., Bauer, N., Popp, A., Humpenöder, F., Leimbach, M., Strefler, J., Baumstark, L., Bodirsky, B. L., Hilaire, J., Klein, D., Mouratiadou, I., Weindl, I., Bertram, C., Dietrich, J.-P., Luderer, G., Pehl, M., Pietzcker, R., Piontek, F., Lotze-Campen, H., Biewald, A., Bonsch, M., Giannousakis, A., Kreidenweis, U., Müller, C., Rolinski, S., Schultes, A., Schwanitz, J., Stevanovic, M., Calvin, K., Emmerling, J., Fujimori, S., and Edenhofer, O. Fossil-fueled development (SSP5): An energy and resource intensive scenario for the 21st century *Glob. Environ. Change* 42 297–315, 2017.
- 1165 Kucharik, C.J., Foley, J.A., Delire, C., Fisher, V.A., Coe, M.T., Lenters, J.D., Young-Molling, C., Ramankutty, N., Norman, J.M. and Gower, S.T. Testing the performance of a dynamic global ecosystem model: water balance, carbon balance, and vegetation structure. *Global Biogeochemical Cycles*, 14(3), pp.795-825, 2000.
- 1170 Lawrence, D. M., Hurtt, G. C., Arneth, A., Brovkin, V., Calvin, K. V., Jones, A. D., et al. The Land Use Model Intercomparison Project (LUMIP) contribution to CMIP6: rationale and experimental design. *Geoscientific Model Development*, 9(9), 2973–2998. <http://doi.org/10.5194/gmd-9-2973-2016>, 2016.
- Le Page, Y., West, T. O., Link, R., and Patel, P. "Downscaling land use and land cover from the Global Change Assessment Model for coupling with Earth system models." *Geosci. Model Dev.* 9(9): 3055-3069, 2016.
- 1175 Le Quéré, C., Andrew, R. M., Friedlingstein, P., Sitch, S., Hauck, J., Pongratz, J., Pickers, P. A., Korsbakken, J. I., Peters, G. P., Canadell, J. G., Arneth, A., Arora, V. K., Barbero, L., Bastos, A., Bopp, L., Chevallier, F., Chini, L. P., Ciais, P., Doney, S. C., Gkritzalis, T., Goll, D. S., Harris, I., Haverd, V., Hoffman, F. M., Hoppema, M., Houghton, R. A., Hurtt, G., Ilyina, T., Jain, A. K., Johannessen, T., Jones, C. D., Kato, E., Keeling, R. F., Goldewijk, K. K., Landschützer, P., Lefèvre, N., Lienert, S., Liu, Z., Lombardozi, D., Metzl, N., Munro, D. R., Nabel, J. E. M. S., Nakaoka, S., Neill, C., Olsen, A., Ono, T., Patra, P., Peregón, A., Peters, W., Peylin, P., Pfeil, B., Pierrot, D., Poulter, B., Rehder, G., Resplandy, L., Robertson, E., Rocher, M., Rödenbeck, C., Schuster, U., Schwinger, J., Séférian, R., Skjelvan, I., Steinhoff, T., Sutton, A., Tans, P. P., Tian, H., Tilbrook, B., Tubiello, F. N., van der Laan-Luijkx, I. T., van der Werf, G. R., Viovy, N., Walker, A. P., Wiltshire, A. J., Wright, R., Zaehle, S., and Zheng, B.: *Global Carbon Budget 2018*, *Earth Syst. Sci. Data*, 10, 2141–2194, <https://doi.org/10.5194/essd-10-2141-2018>, 2018.

- 1185 Le Quéré, C., Andrew, R. M., Friedlingstein, P., Sitch, S., Pongratz, J., Manning, A. C., Korsbakken, J. I., Peters, G. P., Canadell, J. G., Jackson, R. B., Boden, T. A., Tans, P. P., Andrews, O. D., Arora, V. K., Bakker, D. C. E., Barbero, L., Becker, M., Betts, R. A., Bopp, L., Chevallier, F., Chini, L. P., Ciais, P., Cosca, C. E., Cross, J., Currie, K., Gasser, T., Harris, I., Hauck, J., Haverd, V., Houghton, R. A., Hunt, C. W., Hurtt, G., Ilyina, T., Jain, A. K., Kato, E., Kautz, M., Keeling, R. F., Klein Goldewijk, K., Körtzinger, A., Landschützer, P., Lefèvre, N., Lenton, A., Lienert, S., Lima, I., Lombardozzi, D., Metzl, N., Millero, F., Monteiro, P. M. S., Munro, D. R., Nabel, J. E. M. S.,
- 1190 Nakaoka, S.-I., Nojiri, Y., Padín, X. A., Pregon, A., Pfeil, B., Pierrot, D., Poulter, B., Rehder, G., Reimer, J., Rödenbeck, C., Schwinger, J., Séférian, R., Skjelvan, I., Stocker, B. D., Tian, H., Tilbrook, B., van der Laan-Luijkx, I. T., van der Werf, G. R., van Heuven, S., Viovy, N., Vuichard, N., Walker, A. P., Watson, A. J., Wiltshire, A. J., Zaehle, S., and Zhu, D. (2017). Global Carbon Budget 2017. *Earth System Science Data Discussions*.
- 1195 Le Quéré, C., Andrew, R. M., Canadell, J. G., Sitch, S., Korsbakken, J. I., Peters, G. P., Manning, A. C., Boden, T. A., Tans, P. P., Houghton, R. A., Keeling, R. F., Alin, S., Andrews, O. D., Anthoni, P., Barbero, L., Bopp, L., Chevallier, F., Chini, L. P., Ciais, P., Currie, K., Delire, C., Doney, S. C., Friedlingstein, P., Gkritzalis, T., Harris, I., Hauck, J., Haverd, V., Hoppema, M., Klein Goldewijk, K., Jain, A. K., Kato, E., Körtzinger, A., Landschützer, P., Lefèvre, N., Lenton, A., Lienert, S., Lombardozzi, D., Melton, J. R., Metzl, N., Millero, F., Monteiro, P. M. S.,
- 1200 Munro, D. R., Nabel, J. E. M. S., Nakaoka, S.-I., O'Brien, K., Olsen, A., Omar, A. M., Ono, T., Pierrot, D., Poulter, B., Rödenbeck, C., Salisbury, J., Schuster, U., Schwinger, J., Séférian, R., Skjelvan, I., Stocker, B. D., Sutton, A. J., Takahashi, T., Tian, H., Tilbrook, B., van der Laan-Luijkx, I. T., van der Werf, G. R., Viovy, N., Walker, A. P., Wiltshire, A. J., and Zaehle, S. (2016). Global Carbon Budget 2016. *Earth System Science Data*.
- 1205 Le Quéré, C., Moriarty, R., Andrew, R. M., Canadell, J. G., Sitch, S., Korsbakken, J. I., Friedlingstein, P., Peters, G. P., Andres, R. J., Boden, T. A., Houghton, R. A., House, J. I., Keeling, R. F., Tans, P., Arneth, A., Bakker, D. C. E., Barbero, L., Bopp, L., Chang, J., Chevallier, F., Chini, L. P., Ciais, P., Fader, M., Feely, R. A., Gkritzalis, T., Harris, I., Hauck, J., Ilyina, T., Jain, A. K., Kato, E., Kitidis, V., Klein Goldewijk, K., Koven, C., Landschützer, P., Lauvset, S. K., Lefèvre, N., Lenton, A., Lima, I. D., Metzl, N., Millero, F., Munro, D. R., Murata, A., Nabel, J. E. M. S.,
- 1210 Nakaoka, S., Nojiri, Y., O'Brien, K., Olsen, A., Ono, T., Pérez, F. F., Pfeil, B., Pierrot, D., Poulter, B., Rehder, G., Rödenbeck, C., Saito, S., Schuster, U., Schwinger, J., Séférian, R., Steinhoff, T., Stocker, B. D., Sutton, A. J., Takahashi, T., Tilbrook, B., van der Laan-Luijkx, I. T., van der Werf, G. R., van Heuven, S., Vandemark, D., Viovy, N., Wiltshire, A., Zaehle, S., and Zeng, N.: Global Carbon Budget 2015, *Earth Syst. Sci. Data*, 7, 349–396, <https://doi.org/10.5194/essd-7-349-2015>, 2015.
- 1215 Le Quéré, C., Moriarty, R., Andrew, R. M., Peters, G. P., Ciais, P., Friedlingstein, P., Jones, S. D., Sitch, S., Tans, P., Arneth, A., Boden, T. A., Bopp, L., Bozec, Y., Canadell, J. G., Chini, L. P., Chevallier, F., Cosca, C. E., Harris, I., Hoppema, M., Houghton, R. A., House, J. I., Jain, A. K., Johannessen, T., Kato, E., Keeling, R. F., Kitidis, V., Klein Goldewijk, K., Koven, C., Landa, C. S., Landschützer, P., Lenton, A., Lima, I. D., Marland, G., Mathis, J. T., Metzl, N., Nojiri, Y., Olsen, A., Ono, T., Peng, S., Peters, W., Pfeil, B., Poulter, B., Raupach, M. R., Regnier, P., Rödenbeck, C., Saito, S., Salisbury, J. E., Schuster, U., Schwinger, J., Séférian, R., Segsneider, J., Steinhoff, T.,
- 1220 Stocker, B. D., Sutton, A. J., Takahashi, T., Tilbrook, B., van der Werf, G. R., Viovy, N., Wang, Y.-P., Wanninkhof, R., Wiltshire, A., and Zeng, N.: Global carbon budget 2014, *Earth Syst. Sci. Data*, 7, 47–85, <https://doi.org/10.5194/essd-7-47-2015>, 2015.
- 1225 Le Quéré, C., Peters, G. P., Andres, R. J., Andrew, R. M., Boden, T. A., Ciais, P., Friedlingstein, P., Houghton, R. A., Marland, G., Moriarty, R., Sitch, S., Tans, P., Arneth, A., Arvanitis, A., Bakker, D. C. E., Bopp, L., Canadell, J. G., Chini, L. P., Doney, S. C., Harper, A., Harris, I., House, J. I., Jain, A. K., Jones, S. D., Kato, E., Keeling, R. F., Klein Goldewijk, K., Körtzinger, A., Koven, C., Lefèvre, N., Maignan, F., Omar, A., Ono, T., Park, G.-H., Pfeil, B., Poulter, B., Raupach, M. R., Regnier, P., Rödenbeck, C., Saito, S., Schwinger, J., Segsneider, J., Stocker, B. D., Takahashi, T., Tilbrook, B., van Heuven, S., Viovy, N., Wanninkhof, R., Wiltshire, A., and Zaehle, S.: Global carbon budget 2013, *Earth Syst. Sci. Data*, 6, 235–263, <https://doi.org/10.5194/essd-6-235-2014>, 2014.
- Leith, H. Modelling the primary productivity of the world. *Nature and Resources*, UNESCO. VIII, 2:5-10, 1972.
- 1230 Li, S., He, F., Zhang, X., Zhou, T.: Evaluation of global historical land use scenarios based on regional datasets on the Qinghai–Tibet Area, *Science of The Total Environment*, Volume 657, 1615-1628, <https://doi.org/10.1016/j.scitotenv.2018.12.136>, 2019

- 1235 Lotze-Campen, H., Müller, C., Bondeau, A., Rost, S., Popp, A., and Lucht, W. Global food demand, productivity growth, and the scarcity of land and water resources: a spatially explicit mathematical programming approach *Agric. Econ.* 39 325–338, 2008.
- Luderer, G., Leimbach, M., Bauer, N., Kriegler, E., Baumstark, L., Bertram, C., Giannousakis, A., Hilaire, J., Klein, D., Levesque, A., Mouratiadou, I., Pehl, M., Pietzcker, R., Piontek, F., Roming, N., Schultes, A., Schwanitz, V. J., and Strefler, J. Description of the REMIND Model (Version 1.6) (Rochester, NY: Social Science Research Network) Online: <https://papers.ssrn.com/abstract=2697070>, 2015.
- 1240 Ma, L., Hurtt, G. C., Chini, L. P., Sahajpal, R., Pongratz, J., Frohling, S., Stehfest, E., Klein Goldewijk, K., O'Leary, D., and Doelman, J. C.: Global rules for translating land-use change (LUH2) to land-cover change for CMIP6 using GLM2, *Geosci. Model Dev.*, 13, 3203–3220, <https://doi.org/10.5194/gmd-13-3203-2020>, 2020.
- Meehl, G. A., Moss, R., Taylor, K. E., Eyring, V., Stouffer, R. J., Bony, S., and Stevens, B.. Climate model intercomparisons: Preparing for the next phase. *Eos, Trans. Amer. Geophys. Union*, 95, 77, doi:<https://doi.org/10.1002/2014EO090001>, 2014.
- 1245 Messner, S. and Strubegger, M. User's guide for MESSAGE III, 1995.
- Monfreda, C., Ramankutty, N. and Foley, J. Farming the planet: 2. Geographic distribution of crop areas, yields, physiological types, and net primary production in the year 2000. *Global Biogeochemical Cycles*, Vol.22, GB1022, doi:10.1029/2007GB002947, 2008.
- 1250 Moorcroft, P. R., Hurtt, G., and Pacala, S. W. A method for scaling vegetation dynamics: the ecosystem demography model (ED), *Ecological monographs*, 71, 557-586, 2001.
- Müller, C. and Robertson, R. D. Projecting future crop productivity for global economic modeling *Agric. Econ.* 45 37–50, 2014.
- 1255 Müller, C., Stehfest, E., Van Minnen, J.G., Strengers, B., Von Bloh, W., Beusen, A.H.W., Schaphoff, S., Kram, T., Lucht, W. Drivers and patterns of land biosphere carbon balance reversal. *Environmental Research Letters* 11. doi:10.1088/1748-9326/11/4/044002, 2016.
- Olofsson, J., and T. Hickler. Effects of human land-use on the global carbon cycle during the last 6000 years, *Veget. Hist. Archaeobot.*, doi:10.1007/s00334-007-0126-6, 2007.
- 1260 O'Neill, B. C., Tebaldi, C., van Vuuren, D. P., Eyring, V., Friedlingstein, P., Hurtt, G., et al. The Scenario Model Intercomparison Project (ScenarioMIP) for CMIP6. *Geoscientific Model Development*, 9(9), 3461–3482. <http://doi.org/10.5194/gmd-9-3461-2016>, 2016.
- Pan, Y., Birdsey, R.A., Phillips, O.L. and Jackson, R.B. The structure, distribution, and biomass of the world's forests. *Annual Review of Ecology, Evolution, and Systematics*, 44, pp.593-622, 2013.
- 1265 Popp, A., Dietrich, J. P., Lotze-Campen, H., Klein, D., Bauer, N., Krause, M., Beringer, T., Gerten, D., and Edenhofer, O. The economic potential of bioenergy for climate change mitigation with special attention given to implications for the land system *Environ. Res. Lett.* 6 034017, 2011.
- Popp, A., Humpenöder, F., Weindl, I., Bodirsky, B. L., Bonsch, M., Lotze-Campen, H., Müller, C., Biewald, A., Rolinski, S., Stevanovic, M., and Dietrich, J. P. Land-use protection for climate change mitigation *Nat. Clim. Change* 4 1095–8, 2014.
- 1270 Popp, A., Calvin, K., Fujimori, S., Havlik, P., Humpenöder, F., Stehfest, E., et al. Land-use futures in the shared socio-economic pathways. *Global Environmental Change*, 42, 331–345. <http://doi.org/10.1016/j.gloenvcha.2016.10.002>, 2017.

- 1275 Prestele, R., Arneth, A., Bondeau, A., de Noblet-Ducoudré, N., Pugh, T. A. M., Sitch, S., Stehfest, E., and Verburg, P. H.: Current challenges of implementing anthropogenic land-use and land-cover change in models contributing to climate change assessments, *Earth Syst. Dynam.*, 8, 369–386, <https://doi.org/10.5194/esd-8-369-2017>, 2017
- Riahi, K., van Vuuren, D. P., Kriegler, E., Edmonds, J., O'Neill, B. C., Fujimori, S., et al. The Shared Socioeconomic Pathways and their energy, land use, and greenhouse gas emissions implications: An overview. *Global Environmental Change*, 42, 153–168. <http://doi.org/10.1016/j.gloenvcha.2016.05.009>, 2017.
- 1280 Riahi, K., Dentener, F., Gielen, D., Grubler, A., Jewell, J., Klimont, Z., Krey, V., McCollum, D.L., Pachauri, S., Rao, S. and van Ruijven, B. Energy pathways for sustainable development, 2012.
- Riahi, K., Grübler, A. & Nakicenovic, N. Scenarios of long-term socio-economic and environmental development under climate stabilization. *Technol. Forecasting Soc. Change* 74, 887–935. (doi:10.1016/j.techfore.2006.05.026), 2007.
- 1285 Rogelj, J., Popp, A., Calvin, K.V. et al. Scenarios towards limiting global mean temperature increase below 1.5 °C. *Nature Clim Change* 8, 325–332. doi:10.1038/s41558-018-0091-3, 2018.
- Ruthenberg, H. *Farming Systems in the Tropics*. Oxford University Press, 1980.
- Sahajpal, R., Zhang, X., Izaurralde, R. C., Gelfand, I., & Hurtt, G. C. Identifying representative crop rotation patterns and grassland loss in the US Western Corn Belt. *Computers and electronics in agriculture*, 108, 173-182, 2014.
- 1290 Shevliakova, E., Stouffer, R. J., Malyshev, S., Krasting, J. P., Hurtt, G. C., and Pacala, S. W. Historical warming reduced due to enhanced land carbon uptake. *Proceedings of the National Academy of Sciences*. <http://doi.org/10.1073/pnas.1314047110>, 2013.
- 1295 Shevliakova, E., Pacala, S. W., Malyshev, S., Hurtt, G. C., Milly, P. C. D., Caspersen, J. P., et al. Carbon cycling under 300 years of land use change: Importance of the secondary vegetation sink. *Global Biogeochemical Cycles*, 23(2), 1–16. <http://doi.org/10.1029/2007GB003176>, 2009.
- Sitch, S., Smith, B., Prentice, I.C., Arneth, A., Bondeau, A., Cramer, W., Kaplan, J.O., Levis, S., Lucht, W., Sykes, M.T. and Thonicke, K., Evaluation of ecosystem dynamics, plant geography and terrestrial carbon cycling in the LPJ dynamic global vegetation model. *Global Change Biology*, 9(2), pp.161-185, 2003.
- 1300 Smil, V. *Enriching the Earth: Fritz Haber, Carl Bosch, and the Transformation of World Food Production*, MIT Press, 2001.
- Smil, V. *Energy at the Crossroads: Global Perspectives and Uncertainties*, MIT Press, Cambridge MA USA, 2003.
- Stehfest, E., van Vuuren, D., Kram, T., Bouwman, L., Alkemade, R., Bakkenes, M., Biemans, H., Bouwman, A., den Elzen, M., Janse, J., Lucas, P., van Minnen, J., Müller, C., and Prins, A. *Integrated Assessment of Global Environmental Change with IMAGE 3.0. Model description and policy applications*, The Hague, 2014.
- 1305 Thornton, P. E., Calvin, K., Jones, A. D., Di Vittorio, A. V., Bond-Lamberty, B., Chini, L., Shi, X., Mao, J., Collins, W. D., Edmonds, J., Thomson, A., Truesdale, J., Craig, A., Branstetter, M. L., and Hurtt, G. Biospheric feedback effects in a synchronously coupled model of human and Earth systems, *Nature Climate Change*, 2017.
- 1310 van Vuuren, D. P., Edmonds, J., Thomson, A., Riahi, K., Kainuma, M., Matsui, T., Hurtt, G. C., Lamarque, J.-F., Meinshausen, M., Smith, S., Granier, C., Rose, S. K., and Hibbard, K. A. The Representative Concentration Pathways: an overview, *Climatic Change*, 109, 5–31, 2011.

van Vuuren, D. P., Stehfest, E., Gernaat, D. E., Doelman, J. C., van den Berg, M., Harmsen, M., de Boer, H. S., Bouwman, L. F., Diaoglou, V., and Edelenbosch, O. Y. Energy, land-use and greenhouse gas emissions trajectories under a green growth paradigm. *Global Environmental Change*, 42, 237-250, 2017.

1315 Wei, Y.; Liu, S.; Huntzinger, D. N.; Michalak, A. M.; Viovy, N.; Post, W. M.; Schwalm, C. R.; Schaefer, K.; Jacobson, A.R.; Lu, C.; et al. The North American carbon program multi-scale synthesis and terrestrial model intercomparison project—Part 2: Environmental driver data. *Geosci. Model Dev.*, 6, 5375–5422, 2013.

Weindl, I., Popp, A., Bodirsky, B. L., Rolinski, S., Lotze-Campen, H., Biewald, A., Humpenöder, F., Dietrich, J. P., and Stevanović, M. Livestock and human use of land: Productivity trends and dietary choices as drivers of future land and carbon dynamics *Glob. Planet. Change* 159 1–10, 2017

1320 West, T., Le Page, Y., Huang, M., Wolf, J., and Thomson, A. "Downscaling global land cover projections from an integrated assessment model for use in regional analyses: results and evaluation for the US from 2005 to 2095." *Environmental Research Letters* 9(6), 2014.

1325 Wise, M., Calvin, K., Kyle, P., Luckow, P., and Edmonds, J. "Economic and Physical Modeling of Land Use in GCAM 3.0 and an Application to Agricultural Productivity, Land, and Terrestrial Carbon." *Climate Change Economics* 5(2), 2014.

Zhang, X., Davidson, E. A., Mauzerall, D. L., Searchinger, T. D., Dumas, P., and Shen, Y.. Managing nitrogen for sustainable development, *Nature*, 528, 51-59, doi:10.1038/nature15743, 2015.

Zon, R. and Sparhawk, W. N. *Forest Resources of the World, Volume I*. McGraw-Hill, NY, p 493, 1923

1330

Table 1. Historical global population (millions) and land use estimates (million ha) from HYDE 3.2 (Klein Goldewijk et al., 2017).

	800 CE	1000 CE	1500 CE	1700 CE	1850 CE	1950 CE	2015 CE
Population	286	323	503	592	1271	2529	7301
Cropland	140	162	256	293	578	1223	1591
Rainfed area	136	157	252	289	549	1118	1316
Irrigated area	3.6	4.1	4.2	4.5	28	105	276
Rice area	4.2	4.8	8.7	12.5	28	65	118
Paddy rice	1.2	1.5	2.4	2.9	12	36	75
Rainfed rice	2.9	3.3	6.3	9.6	16	29	43
Grazing	314	366	515	664	1192	2611	3241
Pasture	31	55	105	145	253	535	787
Rangeland	282	310	410	519	939	2076	2454
% agric /total land area	3.5%	4.0%	5.9%	7.3%	13.6%	29.4%	37.1%

1335 Table 2. Properties of SSPs used in this analysis. SSP-RCP refers to Shared Socioeconomic Pathway and Representative Concentration Pathway, respectively and Tier refers to ScenarioMIP Tier (O'Neill et al., 2016).

SSP-RCP	IAM	Tier	Crop	Grazing	Wood Harvest	Irrigation	Fertilizer
SSP5-8.5	REMIND-MAGPIE	1	0.5°x0.5°	0.5°x0.5°	NA	0.5°x0.5°	0.5°x0.5°
SSP3-7	AIM	1	0.5°x0.5°	0.5°x0.5°	18 regions	0.5°x0.5°	18 regions
SSP2-4.5	MESSAGE	1	0.5°x0.5°	30 regions	0.5x0.5	30 regions	30 regions
SSP1-2.6	IMAGE	1	0.5°x0.5°	0.5°x0.5°	26 regions	0.5°x0.5°	0.5°x0.5°
SSP4-6.0	GCAM	2	0.25°x0.25°	33 regions	33 regions	33 regions	33 regions
SSP4-3.4	GCAM	2	0.25°x0.25°	33 regions	33 regions	33 regions	33 regions
SSP5-3.4-OS	REMIND-MAGPIE	2	0.5°x0.5°	0.5°x0.5°	NA	0.5°x0.5°	0.5°x0.5°
SSP1-1.9	IMAGE	2	0.5°x0.5°	0.5°x0.5°	26 regions	0.5°x0.5°	0.5°x0.5°

1340

Table 3. Diagnostic table, historical data.

Metric	Units	Time-period	Literature values	LUH2_v2h	LUH1
Transitions					
Total gross transitions	10 ⁶ km ² yr ⁻¹	2000		1.86	2.9
Total net transitions	10 ⁶ km ² yr ⁻¹	2000		0.23	0.17
Human land use impacts					
Secondary land increase that is forested	%	1700-2000		64.5	57.6
U.S. Forests that are secondary	%	2000		92.9	100
Natural vegetation in biodiversity hotspots	%	2005	2.3 ¹	1.6	4.6
Median secondary forest mean age	yr	2005		42.2	27.6
Median secondary forest mean age	yr	2015	30–40 ²	43.0	
Land impacted by human land use	%	2000		58.7	54.0
Secondary land area increase	10 ⁶ km ²	1700-2000		13	17
Secondary land area increase (forest)	10 ⁶ km ²	1700-2000		10	10
Secondary land area increase (non-forest)	10 ⁶ km ²	1700-2000		3	7
Wood harvest and agricultural clearing					
Wood clearing for crop and pasture	Pg C	1500-1990	121.9–356.3 ³	251	278
Total wood harvest	Pg C	1500-1990		170	
Direct wood harvest	Pg C	1500-1990		132	119
Agricultural clearing for wood harvest	Pg C	1500-1990		38	
Shifting cultivation					
Agricultural land for shifting cultivation	10 ⁶ km ² yr ⁻¹	2000	0.3 ⁴	0.3	0.6
Agricultural land for shifting cultivation	10 ⁶ km ² yr ⁻¹	1980	0.2-0.6 ⁵	0.3	0.5
Forest loss and area					
Potential forest area	10 ⁶ km ²	Potential	48.7-55.3 ⁶	47	51
Forest area	10 ⁶ km ²	2015	32.1-41.4 ⁷	37	
Management					
Fuelwood	Pg C	2000	0.72 ⁹	0.7	
Wood-harvest	Pg C	2000	1.30 ⁹	1.3	
Fertilizer use	Tg N yr ⁻¹	2012	100 ⁸	107	
Irrigated area	10 ⁶ km ²	2003	2.77 ⁹	2.5	
Biofuel area (corn, USA)	10 ⁶ km ²	2004	0.033 ¹⁰	0.03	
Biomass					
Plant total biomass on all lands	Pg C	Potential 2007-2008	557.4-923 ¹¹ 187.5-	718 184	731 177
Plant AGB on pantropical forest lands	Pg C		228.7 ¹²		
Plant total biomass on forest lands	Pg C	2005	362.6 ¹³	395	404
Plant total biomass on all lands	Pg C	2005	393.4 ¹³	434	440

References¹Mittermeier et al. 2005⁶Pongratz et al., 2008;
Ramankutty &Foley, 1999¹¹Kucharik, 2000; Sitch, 2003; Pan, 2013²Ben Poulter, NACP 2013⁷Sexton, 2016¹²Saatchi, 2011; Baccini, 2012; Avitabile, 2016³Direct wood harvest LUH1, Kaplan low/high-case (see text)⁸Zhang, 2016¹³Pan, 2013⁴Heinimann et al. 2017⁹FAO⁵Rojstaczer, 2001¹⁰Searchinger, 2008

Table 4. Harmonized Scenarios of Future Land-use: global land-use state areas in year 2100, across all future scenarios (10^6 km²).

	SSP1-1.9	SSP1-2.6	SSP4-3.4	SSP5-3.4OS	SSP2-4.5	SSP4-6.0	SSP3-7.0	SSP5-8.5
C3 annuals	7.86	7.94	9.13	7.72	10.4	8.39	10.5	9.04
C4 annuals	2.67	2.59	3.56	2.95	4.03	3.50	5.18	4.20
C3 perennials	2.78	2.79	2.95	2.22	2.02	1.82	2.17	1.59
C4 perennials	2.87	2.42	11.2	9.04	0.34	2.55	0.35	0.33
C3 N-fixers	2.11	2.11	2.27	2.11	3.03	2.38	3.34	2.77
Managed pasture	3.81	4.35	9.04	4.13	6.23	9.74	8.95	7.11
Rangeland	21.6	22.1	22.2	21.3	22.1	25.8	25.5	23.8
Urban	1.04	1.04	1.11	1.25	1.10	1.11	1.03	1.25
Primary	40.7	40.8	32.0	38.7	36.5	33.7	34.6	37.2
Secondary	44.5	43.8	36.5	40.6	44.1	41.0	38.3	42.6

Table 5. Diagnostic table, future land-use.

Metric	Units	Time period	SSP1 RCP1.9	SSP5 RCP3.4OS	SSP1 RCP2.6	SSP5 RCP8.5	SSP4 RCP3.4	SSP4 RCP6.0	SSP3 RCP7.0	SSP2 RCP4.5
Transitions										
Total gross transitions	10 ⁶ km ² yr ⁻¹	2100	2.02	3.99	2.12	4.21	4.56	4.79	4.60	3.06
Total net transitions	10 ⁶ km ² yr ⁻¹	2100	0.02	0.04	-0.11	0.03	0.16	0.09	0.13	0.03
Human land use impacts										
Secondary land increase that is forested	%	2015-2100	49.7	54.1	48.9	58.4	60.0	71.6	63.6	72.8
U.S. Forests that are secondary	%	2100	100	100	100	100	100	100	100	100
Global area covered by natural vegetation in biodiversity hotspots	%	2100	1.1	0.9	1.1	0.9	0.6	0.8	0.9	0.9
Median secondary forest mean age	yr	2100	74.0	58.5	74.2	67.7	60.8	60.6	68.0	63.0
Land impacted by human land use	%	2100	68.6	70.2	68.6	71.4	75.4	74.1	73.3	71.9
Secondary land increase	10 ⁶ km ²	2100-2015	13	10	13	12	6	10	8	12
Secondary land increase (forest)	10 ⁶ km ²	2100-2015	6	5	6	7	4	7	5	8
Secondary land increase (non-forest)	10 ⁶ km ²	2100-2015	7	5	7	5	2	3	3	3
Wood harvest and agricultural clearing										
Wood clearing for crop and pasture	Pg C	2100-2015	47	56	47	47	88	59	70	44
Total wood harvest	Pg C	2100-2015	93	139	95	141	145	148	131	139
Direct wood harvest	Pg C	2100-2015	93	139	95	141	145	148	131	139
Agricultural clearing for wood harvest	Pg C	2100-2015	0	0	0	0	0	0	0	0
Shifting cultivation										
Agricultural land for shifting cultivation	10 ⁶ km ² yr ⁻¹	2100	0	0	0	0	0	0	0	0
Forest loss and area										
Forest area change	10 ⁶ km ²	2100-2015	0.9	-1.3	0.9	-0.9	-5.1	-1.4	-3.4	0.8
Forest area	10 ⁶ km ²	2100	38.1	35.9	38.1	36.3	32.1	35.8	33.8	38.0
Forest loss	10 ⁶ km ²	2015-2100	12.0	17.6	12.1	15.3	20.3	17.9	15.1	15.0
Management										
Fuelwood	Pg C	2100	0.2	0.7	0.2	0.9	0.9	0.9	0.8	0.7
Wood-harvest	Pg C	2100	0.9	1.6	0.9	1.7	1.8	1.9	1.5	1.5
Fertilizer use	Tg N yr ⁻¹	2100	140	223	177	110	240	145	173	210
Irrigated area	10 ⁶ km ²	2100	2.9	2.8	2.9	3.4	2.7	2.7	4.1	2.6
Flooded area	10 ⁶ km ²	2100	0.9	0.2	0.9	0.6	0.8	0.9	0.9	1.0
Biofuel area	10 ⁶ km ²	2100	3.6	10.9	3.4	0.2	18.0	3.7	0.0	0.0
Biomass										
Plant total biomass on all lands	Pg C	2100	433	380	434	386	319	367	355	401

Plant AGB on pantropical forest lands	Pg C	2100	239	217	239	213	170	198	178	221
Plant total biomass on forest lands	Pg C	2100	390	343	391	349	290	335	322	366

1350 Table 6. Regional results for 1700-2000 (historical period).

	Secondary area (10 ⁶ km ²)	Secondary Age (yr)	Gross Transitions (10 ³ km ² yr ⁻¹)	Net Transitions (10 ³ km ² yr ⁻¹)
1700-1799 mean				
North America	0.3	150	12	3
South America	0.3	77	40	1
Eurasia	8.5	429	456	41
Africa	6.0	245	165	10
Oceania	0.1	98	5	1
1800-1899 mean				
North America	0.3	144	52	33
South America	0.4	79	61	11
Eurasia	9.8	377	660	76
Africa	6.5	257	191	19
Oceania	0.1	116	13	10
1900-1999 mean				
North America	1.7	52	108	48
South America	0.8	53	145	48
Eurasia	12.4	289	604	121
Africa	6.8	232	404	80
Oceania	0.1	99	40	33

Table 7. Regional results averaged over years 2000-2099.

	Secondary area (10 ⁶ km ²)	Secondary Age (yr)	Gross Transitions (10 ³ km ² yr ⁻¹)	Net Transitions (10 ³ km ² yr ⁻¹)
SSP1 RCP1.9				
North America	4.5	64	89	4
South America	2.5	46	129	9
Eurasia	18.4	210	1080	13
Africa	10.9	77	959	35
Oceania	0.9	46	20	-4
SSP1 RCP2.6				
North America	4.4	65	86	6
South America	2.5	47	128	9
Eurasia	18.2	213	1070	19
Africa	10.9	76	975	34
Oceania	0.9	48	18	-4
SSP4 RCP3.4				
North America	4.1	60	153	19
South America	3.0	45	109	-3
Eurasia	17.1	197	1790	93
Africa	9.2	69	1630	143
Oceania	0.8	48	21	1
SSP5 RCP3.4OS				
North America	4.0	62	171	15
South America	2.0	49	135	16
Eurasia	17.8	195	1940	50
Africa	10.6	81	798	49
Oceania	0.8	49	18	-3
SSP2 RCP4.5				
North America	4.2	65	92	7
South America	2.3	45	147	13
Eurasia	17.7	206	1380	44
Africa	10.9	69	1340	71
Oceania	0.8	49	20	-4
SSP4 RCP6.0				
North America	4.1	63	107	12
South America	2.4	45	130	3
Eurasia	17.9	201	1750	53
Africa	9.5	64	1610	133
Oceania	0.7	50	18	-2
SSP3 RCP7.0				
North America	3.8	66	94	17
South America	2.0	49	132	24
Eurasia	18.1	208	1450	32
Africa	9.5	70	1880	133
Oceania	0.7	53	16	1
SSP5 RCP8.5				
North America	4.0	67	81	15
South America	2.1	49	126	19
Eurasia	17.7	209	1590	48
Africa	10.8	70	1540	62
Oceania	0.9	50	16	-4

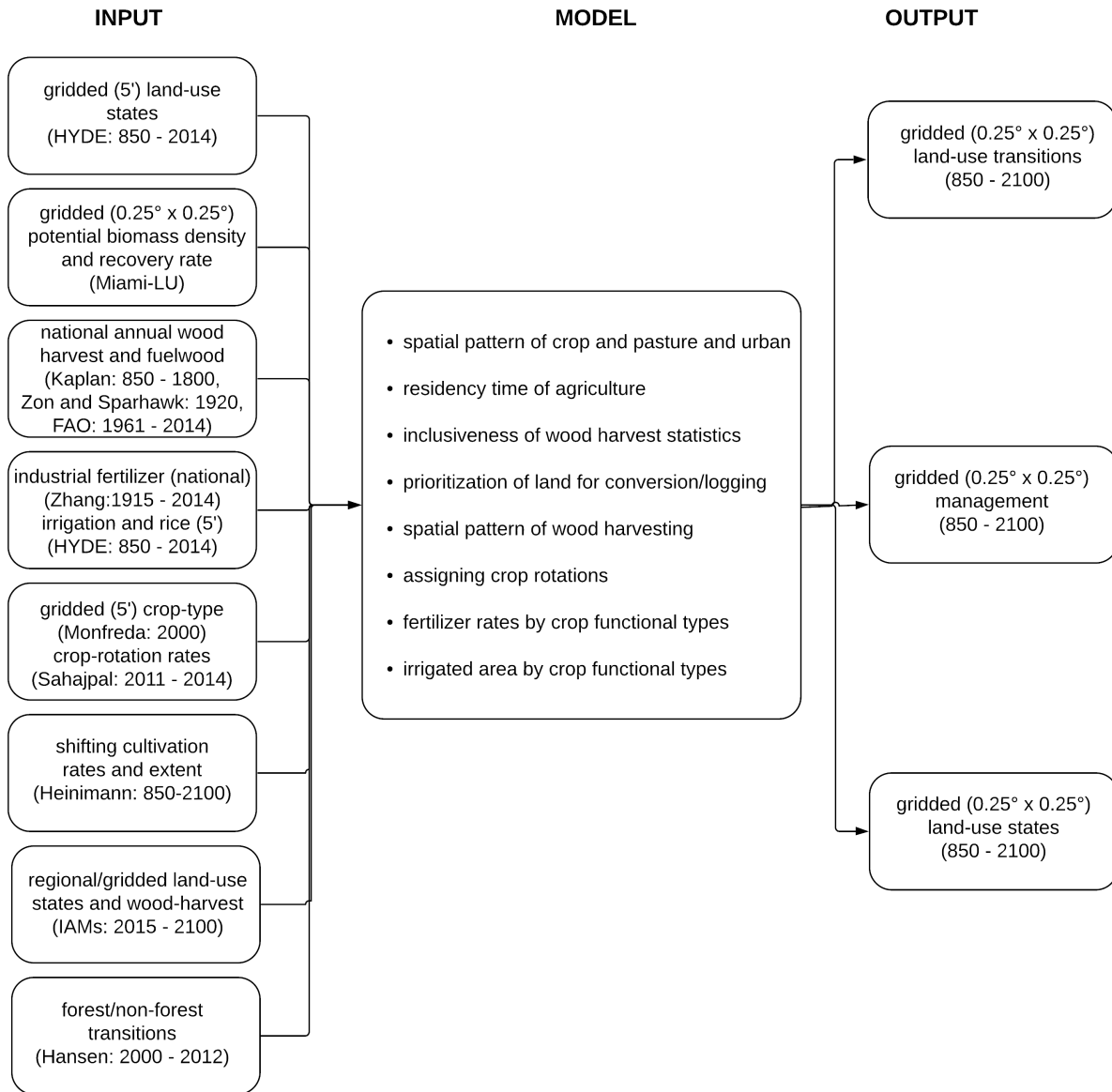


Figure 1. Schematic diagram of major model inputs, decisions, and outputs.

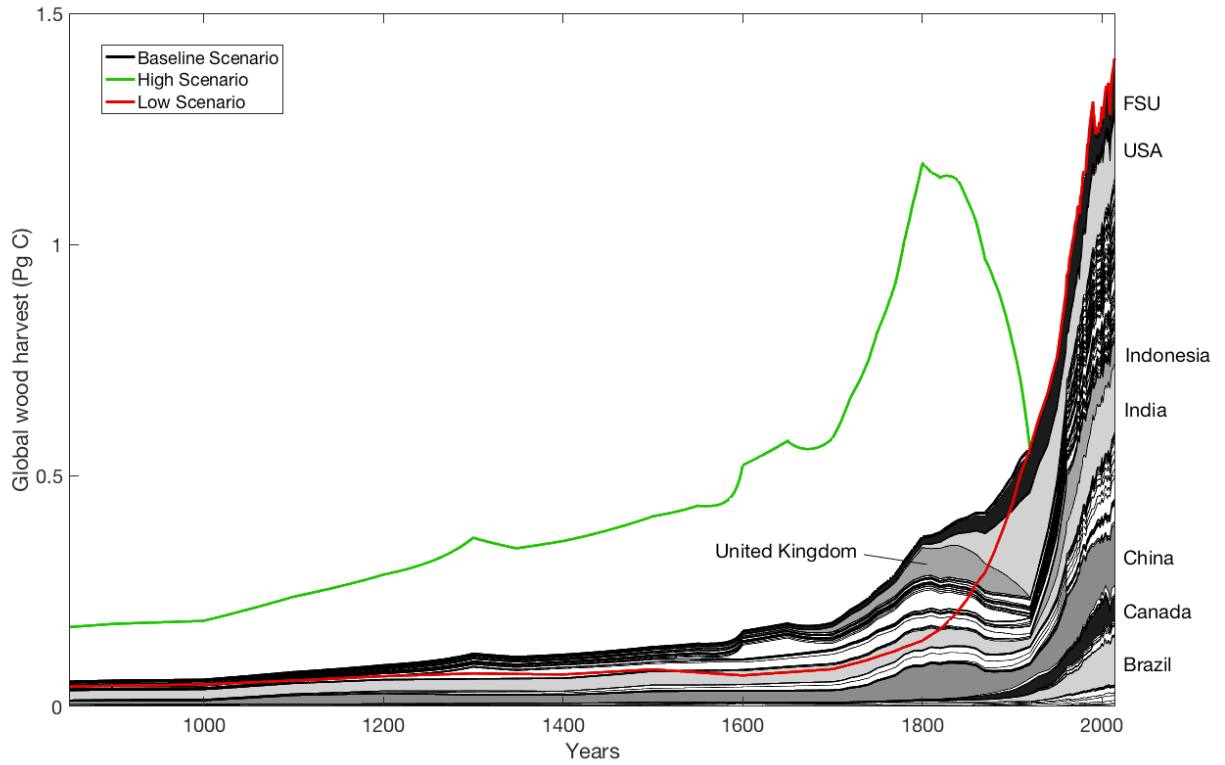


Figure 2. (a) Annual national wood harvest (in Pg C/y) for 850-2015, for low, baseline and high scenarios. (FSU= Former Soviet Union.) Integrated total wood harvest in baseline scenario was 259 Pg C (including slash).

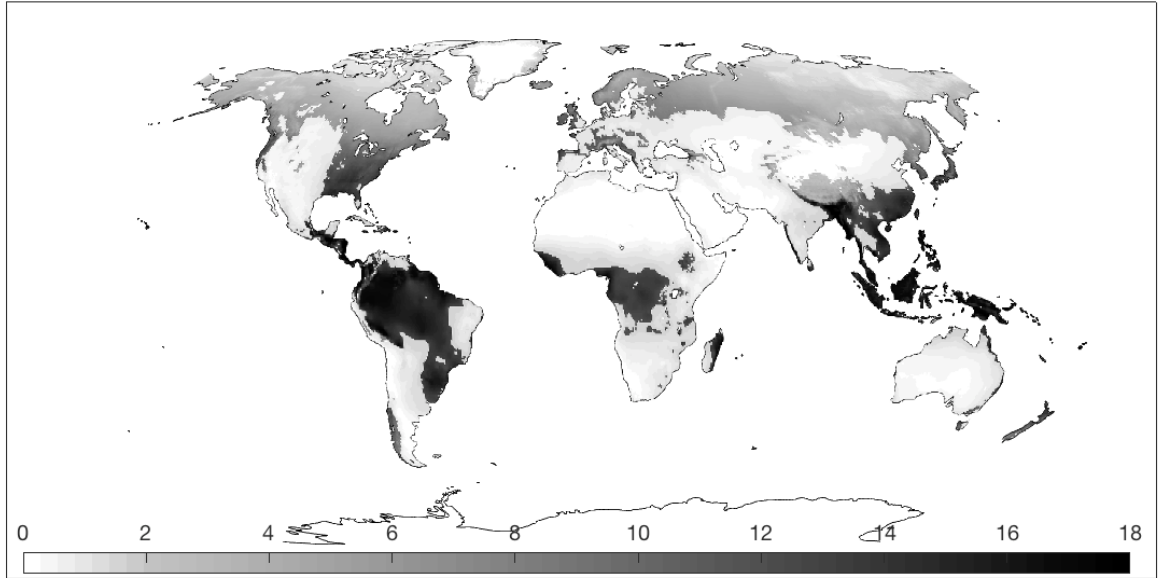


Figure 3. Global potential above-ground biomass (kg C m^{-2}) as estimated by Miami-LU model. Land is considered to be potential forest if the potential biomass density is $>2 \text{ kg C m}^{-2}$ (after Hurtt et al., 2006; 2011).

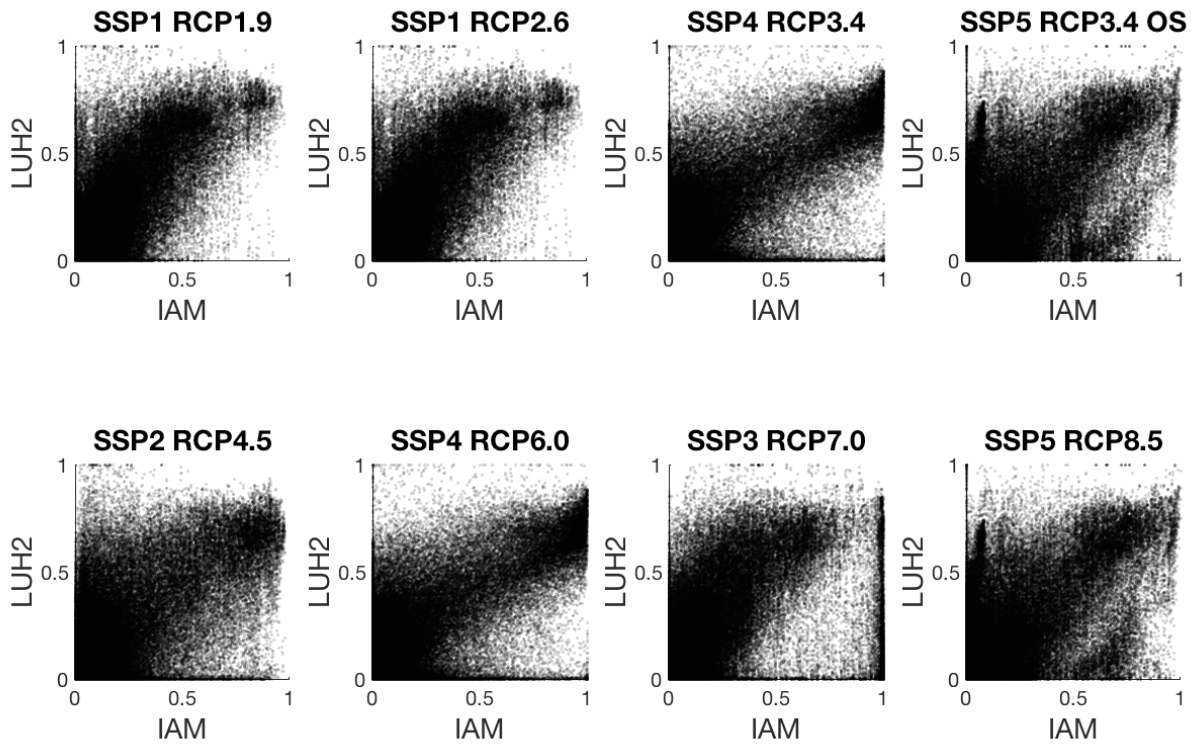
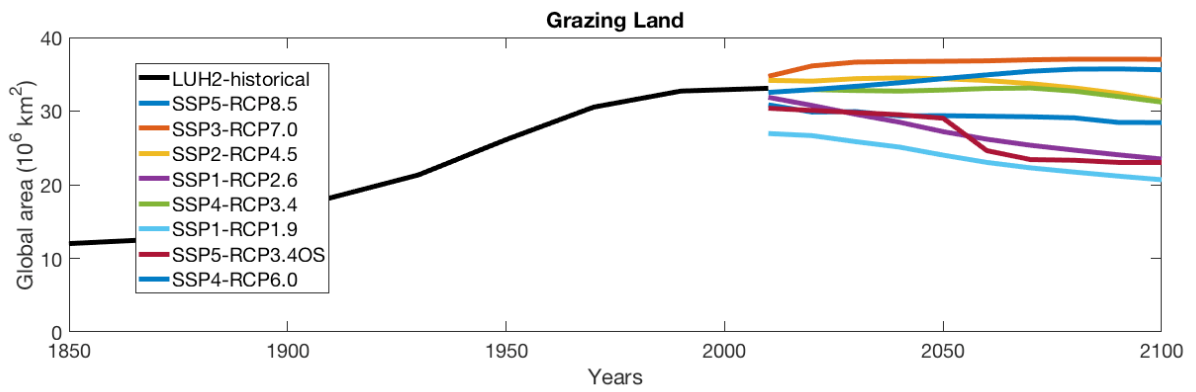
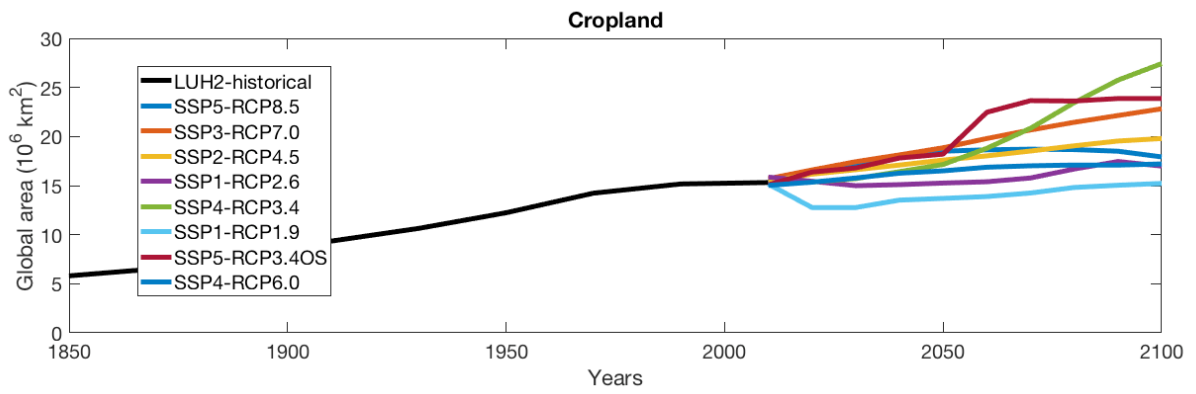
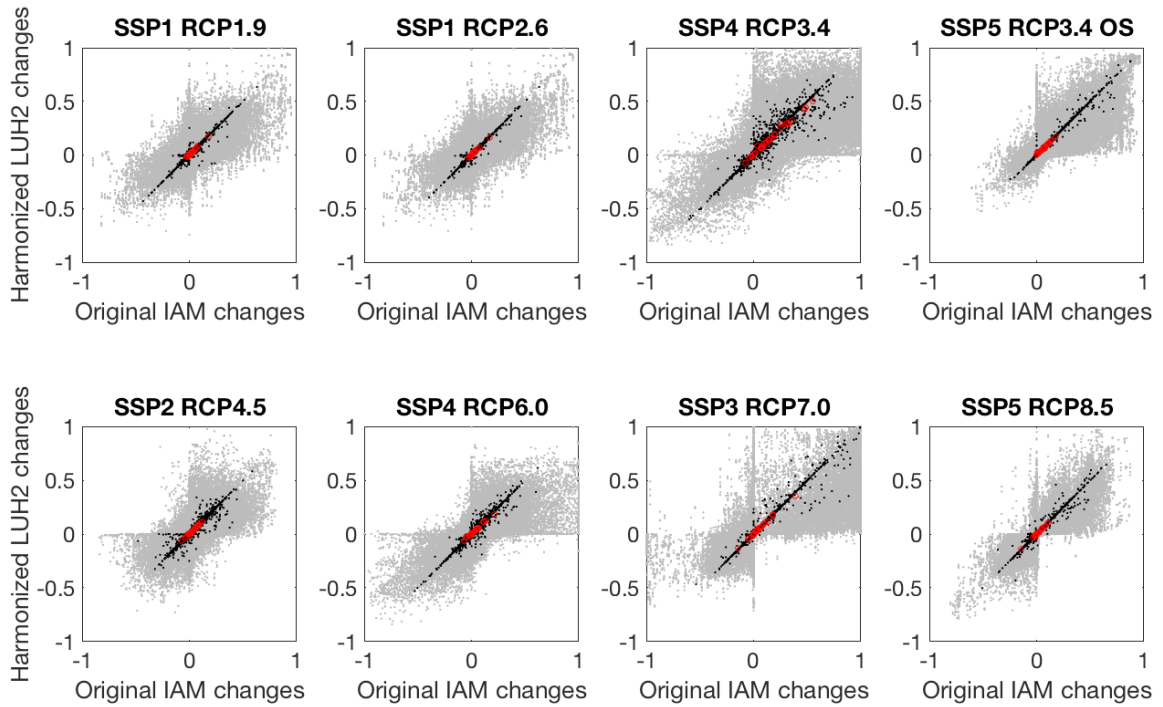


Figure 4. Pre-harmonization (a) global cropland, (b) global grazing land, (c) 0.25° grid cell comparison of 2015 crop fraction of grid cell areas (excluding water and ice): LUH2 (x-axis), IAM (y-axis).

(a)



(b)

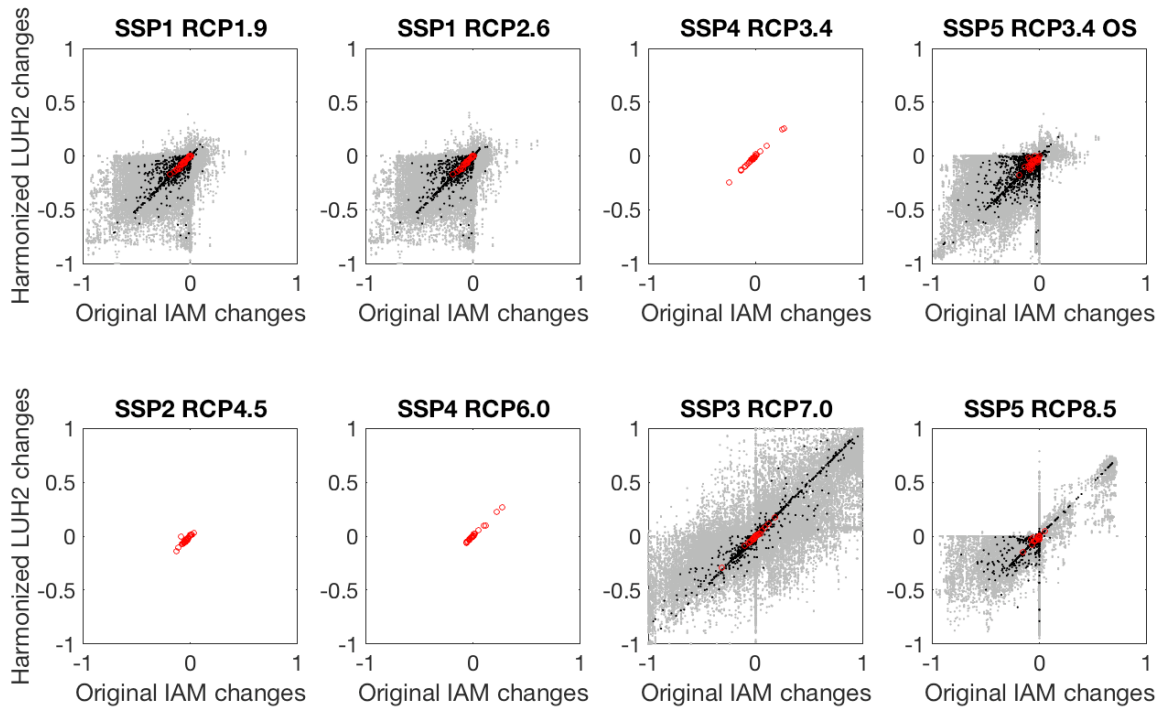


Figure 5. Post-harmonization comparison of projected changes 2015-2100 at multiple scales: 0.25 degree (grey), 2 degree (black), regional (red); as fraction of total area. Original IAM change (x-axis), harmonized change (y-axis), for (a) Cropland, and (b) grazing land. Note that for SSP4 RCP3.4, SSP2 RCP4.5, and SSP4 RCP6.0, pasture was only reported by IAMs as regional totals, so LHU2 comparisons at 0.25° and 2° are not possible.

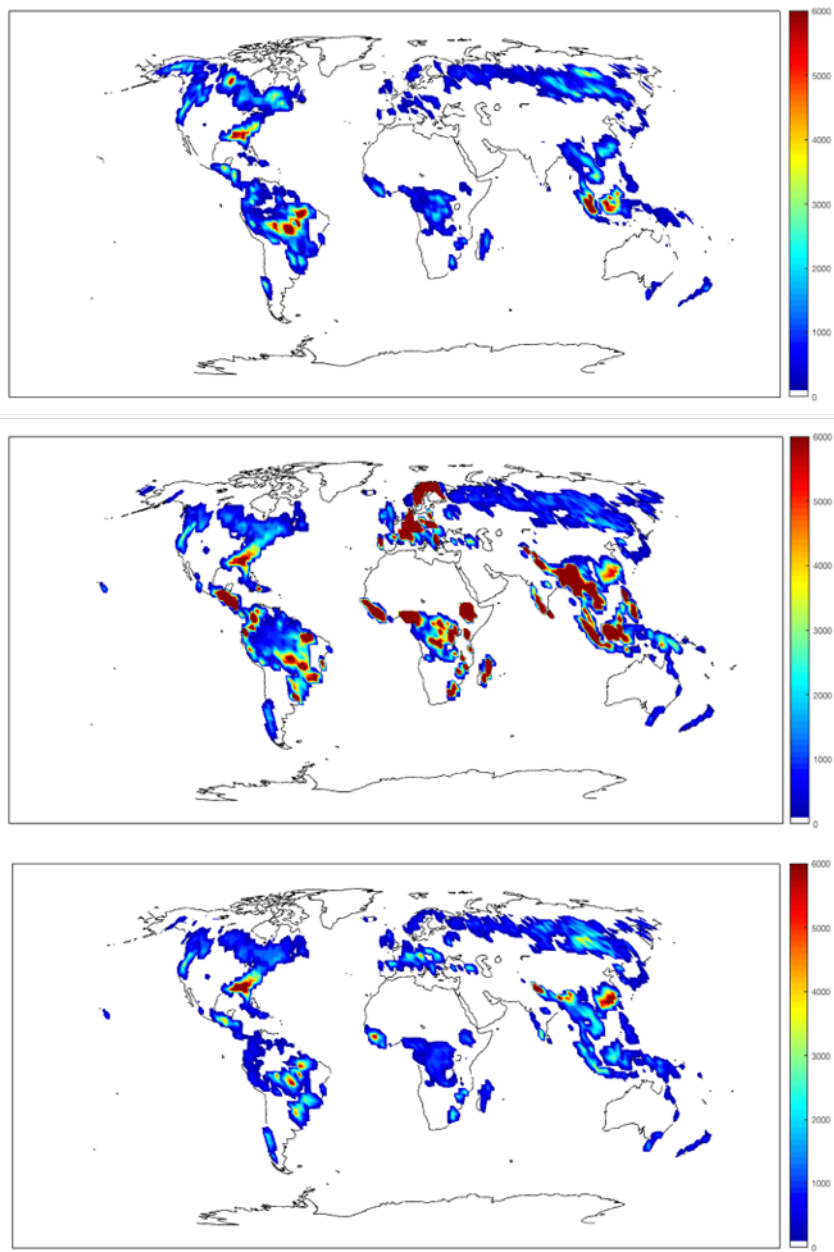


Figure 6. Forest loss 2000-2012 (a) Landsat forest loss (Hansen et al. 2013), (b) LUH2 forest loss without Landsat constraint, (c) LUH2 forest loss with Landsat constraint.

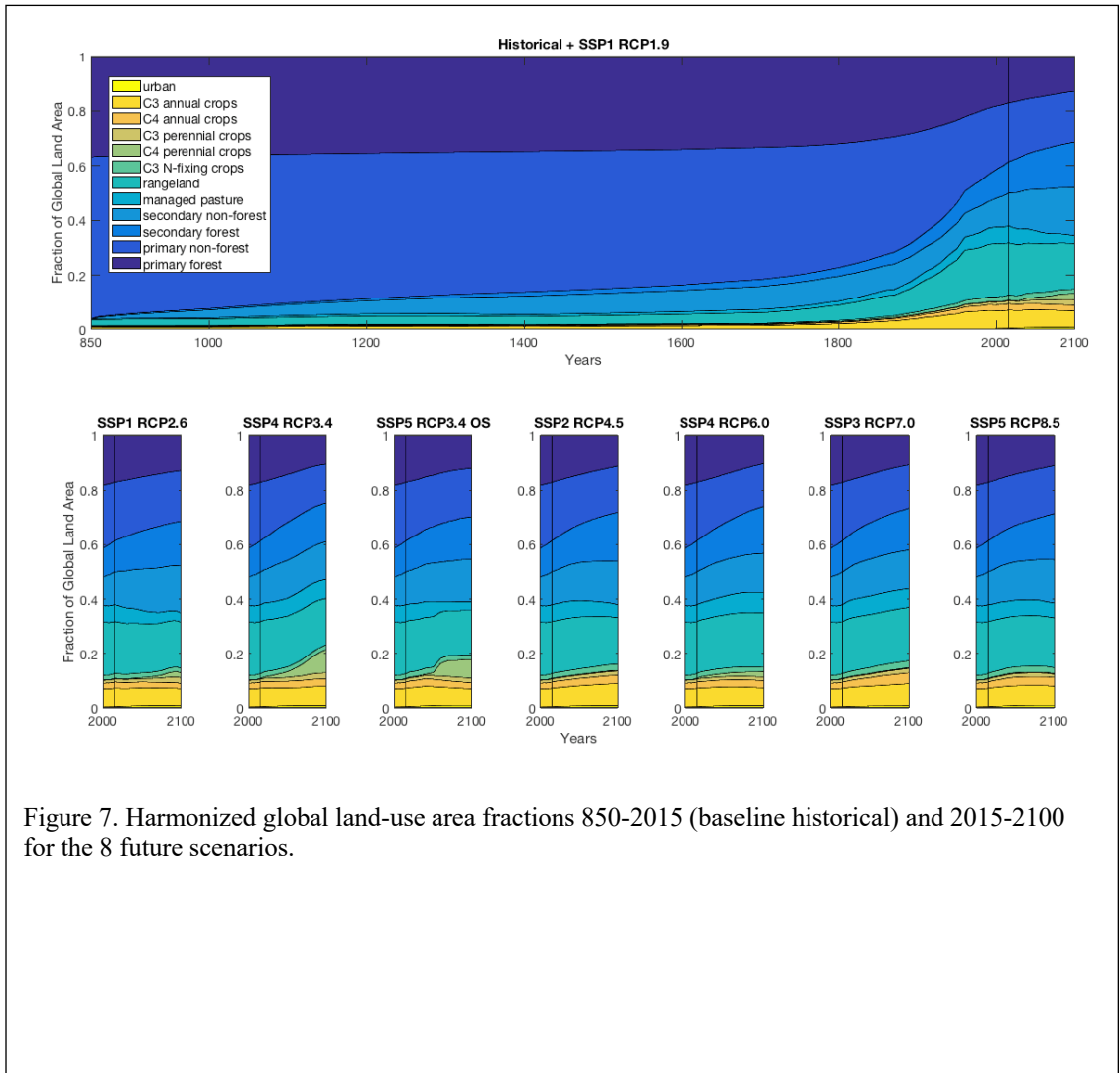


Figure 7. Harmonized global land-use area fractions 850-2015 (baseline historical) and 2015-2100 for the 8 future scenarios.

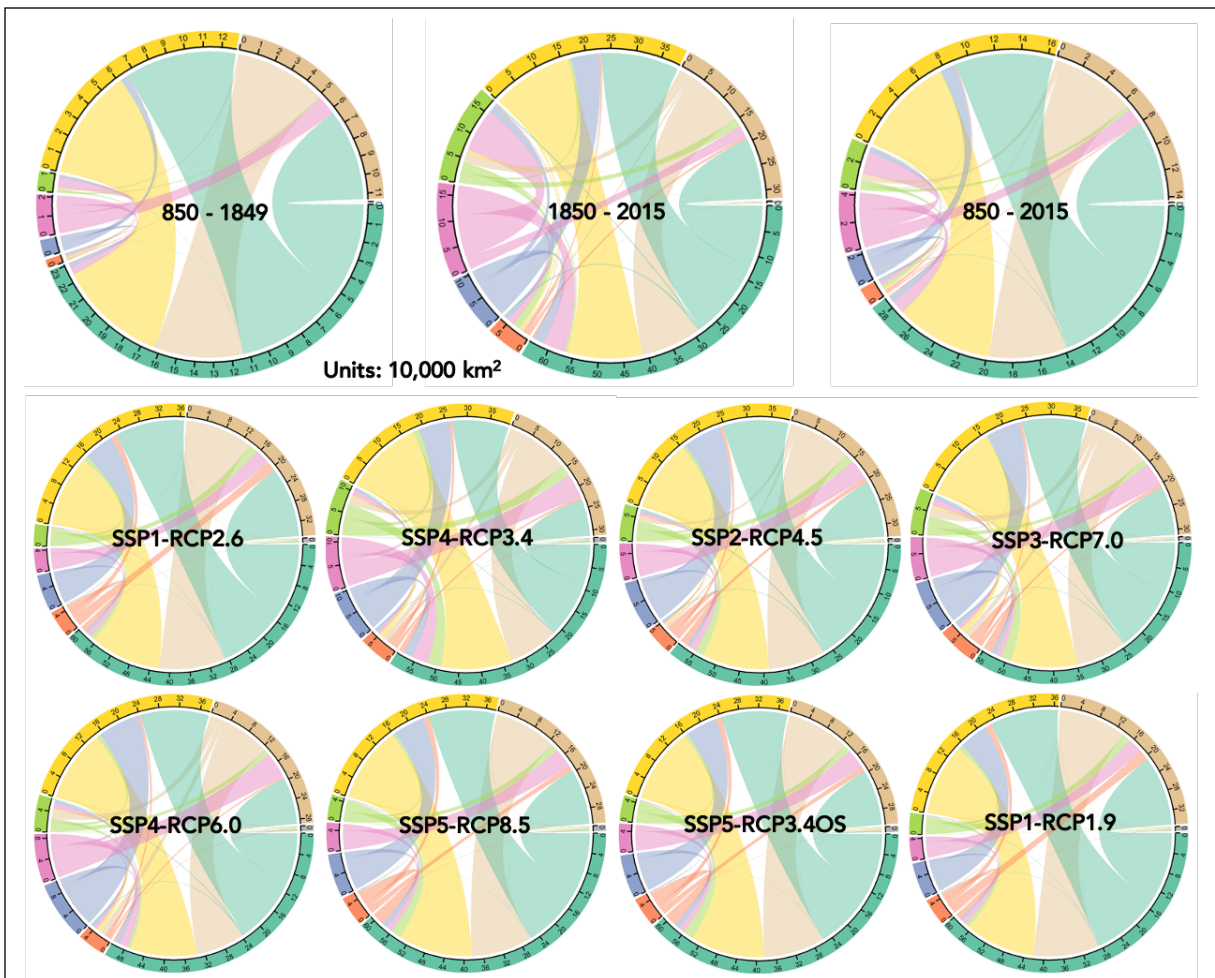
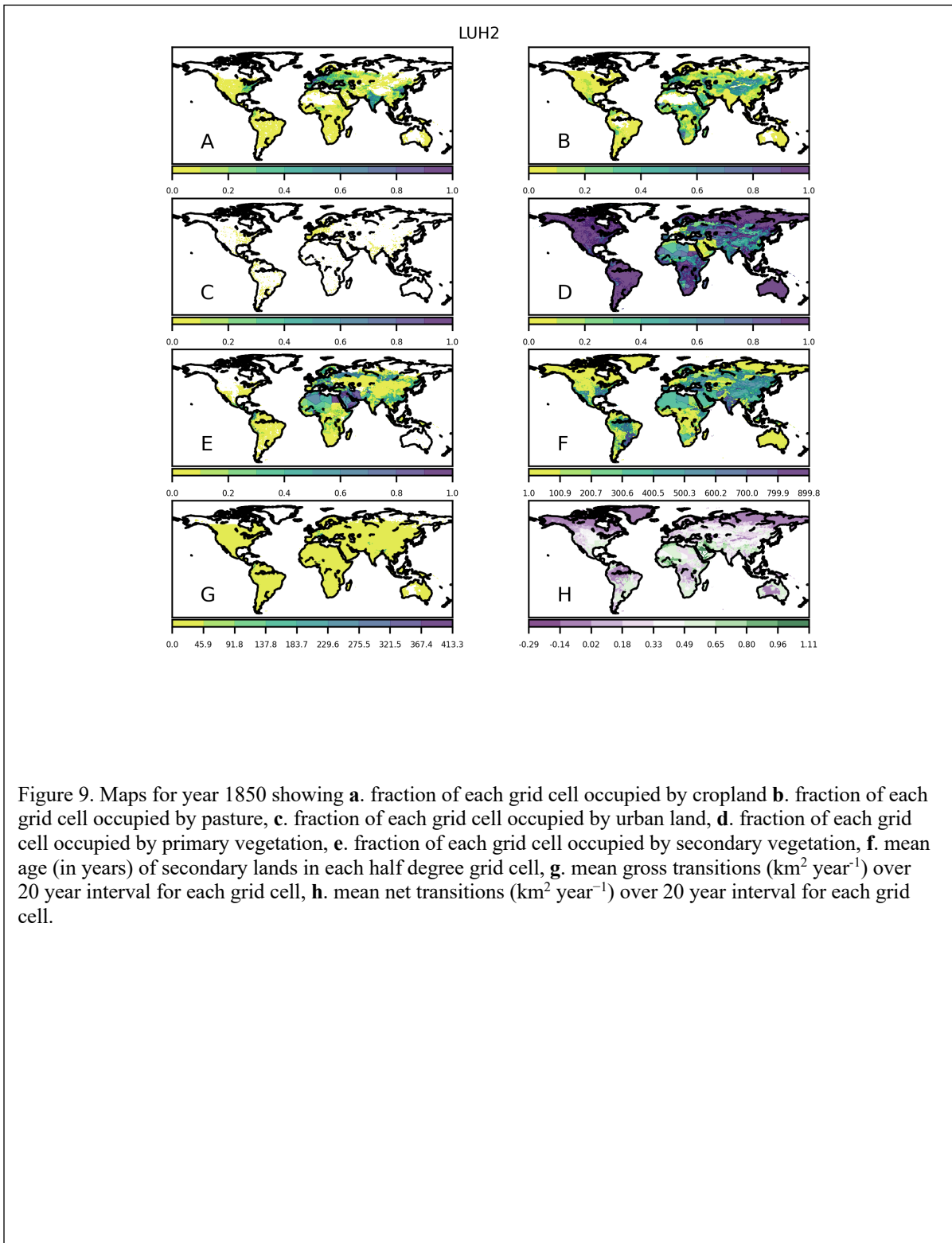
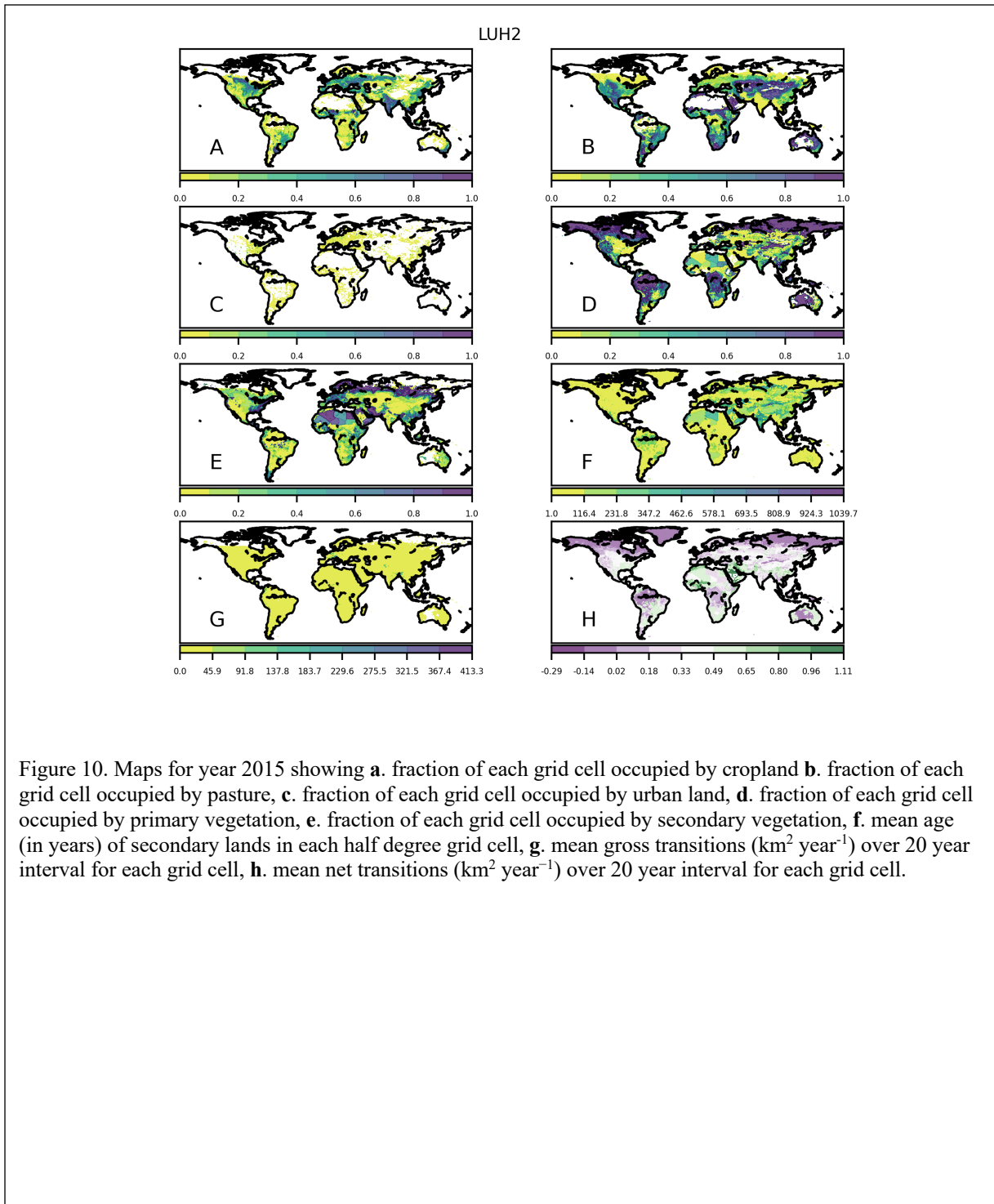


Figure 8. Global land-use transitions by time-period and by future scenario. Each color represents transitions from a specific land-use type to the other land-use types: dark green for cropland, orange for managed pasture, blue for primary forest, pink for primary non-forest, light green for rangeland, yellow for secondary forest, brown for secondary non-forest, and grey for urban.





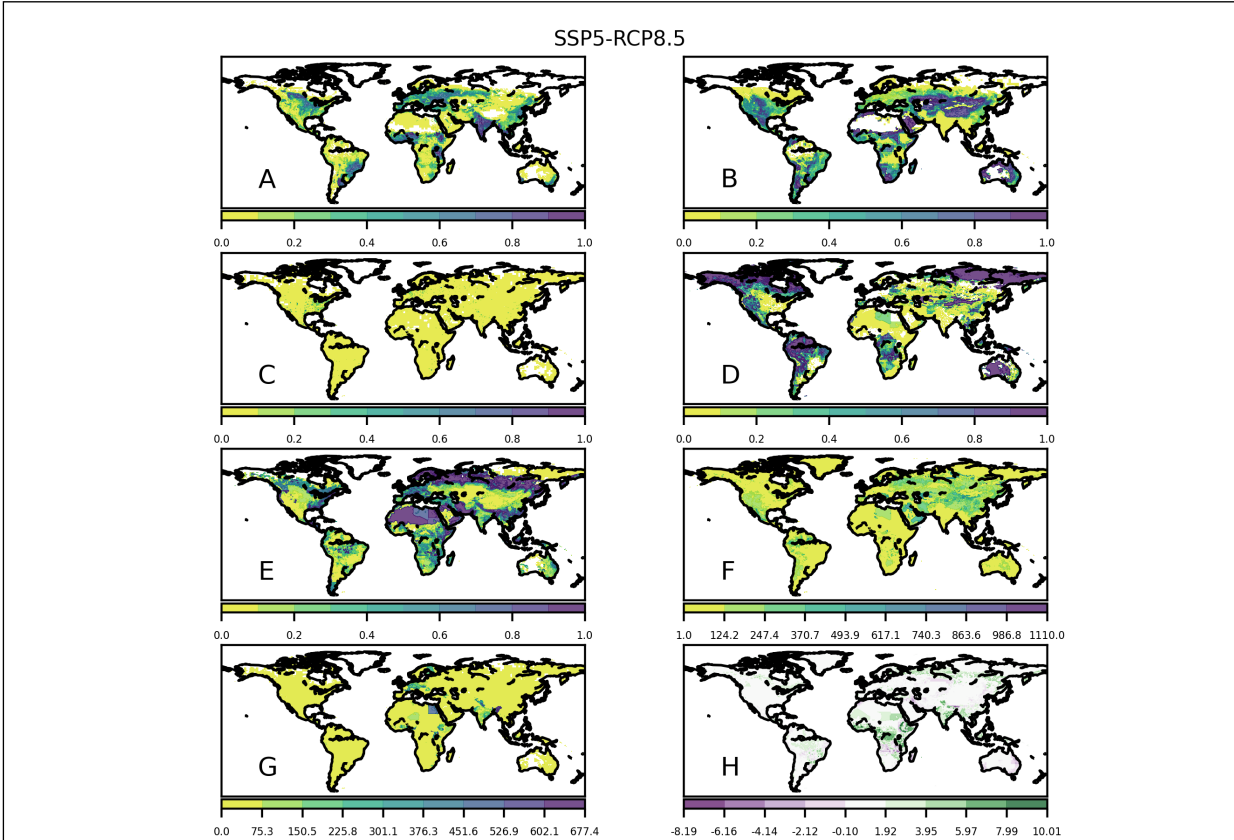
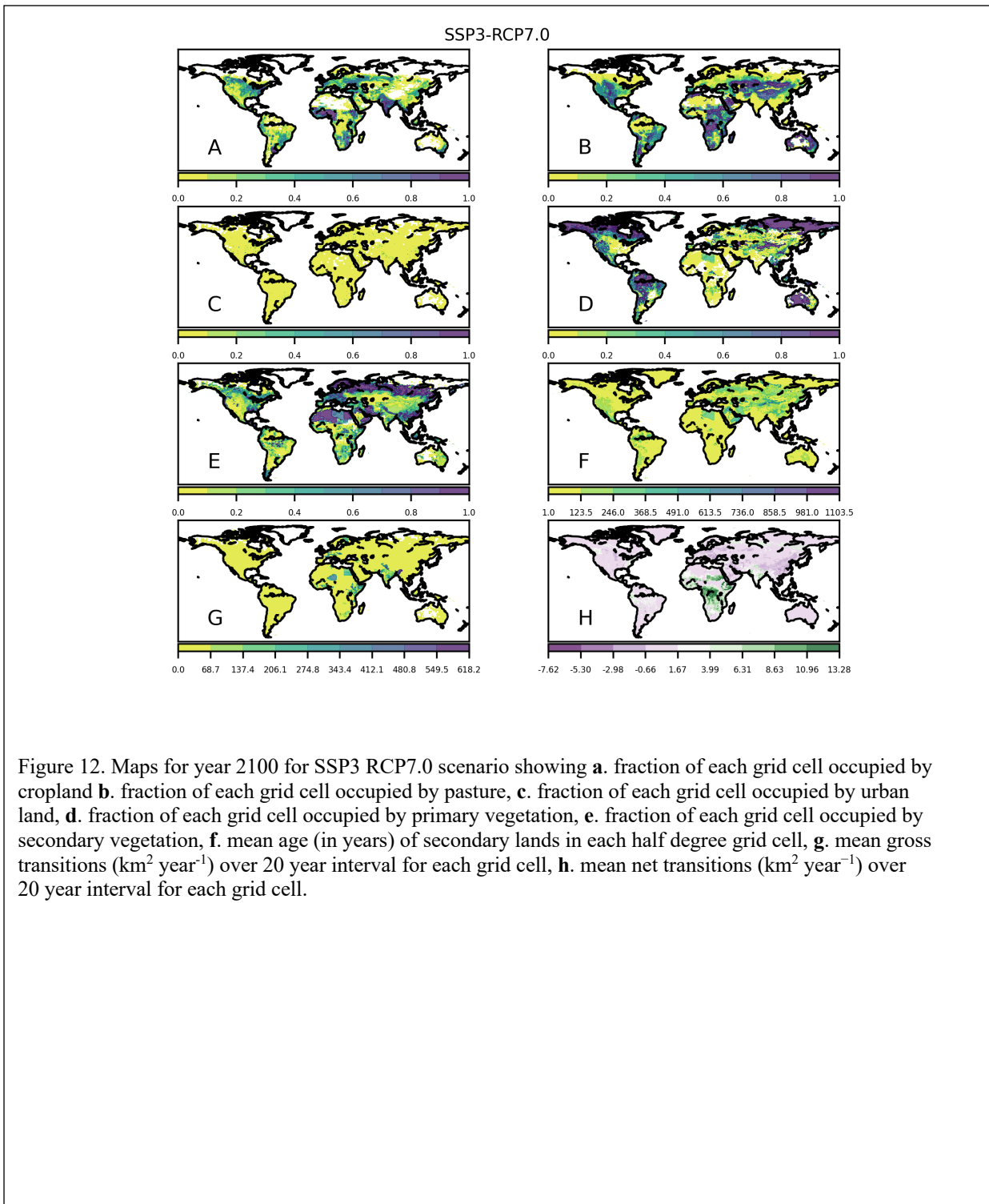


Figure 11. Maps for year 2100 for SSP5 RCP8.5 scenario showing **a.** fraction of each grid cell occupied by cropland **b.** fraction of each grid cell occupied by pasture, **c.** fraction of each grid cell occupied by urban land, **d.** fraction of each grid cell occupied by primary vegetation, **e.** fraction of each grid cell occupied by secondary vegetation, **f.** mean age (in years) of secondary lands in each half degree grid cell, **g.** mean gross transitions ($\text{km}^2 \text{ year}^{-1}$) over 20 year interval for each grid cell, **h.** mean net transitions ($\text{km}^2 \text{ year}^{-1}$) over 20 year interval for each grid cell.



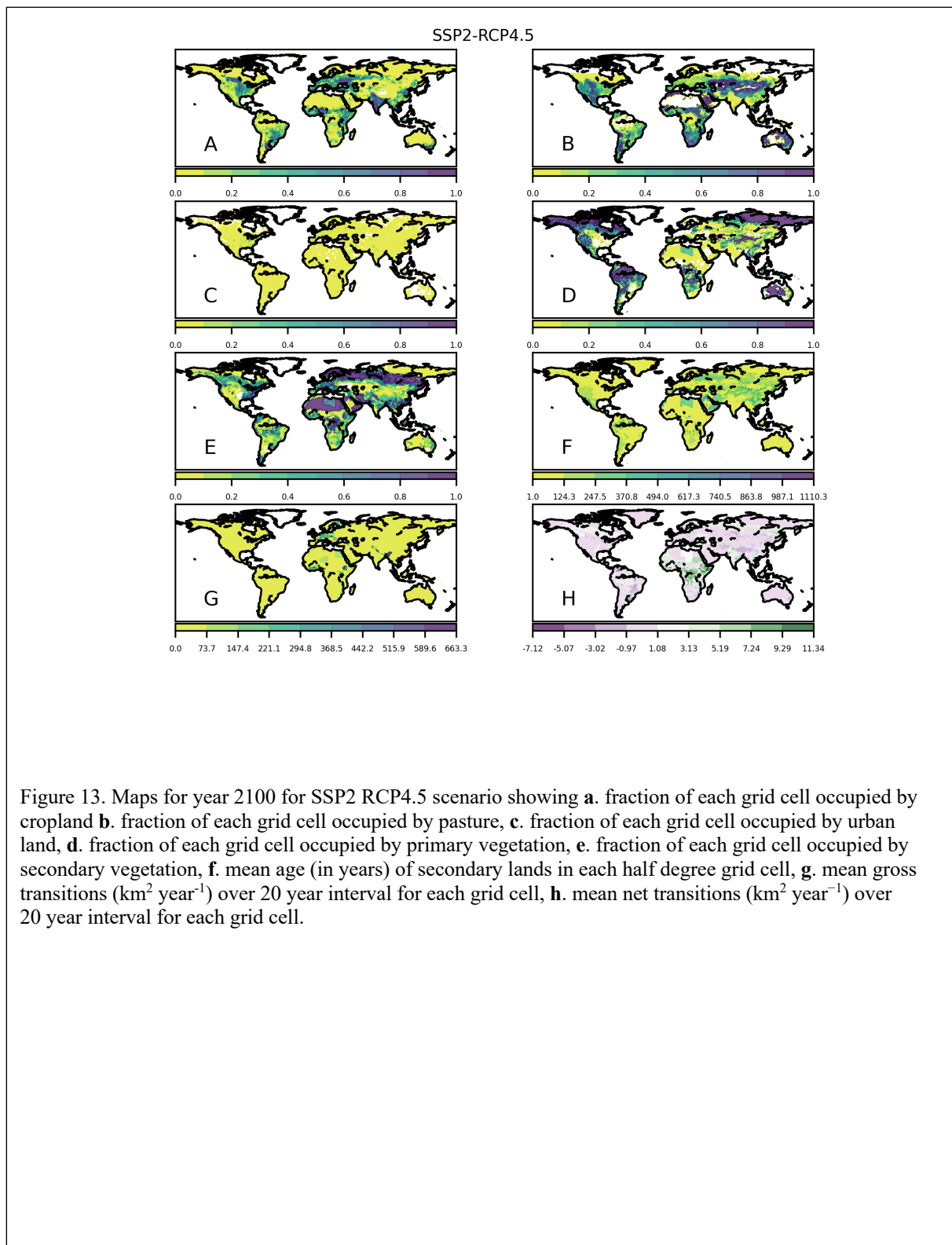
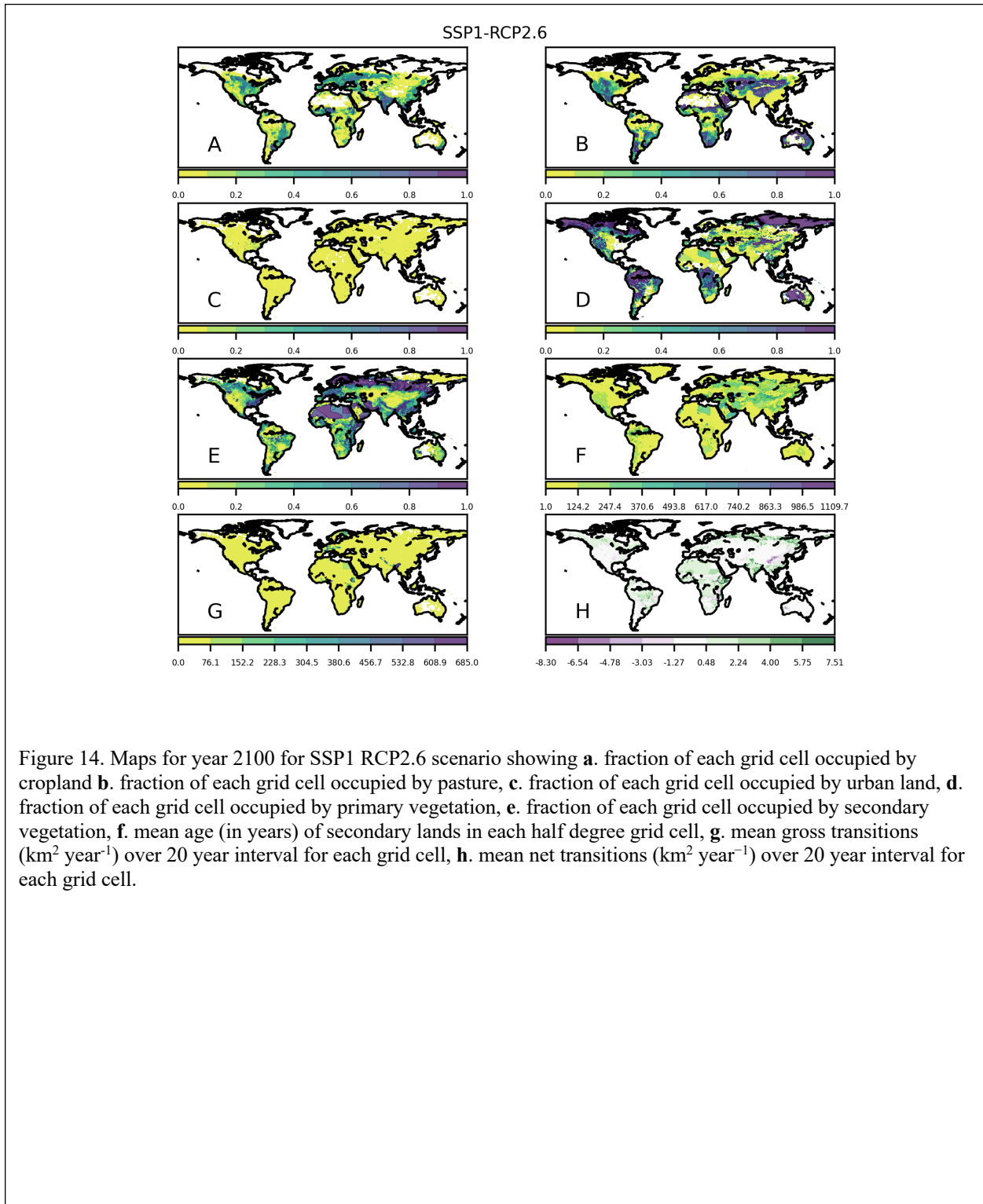


Figure 13. Maps for year 2100 for SSP2 RCP4.5 scenario showing **a.** fraction of each grid cell occupied by cropland **b.** fraction of each grid cell occupied by pasture, **c.** fraction of each grid cell occupied by urban land, **d.** fraction of each grid cell occupied by primary vegetation, **e.** fraction of each grid cell occupied by secondary vegetation, **f.** mean age (in years) of secondary lands in each half degree grid cell, **g.** mean gross transitions ($\text{km}^2 \text{ year}^{-1}$) over 20 year interval for each grid cell, **h.** mean net transitions ($\text{km}^2 \text{ year}^{-1}$) over 20 year interval for each grid cell.



1385

1390

1395

1400

1405

1410

1415

1420

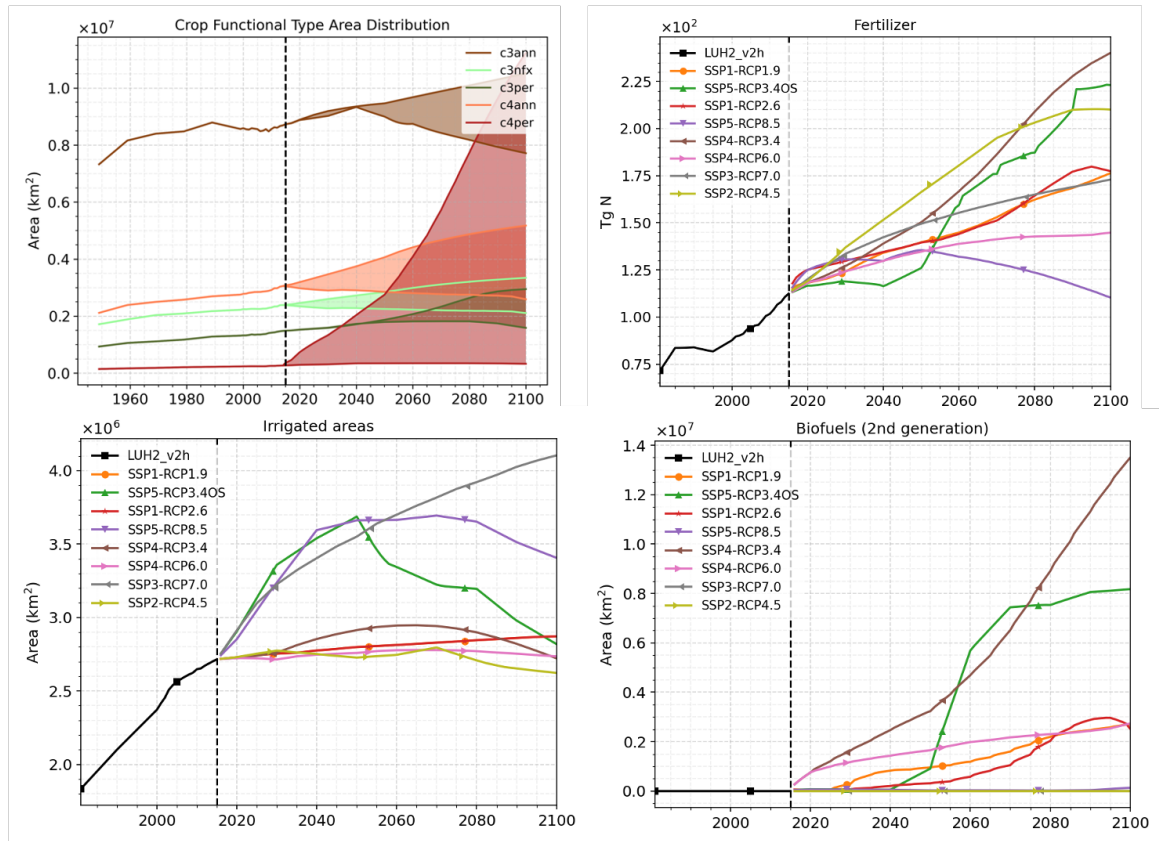


Fig. 15. Time series of harmonized management variables.

Appendix

Mapped patterns of Tier 2 Scenarios

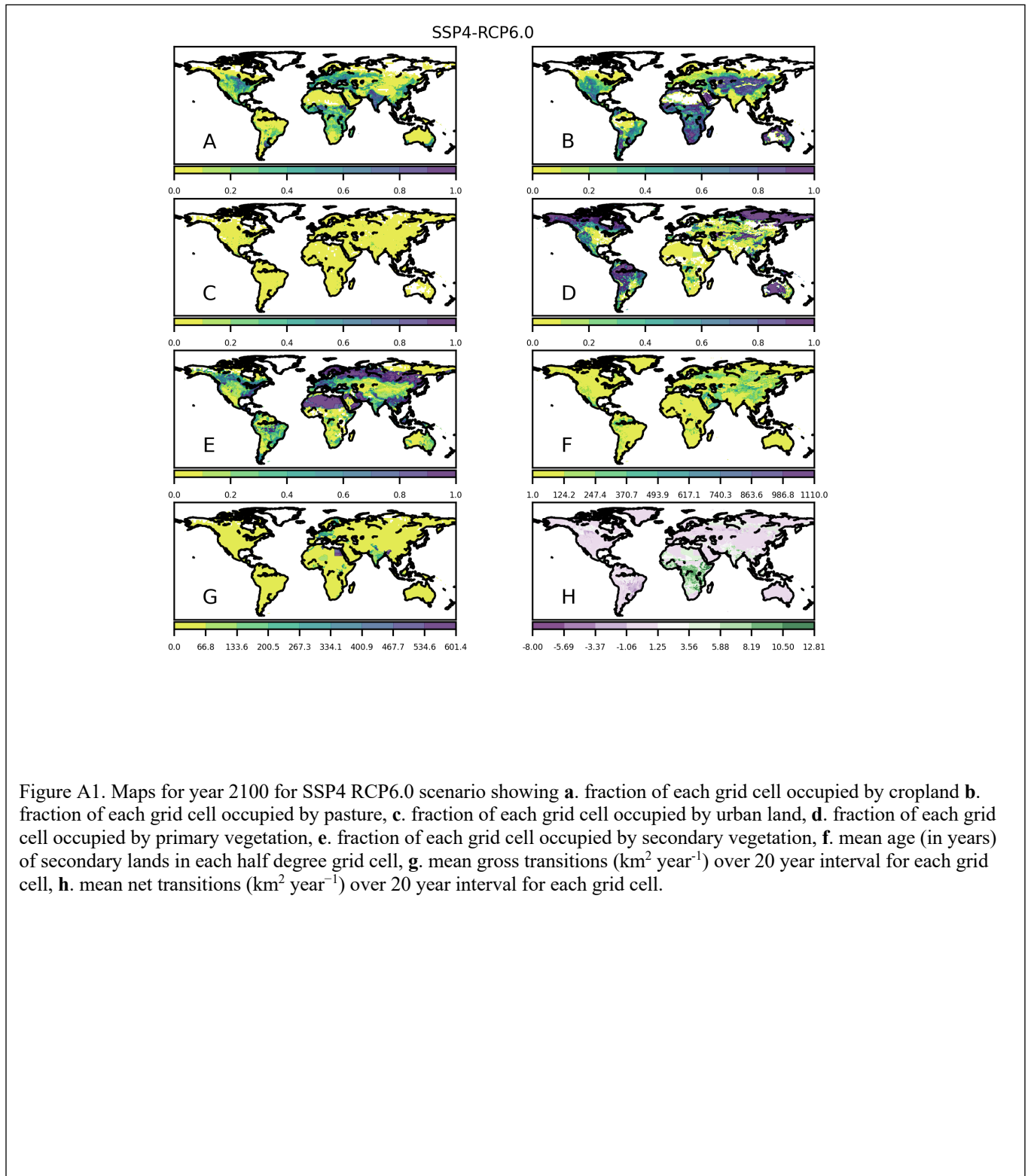
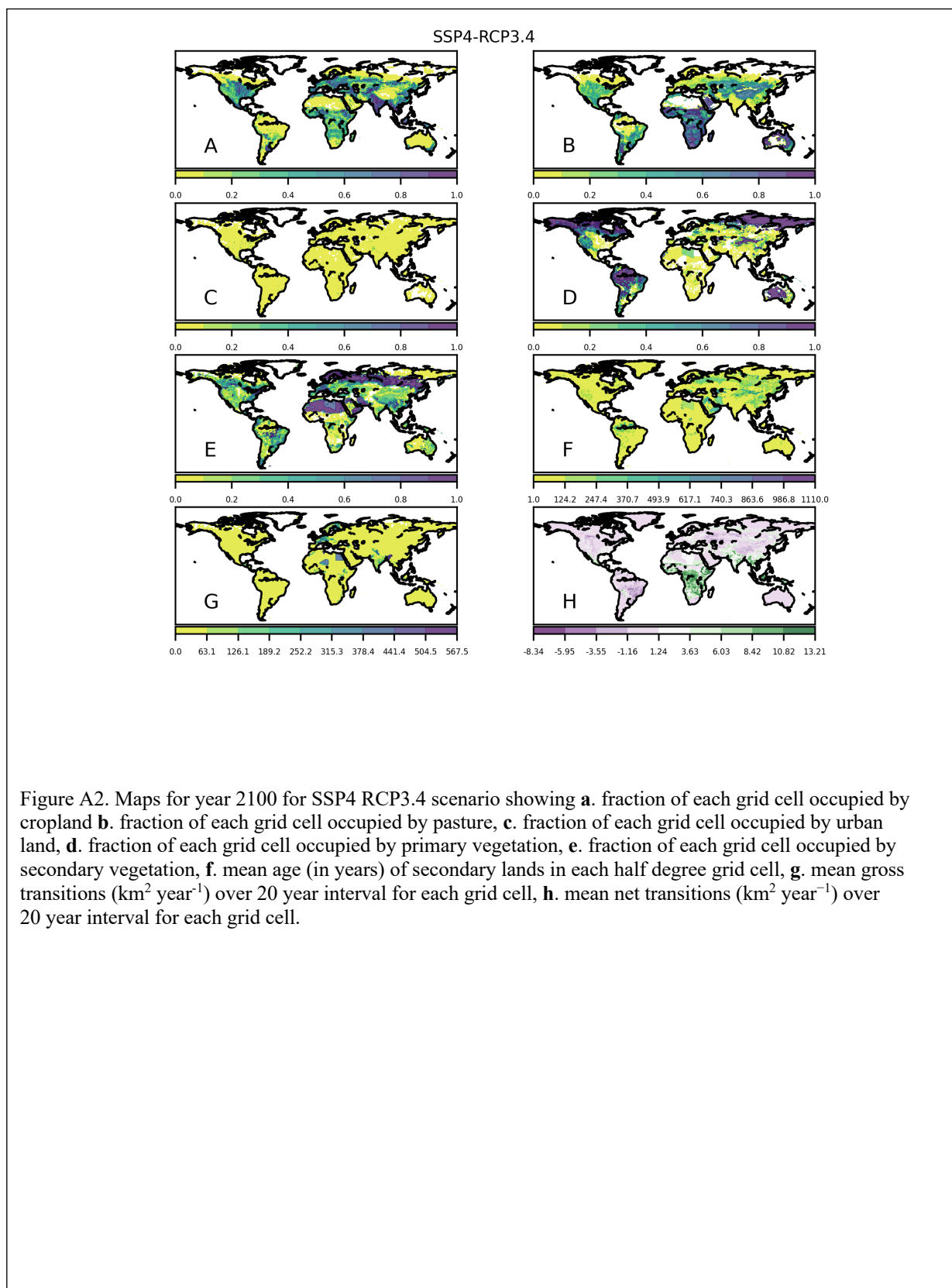


Figure A1. Maps for year 2100 for SSP4 RCP6.0 scenario showing **a.** fraction of each grid cell occupied by cropland **b.** fraction of each grid cell occupied by pasture, **c.** fraction of each grid cell occupied by urban land, **d.** fraction of each grid cell occupied by primary vegetation, **e.** fraction of each grid cell occupied by secondary vegetation, **f.** mean age (in years) of secondary lands in each half degree grid cell, **g.** mean gross transitions ($\text{km}^2 \text{ year}^{-1}$) over 20 year interval for each grid cell, **h.** mean net transitions ($\text{km}^2 \text{ year}^{-1}$) over 20 year interval for each grid cell.



SSP5-RCP3.4OS

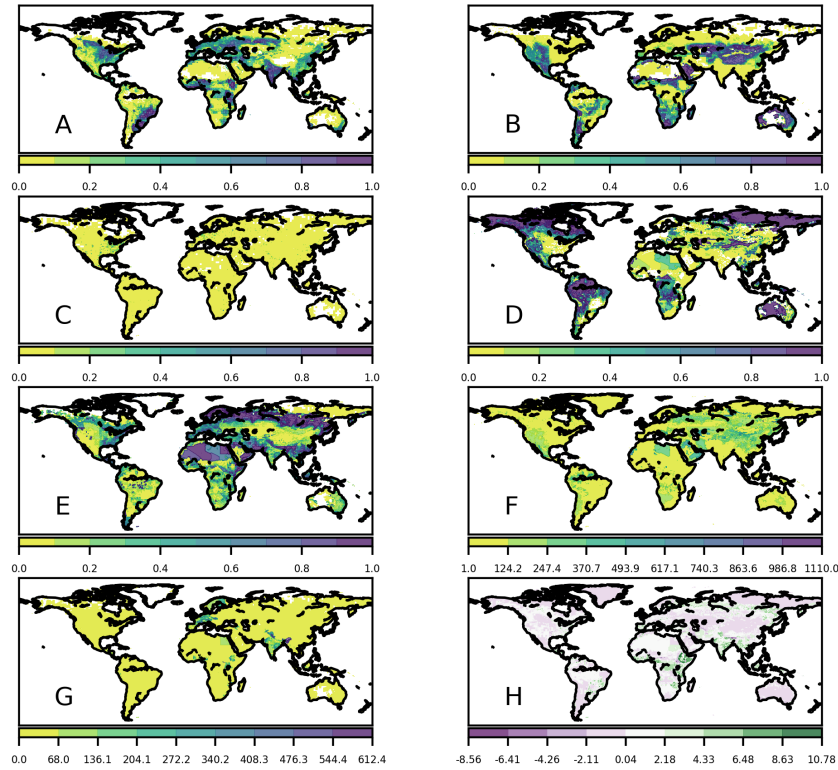


Figure A3. Maps for year 2100 for SSP5 RCP3.4OS scenario showing **a.** fraction of each grid cell occupied by cropland **b.** fraction of each grid cell occupied by pasture, **c.** fraction of each grid cell occupied by urban land, **d.** fraction of each grid cell occupied by primary vegetation, **e.** fraction of each grid cell occupied by secondary vegetation, **f.** mean age (in years) of secondary lands in each half degree grid cell, **g.** mean gross transitions ($\text{km}^2 \text{ year}^{-1}$) over 20 year interval for each grid cell, **h.** mean net transitions ($\text{km}^2 \text{ year}^{-1}$) over 20 year interval for each grid cell.

